Physics potential of Tokai-to-Kamioka-and-Korea neutrino oscillation experiment

Ken-ichi Senda

Department of Particle and Nuclear Physics,
School of High Energy Accelerator Science,
the Graduate University for Advanced Studies (SOKENDAI)

Abstract

The Tokai-to-Kamioka (T2K) neutrino oscillation experiment will start in 2009. In T2K, the center of the neutrino beam from J-PARC at Tokai will go through underground beneath Super-Kamiokande (SK), reach the sea level in the Japan (east) sea near Korean shore. When the beam center is 2.5° (3.0°) downward SK, the neutrino beam with an off-axis angle greater than 1.0° (0.5°) can be observed in Korea. We study the physics potential of the Tokai-to-Kamioka-and-Korea (T2KK) experiment when an additional 100 kt-level Water Čerenkov detector is placed in Korea during the T2K experimental period. We find that the matter effect, which arises from the coherent interaction of ν_e (or $\bar{\nu}_e$) off the electrons in the earth matter, is a powerful tool to determine the sign of $(m_3^2 - m_1^2)$, and the CP phase, $\delta_{\rm MNS}$, of the lepton flavor mixing matrix. The best combination of the off-axis angles at each detector and the length for the Tokai-to-Korea baseline is found to be 3.0° at SK ($L = 295$km) and 0.5° at $L = 1000$km. If we choose this combination, and if the densities along the baselines are 2.8 g/cm^3 for Tokai-to-Kamioka baseline and 3 g/cm^3 for Tokai-to-Korea baseline with 3% uncertainties, the mass hierarchy pattern can be determined at 3-σ level for $\sin^2 2\theta_{\rm RCT} \gtrsim 0.09$, and the CP phase can be constrained with ±30° error for $\sin^2 2\theta_{\rm RCT} \gtrsim 0.06$, after 5 years of running (5×10^{21} POT). When we combine the result of the future reactor neutrino experiments, such as Double-CHOOZ, RENO, DAYA-BAY, the capability of determining the mass hierarchy pattern in T2KK is enhanced, and the hierarchy pattern can be constrained at 3-σ level for $\sin^2 2\theta_{\rm RCT} \gtrsim 0.055$. Because of the importance of the matter effect, we study the matter profile along the baselines of the T2KK experiment by using the recent geophysical measurements. The average matter density along the Tokai-to-Korea baselines is found to be 2.96, 3.01, and 3.03 g/cm^3 for the baseline length of L = 1000, 1100, and 1200 km, respectively, with about 6% uncertainty. Only the real part of the first Fourier mode gives non-negligible but very small contribution to the $\nu_\mu \to \nu_e$ oscillation probability. We find that, even if we enhance the error of the average matter density from 3% to 6%, the capability of determining the neutrino mass hierarchy pattern in T2KK does not deteriorate significantly because the measurement error is dominated by statistics.

Contents

1 Introduction

Before 1998, neutrinos had been thought to be massless particles by a lot of people. In 1998, Super-Kamiokande collaboration reported that they discovered the neutrino oscillation from the atmospheric neutrinos [1] Because neutrinos should be massive particles and have the finite lepton-flavor mixing angles in order to explain the neutrino oscillation, the idea that the neutrinos are massless was overturned by the discovery of neutrino oscillation.

After the discovery of the neutrinos oscillation, many people have been interested in the origin of the neutrino mass and the flavor mixing, and the related topics such as mass matrix at the GUT scale, the leptogenesis and so on. When we consider such models, the value of the neutrino oscillation parameters are hints about the symmetry and the picture of the mass matrix at the GUT scale. In other words, constraints on the unmeasured oscillation parameters give us more hints to beyond the standard model.

In the three neutrino model, totally nine parameters are related to the mass matrix. Those are three neutrino masses, three lepton-flavor mixing angles, and three CP violating phase. About the CP phase, one is the lepton-conserving phase, which is the same as the KM phase in the quark sector, and the others are lepton-number violating phases, which can be taken non-zero value when neutrinos are Majorana particles. Among the nine, the six parameters, two mass-squared differences, three flavor-mixing angles, and the lepton conserving phase, are observables in the neutrino oscillation experiments.

As of December 2007, four of the six oscillation parameters have been measured in neutrino oscillation experiments. From the atmospheric neutrino oscillation experiments [2], we have measured the magnitude of the larger mass-squared difference and one of the lepton flavor mixing angles, of which values are confirmed by the accelerator based long baseline (LBL) neutrino oscillation experiments, K2K [3] and MINOS citeminos. The another mass-squared difference and the mixing angle are measured in the solar neutrino oscillation experiments [5, 6] and the KamLAND [7, 8] experiments which have observed the $\bar{\nu}_e$ survival probability from the reactor power plant at about 100 km distance. Regarding as the last mixing angle, CHOOZ [9] and Palo Verde [10] reactor (RCT) neutrino experiment tried to measure the third mixing angle, $\theta_{\rm RCT}$, by the $\bar{\nu}_e$ survival probability at about 1km distance, because the magnitude of the disappearance probability is roughly proportional to $\sin^2 2\theta_{\rm RCT}$. But these experiments could not observe the neutrino oscillation phenomena, and only give the upper limit on the value of $\sin^2 2\theta_{\rm RCT}$. The value of $\theta_{\rm RCT}$ will be expected to be measured in the future experiments which will start from 2008 to 2009 [13, 15, 14, 11, 12]. Because the contribution from δ is proportional to $\sin\theta_{\rm RCT}$, we do not know about δ at all now. There are other problem for

already measured parameters, so called degeneracy problem. For example, the absolute value of the lager mass-squared difference is already measured, but its sign have not been constrained yet. So the tasks of the future neutrino oscillation experiments are the measurements of the least mixing angle, and the CP phase, and solving the degeneracy problems.

Here we briefly introduce the Tokai-to-Kamioka (T2K) neutrino oscillation experiment, which will start in 2009[11]. In the T2K experiment, the great number of charged π by 50 GeV proton accelerator at Tokai village, J-PARC [16]. Then large number of μ neutrinos are made by the decay of the pions, and shot through Super-Kamiokande (SK). The main purpose of the T2K experiment is observing $\nu_\mu \to \nu_e$ oscillation. Because the magnitude of this transition probability is roughly proportional to $\sin^2 2\theta_{\mathrm{RCT}}$, measurement of the $\nu_\mu \to \nu_e$ transition means the measurements of θ_{RCT}. In order to observe the oscillation maximum of the $\nu_\mu \to \nu_e$ at SK effectively, the center of the T2K neutrino beam is planed to be aimed the underground beneath SK and the Japan sea (East sea), and then the upper side of the neutrino beam reaches SK. The interesting point that the lower side of the T2K neutrino beam will appear in Korea at the same time [17, 19]. Recently, the possibility of placing second detector in Korea to measure the lower side of the T2K neutrino beam have been discussed [18, 19, 20, 21, 22, 23]. These works point out that if we place the 100 kt level neutrino detector in Korea and measure the T2K neutrino beam, we can measure the CP phase, and solv the degeneracy problem by the two detector system when $\sin^2 2\theta_{\mathrm{RCT}}$ is enough large to be measured in T2K.

In this thesis, we study the mechanism of determining the neutrino mass hierarchy pattern and the CP phase by the two detector system, and explore the physics potential of T2KK experiment. This paper is organized as follows. The sections 2, and 3 are the review parts about the fundamental of the neutrino oscillation phenomena. We study the formalism of the neutrino oscillation in section 2. In section 3, we review the coherent interaction between the neutrinos and the electrons inside the matter and its effect to the neutrino oscillation. In section 4, we learn the present status of the neutrino oscillation parameters, and investigate how to detect the contribution from the unmeasured parameters. In section 5, we briefly introduce the T2K experiment. Furthermore we explain the basic idea of the T2KK experiment, and study the importance of the matter effect in the T2KK experiment. In section 6, we checke the physics potential of T2KK by the numerical calculations. In section 7, we discuss what happen if we combine the T2KK experiment and the future reactor neutrino experiments, then confirms its effect. In section 8, we estimate the earth profile along the Tokai-to-Kamioka and the Tokai-to-Korea baselines by using the recent geophysics research, and then study the earth

matter effect in T2KK. Finally, we conclude this paper in section 9. In the appendix, we derive the approximation formula for the time-evolution operator, which is useful for understanding the neutrino oscillation.

2 Neutrino Oscillation

2.1 Neutrino oscillation in the two flavor model

In this section, we would like to review of the neutrino oscillation in the vacuum. At first, we study the simplest case, two flavor neutrino model.

Here we consider the case that neutrino flavors are only e, and μ. When neutrinos are massive particle, generally the flavor eigen-states do not correspond to the mass eigen-states. The relation between flavor eigen-states, $|\nu_\alpha\rangle$ ($\alpha = e,\ \mu$), and mass eigen-states, $|\nu_i\rangle$ ($i = 1, 2$) can be expressed as

$$|\nu_\alpha\rangle = O_{\alpha i}\,|\nu_i\rangle\ . \tag{1}$$

Here $O_{\alpha i}$ is the flavor mixing matrix, of which elements are

$$O_{e1} = O_{\mu 2} = \cos\theta\,, O_{\mu 2} = -O_{e1} = \sin\theta\,. \tag{2}$$

We can always take both $\sin\theta$ and $\cos\theta$ to be positive by redefinition of the field (state). These sine and cosine function can be interpreted as the rates of the mass eigen-states in the flavor eigen-states. At the following discussion, we take the frame that the mass eigen-value for ν_1, m_1, is lighter than that for ν_2 m_2. Hamiltonian in the flavor representation is given as,

$$\begin{aligned} H_{\beta\alpha} &= O_{\beta i}\left\{\delta_{i1}\delta_{j1}\sqrt{m_1^2+p^2} + \delta_{i2}\delta_{j2}\sqrt{m_2^2+p^2}\right\}O_{\alpha j} \\ &\approx O_{\beta i}\left(\delta_{i1}\delta_{j1}\frac{m_1^2+E^2}{2E} + \delta_{i2}\delta_{j2}\frac{m_2^2+E^2}{2E}\right)O_{\alpha j}\,. \end{aligned} \tag{3}$$

From the first line to the second line in eq. (3), we take the relativistic limit, $p^2 \approx E^2 \gg m^2$. Then the time evolution operator, $S_{\beta\alpha}$, can be expressed as,

$$\begin{aligned} S_{\beta\alpha} = \left(e^{-iHt}\right) &= O_{\beta i}\left(\delta_{i1}\delta_{j1}e^{-i\frac{m_1^2+E^2}{2E}L} + \delta_{i2}\delta_{j2}e^{-i\frac{m_2^2+E^2}{2E}L}\right)O_{\alpha j} \\ &= e^{-i\frac{m_1^2+E^2}{2E}L}\left(O_{\beta 1}O_{\alpha_1} + O_{\beta 2}O_{\alpha_2}e^{i\frac{m_2^2-m_1^2}{2E}}\right)\,. \end{aligned} \tag{4}$$

Here we assume that neutrino travels in light speed, and we use the traveling length of neutrino, L, instead of the traveling time, t in eq. (4). Since the non-diagonal elements of

$S_{\beta\alpha}$ are not zero, flavor eigen-states transit by the time evolution. The flavor-transition probability and the flavor-survival probability can be obtain as

$$P_{e\to e} = P_{\mu\to\mu} = 1 - \sin^2 2\theta \sin^2\left(\frac{m_2^2 - m_1^2}{2E}L\right), \tag{5}$$

$$P_{e\to\mu} = P_{\mu\to e} = \sin^2 2\theta \sin^2\left(\frac{m_2^2 - m_1^2}{2E}L\right). \tag{6}$$

We find in eqs. (5) and (6) that the magnitude of the transition rate tells us the size of the flavor-mixing angle, and when we fix the traveling length, L, the energy dependence of the neutrino oscillation tells us the absolute value of the mass-squared difference. Notice that the observed mixing angle, θ, have the degeneracy solution; $\sin^2 2\theta = \sin^2(\pi - 2\theta)$. Because of this degeneracy solution, we can not understand which states are dominant component in the ν_e state from the two-flavor neutrino oscillation experiment in the vacuum. We will study that this degeneracy can be solved by the interaction between neutrinos and electrons inside the matter in section 3.

2.2 Neutrino Oscillation in three flavor model

Here we study the neutrino oscillation in the three flavor model. Now the flavor eigenstates are ν_e, ν_μ, and ν_τ. Mass eigen-states are ν_1, ν_2, and ν_3 and their eigen-values are m_1, m_2, and m_3. Flavor eigen-states are related to the mass eigen-states through the 3×3 unitary matrix.

$$\begin{pmatrix} \nu_e \\ \nu_\mu \\ \nu_\tau \end{pmatrix} = U_{\rm MNS} \begin{pmatrix} \nu_1 \\ \nu_2 \\ \nu_3 \end{pmatrix}. \tag{7}$$

Here $U_{\rm MNS}$ is the lepton flavor mixing matrix, so called Maki-Nakagawa-Sakata matrix [24]. MNS matrix can be parametrize as,

$$U_{\rm MNS} = UV,$$

$$U = \begin{pmatrix} U_{e1} & U_{e2} & U_{e3} \\ U_{\mu 1} & U_{\mu 2} & U_{\mu 3} \\ U_{\tau 1} & U_{\tau 2} & U_{\tau 3} \end{pmatrix}$$

$$= O_{12} P_\delta O_{13} P_\delta^\dagger O_{12}$$

$$= \begin{pmatrix} 1 & 0 & 0 \\ 0 & \cos\theta_{23} & -\sin\theta_{23} \\ 0 & -\sin\theta_{23} & -\cos\theta_{23} \end{pmatrix} \begin{pmatrix} 1 & 0 & 0 \\ 0 & 1 & 0 \\ 0 & 0 & e^{i\delta} \end{pmatrix} \begin{pmatrix} \cos\theta_{13} & 0 & \sin\theta_{13} \\ 0 & 1 & 0 \\ -\sin\theta_{13} & 0 & \cos\theta_{13} \end{pmatrix}$$

$$\times \begin{pmatrix} 1 & 0 & 0 \\ 0 & 1 & 0 \\ 0 & 0 & e^{-i\delta} \end{pmatrix} \begin{pmatrix} \cos\theta_{12} & \sin\theta_{12} & 0 \\ -\sin\theta_{12} & \cos\theta_{12} & 0 \\ 0 & 0 & 1 \end{pmatrix}, \tag{8}$$

$$V = \begin{pmatrix} 1 & 0 & 0 \\ 0 & e^{-i\phi_1} & 0 \\ 0 & 0 & e^{-i\phi_2} \end{pmatrix}. \tag{9}$$

U and V are unitary metrics. U is the flavor mixing matrix which is same as the CKM matrix in quark sector [25]. The independent parameters of U are three flavor mixing angles, θ_{12}, θ_{13}, and θ_{23}, and one lepton number conserving CP violating phase, δ . V is the contribution of the Majorana phase. If neutrinos are Majorana particles, two lepton number violating CP phase, ϕ_1, ϕ_2, can take the finite values. Totally, the number of parameters in the MNS matrix is six.

In the same way as the two flavor model, time evolution operator can be obtained as

$$S_{\beta\alpha} = U_{\beta 1}U^*_{\alpha_1} + U_{\beta 2}U^*_{\alpha_2}e^{-i\Delta_{12}} + U_{\beta 3}U^*_{\alpha_3}e^{-i\Delta_{13}}, \tag{10}$$

where Δ_{ij} represents the oscillation phase,

$$\Delta_{ij} = \frac{\delta m^2_{ij}}{2E}L \simeq 2.534\frac{\delta m^2_{ij}[\mathrm{eV}^2]}{E[\mathrm{GeV}]}L[\mathrm{km}], \tag{11}$$

$$\delta m^2_{ij} = m^2_j - m^2_i. \tag{12}$$

Please notice that the contribution from the Majorana phases is canceled in eq. (10). Therefore we can not determine whether neutrinos are Dirac particles or Majorana particles in the neutrino oscillation experiments.

We can calculate the flavor transition probability from eq. (10);

$$\begin{aligned} P_{\nu_\alpha\to\nu_\beta} = \delta_{\beta\alpha} - 4Re\Big\{ & U_{\beta 1}U^*_{\alpha 1}U_{\beta 2}U^*_{\alpha 2}\sin^2\left(\frac{\Delta_{12}}{2}\right) \\ & + U_{\beta 2}U^*_{\alpha 2}U_{\beta 3}U^*_{\alpha 3}\sin^2\left(\frac{\Delta_{23}}{2}\right) + U_{\beta 3}U^*_{\alpha 3}U_{\beta 1}U^*_{\alpha 1}\sin^2\left(\frac{\Delta_{13}}{2}L\right)\Big\} \\ & - 2[\sin(\Delta_{12}) + \sin(\Delta_{23}) - \sin(\Delta_{13})]J_{\mathrm{MNS}}. \end{aligned} \tag{13}$$

Here J_{MNS} is the Jarscov parameter in the lepton sector.

$$J_{\mathrm{MNS}} = Im[U_{\beta i}U^*_{\alpha i}U^*_{\beta j}U_{\alpha j}], \tag{14}$$

J_{MNS} is invariant by changing the combination of α and β and that of i and j, such as $(\alpha,\ \beta) = (e,\mu),(\mu,\tau),(\tau,e)$ and $(i,\ j) = (1,2),(2,3),(3,1)$. From eq. (13), we learn that

the observables in the neutrino oscillation experiments are the component of the mixing matrix, U, and two mass squared differences.

As we study in section 4, a lot of experiments made clear that the $|\delta m^2_{13}| \gg |\delta m^2_{12}|$. This large hierarchy of the mass squared differences gives approximation formulas of the neutrino oscillation, which are useful to understand contributions of each parameters. When $|\Delta_{12}| \ll |\Delta_{13}| \sim O(1)$, we can set $\sin\Delta_{12} \sim 0$ and $\cos\Delta_{12} \sim 1$. Then eq. (13) can be expressed as,

$$P_{\nu_\alpha \to \nu_\alpha} = 1 - 4|U_{\alpha 3}|^2|1 - U_{\alpha 3}|^2 \sin^2\left(\frac{\Delta_{13}}{2}\right) + O(\Delta_{12})\,, \tag{15a}$$

$$P_{\nu_\alpha \to \nu_\beta}(\alpha \neq \beta) = 4|U_{\beta 3}U_{\alpha 3}|^2 \sin^2\left(\frac{\Delta_{13}}{2}\right) + O(\Delta_{12})\,. \tag{15b}$$

In this limit, we can measure the absolute value of the $|\delta m^2_{13}|$ by measuring the oscillation phase, and the elements of the MNS matrix can be measured from the oscillation amplitude. Especially, we find that the formula of eq. (15a) is the same as that of eq. (5). In other words, we can analyze the neutrino oscillation in the two flavor model, and hence the measurement of survival probability suffer from the degeneracy problem, $|U_{\alpha 3}|^2 > 0.5$ or < 0.5. We also find that the we can not determine the sign of δm^2_{13} in this limit.

There is another approximation formula which is sensitive to the Δ_{12}. When $\Delta_{13} \gg \Delta_{12} \sim O(1)$, $\sin^2\frac{\Delta_{13}}{2}$ terms in eq. (13) oscillate very frequently in the width of the energy bin, energy resolution. Then the contributions from the Δ_{13} terms in eq. (13) are averaged out. eq. (13) can be approximated as,

$$\begin{aligned} P_{\nu_\beta \to \nu_\alpha} \approx\ & \delta_{\beta\alpha} - 2Re\left\{U_{\beta 3}U^*_{\alpha 3}\left(\delta_{\beta\alpha} - U_{\beta 3}U^*_{\alpha 3}\right)\right\} \\ & -4Re(U_{\beta 1}U^*_{\alpha 1}U^*_{\beta 2}U_{\alpha 2}) \sin^2\left(\frac{\Delta_{12}}{2}\right) - 2J_{\rm MNS}\sin\Delta_{12}\,. \end{aligned} \tag{16}$$

Especially, the approximation for the flavor survival mode, $\nu_\alpha \to \nu_\alpha$, is very similar to the that in the two flavor model. Actually, in the solar neutrino experiment, which measures the ν_e survival probability from the sun, the condition of the oscillation phase is the satisfied with condition for the approximation, $\Delta_{12} \sim O(1)$. Therefore we can constrain the values of $|U_{e1}U_{e2}|^2$ and δm^2_{12} from the solar neutrino experiments.

3 Matter effect

3.1 Matter effect in the two flavor model

In this section, we study the matter effect, which comes from the interaction between the neutrinos and the electrons inside the matter. When neutrinos are going through the matter, neutrinos interact with the nucleons and the electrons inside the matter via the weak boson exchange. The cross sections of the most of all scattering modes are strongly suppressed by square of Fermi coupling constant, G_F^2, and hence contribution of scattering process in the neutrino oscillation experiment is negligibly small. Only the scattering of which the transfer momentum is zero can interfere with the non-scattering process. This interference term, which is order G_F, gives the potential energy to neutrinos. We shows the possible forward scattering processes between neutrinos and electrons inside the matter in Fig. 1.

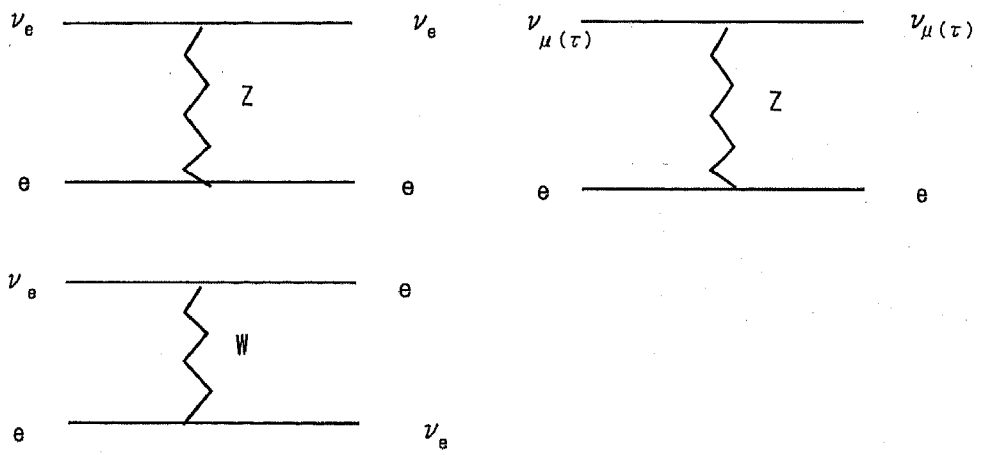

Figure 1: The possible coherent interactions between the neutrinos and the electrons inside the matter. Only ν_e have the additional charged current interaction.

In Fig. 1, we find that the all flavor neutrinos interactions with the electrons inside the matter via a Z boson. The neutral current interactions are flavor diagonal, and all neutrinos receive the just same potential energy. Because such scalar like potential does not give any effects on the disorganization of the Hamiltonian, we can ignore the potential from the neutral current in the neutrino oscillation. Although the protons and neutrons in the matter also interact with neutrinos via Z boson exchange, these interactions gives no contributions to the neutrino oscillation as the above reason. For the charged current process, only ν_e have the W boson exchange process. The potential energy from the charged current changes the diagonazation of the Hamiltonian, then the

effective mass-squared differences and the mixing angles is different from the that in the vacuum [26].

So let us check the effect of the charged current interaction to the neutrino oscillation. In this sub section, we consider the matter effect in the two flavor model, e and μ to understand the matter effect more clearly. The Hamiltonian of this system can be expressed as, in the flavor representation,

$$H(t) = \frac{1}{2E} O \begin{pmatrix} 0 & 0 \\ 0 & \delta m_{12}^2 \end{pmatrix} O^T + \frac{1}{2E} \begin{pmatrix} a(t) & 0 \\ 0 & 0 \end{pmatrix}, \tag{17}$$

where we use the mixing matrix in the two flavor model, O, defined in section 2.1, and $a(t)$ represents the potential from the charged current interaction;

$$\begin{aligned} a(t) &= 2\sqrt{2}\frac{G_F}{E} \int d^3x j_\nu^\mu j_{e\mu} = \sqrt{2} G_F n_e(t) \\ &= 7.56 \times 10^{-5} (\mathrm{eV}^2) \left(\frac{\rho(t)}{\mathrm{g/cm}^3} \right) \left(\frac{E}{\mathrm{GeV}} \right) . \end{aligned} \tag{18}$$

Notice that the matter effect term, $a(t)$, is a function of time because the electron number density depends on the matter density around neutrinos. In other words, the matter effect have local dependence, x. We use the x instead of t following discussion to make clear the local dependence of the matter effect. We can diagonalize the Hamiltonian in eq. (17). The effective mixing angle, Φ, and the effective mass squared difference, Δ, can be expressed in terms of the matter effect, mass squared difference, and the mixng angle in the vacuum,

$$\Delta = \sqrt{a^2 + 4(\delta m_{12}^2)^2 - 4a\delta m_{12}^2 \cos 2\theta}, \tag{19}$$

$$\cos^2 \Phi = \frac{a + \Delta - 2\delta m_{12}^2 \cos 2\theta}{2\Delta} . \tag{20}$$

We find that Δ and Φ depends on the sign of $\cos 2\theta$. Because sign of $\cos \Phi$ is determined by whether ν_1 or ν_2 are dominant state in ν_e, we can solve the degeneracy problem discussed in section 2.1, $\sin^2 2\theta = \sin^2(\pi - 2\theta)$. This $\cos\theta$ dependence can be interpreted as follows. When electron neutrinos receive the potential energy, electron neutrino becomes effectively heavy. Then the heavier mass eigen states becomes to dominate the electron neutrino states. If electron neutrinos are dominated by the lighter state in the vacuum, $\theta < \frac{\pi}{4}$, the effective mixing angles gets to close the maximum mixing as a grows. The resonance density, when the effective mixing angle is maximum, is calculated from

eq. (20),

$$n_e^r = \frac{\delta m_{12}^2 \cos 2\theta}{2\sqrt{2} G_{\rm F} E}. \tag{21}$$

Furthermore when a is over the resonance region, the heavier states dominate the neutrino energy then $\cos 2\Phi$ gets close to zero. *Vice versa*, when the heavier states, $\theta > \frac{\pi}{4}$ dominates electron neutrino in the vacuum, $\cos 2\Phi$ goes to zero directly.

Let us consider the time evolution in this system. Time evolution in this system is slightly difficult because Hamiltonian depends time, t (position, x). In order to check it, we relieve the Schorondiger equation for the mass eigen-state from the flavor eigen-state.

$$\begin{aligned}
i\frac{d}{dx}\nu_{\rm flavor} &= H_{\rm flavor}\nu_{\rm flavor} \\
i\frac{d}{dx}(O\nu_{mass}) &= OH_{mass}O^T O\nu_{mass} \\
iO\begin{pmatrix} 0 & -\dot{\Phi} \\ \dot{\Phi} & 0 \end{pmatrix}\nu_{mass} + O\frac{d}{dx}\nu_{mass} &= OH_{mass}\nu_{mass} \\
\frac{d}{dx}\nu_{mass} &= (H_{mass} + \begin{pmatrix} 0 & -i\dot{\Phi} \\ i\dot{\Phi} & 0 \end{pmatrix})\nu_{mass}
\end{aligned} \tag{22}$$

Here $\dot{\Phi}$ is $\frac{d\Phi}{dx}$, and index "flavor" ("mass"), means the flavor (mass) representation, respectively. In this system, a mass eigen-state can be transit the other mass eigen-state, because of the second term of the right side in eq. (22). Such system is very difficult to solve the equation analytically, so we often use the adiabatic condition;

$$\frac{d\Phi}{dx} \sim 0. \tag{23}$$

Fortunately, most of all neutrino oscillation experiments satisfies the adiabatic condition. We assume that the adiabatic condition is satisfied following part of this paper. The second difficulty in this system is that still $H_{\rm mass}$ depends on the x. We have to use $\mathcal{T}e^{-i\int_0^L dx H_{mass}}$ instead of naive $e^{-iH_{mass}L}$ as the time evolution operator. When $\rho(x)$ is a constant function, of course, we can use $e^{-iH_{mass}L}$ as the time evolution operator, and then we can calculate transition probability and the survival probability by using the effective mass squared difference, Δ, and effective mixing angle, Φ.

Though this is very difficult to solve differential equation, eq. (22) exactly, but we can roughly estimate magnitude of the transition probability and the survival probability.

The matrix element of the time evolution can be calculated as

$$\begin{aligned} S_{\beta\alpha} &= \langle \nu_\beta(x) \, | \nu_\alpha(0) \rangle \\ &= \langle \nu_i | \, O'_{\beta i}(x) e^{-i \int_0^x dy H(y)} O'_{\alpha j}(x) \, | \nu_j \rangle \ . \end{aligned} \tag{24}$$

Here O' is the effective mixing matrix, of which elements can be written by $\cos\Phi$ and $\sin\Phi$. The point is that the magnitude of the transition (survival) probability strongly depends on the initial and final mixing matrix. Therefore we can roughly discuss the oscillation amplitude without solving eq. (22). For the practice, we consider the following cases;

- $\Phi(0) \sim \pi$ or 0: In that case, a flavor eigen-state is a almost pure mass eigen-state at the initial. Because the almost only one energy eigen-state is produced at the initial, the interference between the mass eigen-states is very small, and neutrino oscillation does not occur. Then the transition and the survival probabilities are controlled by the final effective mixing angle.

- The initial $\Phi(0) > \pi/2$ but the final $\Phi(x) < \pi/2$: In this case, $|\nu_2\rangle$ is mainly composed by ν_e, and ν_μ is mainly composed by $|\nu_1\rangle$ at first. However this relation between turned over at the final. Therefore amplitude of the transition mode tends to be larger than that of the survival mode. For example, when the electron neutrino is produced at the initial, the traveling neutrino is mainly ν_2. However ν_2 is mainly composed by ν_μ at position x. So the number of ν_μ tends to be larger than ν_e.

At the last of this sub section, we would like to comment about the CP symmetry. For the anti-neutrino, S-channel interaction can be added to the Hamiltonian instead of the T-channel interaction in Fig. 1, and the sign of the matter effect becomes negative. Even when the neutrino is two flavor, the mixing matrix is positive. CP symmetry is broken by the matter effect.

3.2 Matter effect in the three flavor model

In this section, we consider about the matter effect in the three flavor model, but that the matter density is constant, in order to simplify the system. In the three flavor neutrino model, the mixing matrix is complex matrix so it seems that we can not diagonalize analytically. But actually we do not have to diagonalize complex matrix, when we choose the parametrization of MNS matrix shown in eq. (8) [27]. This is because the

potential term are not affected by the O_{23} and P_δ defined in eq. (8).

$$
\begin{aligned}
& P_\delta^\dagger O_{12} \begin{pmatrix} 0 & 0 & 0 \\ 0 & \delta m_{12}^2 & 0 \\ 0 & 0 & \delta m_{13}^2 \end{pmatrix} O_{12}^\dagger P_\delta \\
&= \begin{pmatrix} 1 & & \\ & 1 & \\ & & e^{i\delta} \end{pmatrix} \begin{pmatrix} s_{12}^2 \delta m_{12}^2 & s_{12}c_{12}\delta m_{13}^2 & 0 \\ s_{12}c_{12}\delta m_{13}^2 & c_{12}^2 & 0 \\ 0 & 0 & \delta m_{13}^2 \end{pmatrix} \begin{pmatrix} 1 & & \\ & 1 & \\ & & e^{-i\delta} \end{pmatrix} \\
&= O_{12} \begin{pmatrix} 0 & & \\ & \delta m_{12}^2 & \\ & & \delta m_{13}^2 \end{pmatrix} O_{12}^T
\end{aligned} \tag{25}
$$

$$
O_{23} P_\delta \begin{pmatrix} a & & \\ & 0 & \\ & & 0 \end{pmatrix} P_\delta^\dagger O_{23}^T = \begin{pmatrix} a & & \\ & 0 & \\ & & 0 \end{pmatrix} \tag{26}
$$

By using this relation, the Hamiltonian can be expressed as

$$
\begin{aligned}
H &= \frac{1}{2E} \{ O_{23} P_\delta O_{13} P_\delta^\dagger O_{12} \begin{pmatrix} 0 & & \\ & \delta m_{12}^2 & \\ & & \delta m_{13}^2 \end{pmatrix} O_{12}^T P_\delta O_{13}^T P_\delta^\dagger O_{23}^T + \begin{pmatrix} a & & \\ & 0 & \\ & & 0 \end{pmatrix} \} \\
&= \frac{1}{2E} \{ O_{23} P_\delta O_{13} O_{12} \begin{pmatrix} 0 & & \\ & \delta m_{12}^2 & \\ & & \delta m_{13}^2 \end{pmatrix} O_{12}^T O_{13}^T P_\delta^\dagger O_{23}^T + \begin{pmatrix} a & & \\ & 0 & \\ & & 0 \end{pmatrix} \} \\
&= \frac{1}{2E} O_{23} P_\delta \{ O_{13} O_{12} \begin{pmatrix} 0 & & \\ & \delta m_{12}^2 & \\ & & \delta m_{13}^2 \end{pmatrix} O_{12}^T O_{13}^T + \begin{pmatrix} a & & \\ & 0 & \\ & & 0 \end{pmatrix} \} P_\delta^\dagger O_{23}^T .
\end{aligned} \tag{27}
$$

We find that the matrix which we diagonalize is real symmetric matrix. Therefore we can derive the energy eigen-state and eigen-value analytically.

In actual analysis, however, solving the eigen value equation analytically is still difficult and its solution looks complicated to understand the role of the matter effect in the neutrino oscillation experiment. The perturbation formula in term of δm_{12}^2 and a is very powerful to understand their contribution in the neutrino oscillation experiment, more directly. Now we consider the situation that Δ_{13} is order unity, and Δ_{12} and $\frac{aL}{2E}$. The schrödinger equation in the interaction representation can be expressed as

$$
i\frac{d}{dx} |\nu\rangle_{\rm I} = -H_{0,\rm S} |\nu\rangle_{\rm I} + ie^{H_{0,\rm S}x} \frac{d}{dt} |\nu\rangle_{\rm S}
$$

$$= e^{iH_{0,\mathrm{S}}t} H_{1,\mathrm{S}} e^{-iH_{0,\mathrm{S}}t} |\nu\rangle_{\mathrm{I}} , \tag{28}$$

Here the index S and I mean schrödinger representation and Interaction, respectively. We divided the Hamiltonian into two parts, in eq. (28), the leading term, H_0, and the next-leading term, H_1;

$$H = H_0 + H_1$$

$$H_0 = \frac{1}{2E} U \begin{pmatrix} 0 & 0 & 0 \\ 0 & 0 & 0 \\ 0 & 0 & \delta m^2_{13} \end{pmatrix} U^\dagger , \tag{29}$$

$$H_1 = \frac{1}{2E} U \begin{pmatrix} 0 & 0 & 0 \\ 0 & \delta m^2_{12} & 0 \\ 0 & 0 & 0 \end{pmatrix} U^\dagger + \begin{pmatrix} a & 0 & 0 \\ 0 & 0 & 0 \\ 0 & 0 & 0 \end{pmatrix} . \tag{30}$$

The solution of this schrödinger equation is

$$|\nu(L)\rangle_{\mathrm{I}} = |\nu(0)\rangle_{\mathrm{I}} - i \int_0^L dx e^{iH0,\mathrm{S}x} H_{1,\mathrm{S}} e^{-iH_{0,\mathrm{S}}x} |\nu(x)\rangle_{\mathrm{I}} . \tag{31}$$

The first order approximation in term of H_1 is obtained by substituting the left-hand side of eq. (31) to the second term of the right hand side.

$$|\nu(L)\rangle_{\mathrm{I}} = |\nu(0)\rangle_{\mathrm{I}} - i \int_0^L dx e^{iH^0_{\mathrm{S}}x} H_{1,\mathrm{S}} e^{-iH^0_{\mathrm{S}}x} |\psi(0)\rangle_{\mathrm{I}} + O(H_1) .$$

$$|\nu(L)\rangle_{\mathrm{S}} = e^{-iH_0 L} |\nu(0)\rangle_{\mathrm{S}} - i \int_0^L dx e^{iH^0_{\mathrm{S}}(x-L)} H_{1,\mathrm{S}} e^{-iH^0_{\mathrm{S}}x} |\nu(0)\rangle_{\mathrm{S}} + O(H_1) . \tag{32}$$

Then we can calculate the matrix element, $S_{\beta\alpha}$ as,

$$S_{\beta\alpha} = \langle \nu_\beta | e^{-i\int_0^L (H_0+H_1)dx} |\nu_\alpha\rangle \approx (S_0(L) + S_1(L))_{\beta\alpha} , \tag{33}$$

$$S_0(L)_{\beta\alpha} = \langle \nu_\beta | e^{-iH_0 L} |\nu_\alpha\rangle , \tag{34}$$

$$S_1(L)_{\beta\alpha} = -i \langle \nu_\beta | \left(\int_0^L dx e^{iH^0(x-L)} V(t') e^{-iH^0 x} \right) |\nu_\alpha\rangle . \tag{35}$$

The each of S_0 and S_1 term can be expressed in terms of $U_{\beta\alpha}, \Delta_{ij}, and a$ as,

$$S_0 = \delta_{\beta\alpha} + U_{\beta 3} U^*_{\alpha 3} \left(e^{-i\Delta_{13}} - 1 \right) , \tag{36}$$

$$\begin{aligned} S^{(1)}_1(L)_{\beta\alpha} &= -i \langle \nu_\beta | \left(\int_0^L dx e^{iH^0(x-L)} H^1(x) e^{-iH^0 x} \right) |\nu_\alpha\rangle \\ &= -iU_{\beta 2} U^*_{\alpha 2} \Delta_{12} + \left(U_{\beta 3} U^*_{e3} \delta_{\alpha e} + \delta_{\beta e} U_{e3} U^*_{\alpha 3} - 2U_{\beta 3} U^*_{\alpha 3} |U_{e3}|^2 \right) \left(e^{-i\Delta_{13}} - 1 \right) \frac{a}{\delta m^2_{13}} \\ &\quad -i \left[\delta_{\beta e}\delta_{\alpha e} - U_{\beta 3} U^*_{e3} \delta_{\alpha e} - \delta_{\beta e} U_{e3} U^*_{\alpha 3} + U_{\beta 3} U^*_{\alpha 3} |U_{e3}|^2 \left(e^{-i\Delta_{13}} + 1 \right) \right] \frac{aL}{2E} . \end{aligned} \tag{37}$$

We find in eq. (89) that there are two type of matter effect terms, $\frac{aL}{2E}$ and $\frac{a}{\delta m^2_{13}}$. The first type, $\frac{a}{\delta m^2_{13}}$, is proportional to neutrino energy, and depends on the sign of δm^2_{13}. Therefore the neutrino oscillation experiment which use the high energy neutrino beam have the capability of determining the neutrino mass hierarchy. The second type, $\frac{aL}{2E}$, does not depend on the neutrino energy but the baseline length, L, which ordinary comes from integration of the potential term, $\int \frac{a}{2E} dx$. This effect is negligibly small for the short baseline experiment, but significantly large for the very long long baseline experiment even when the neutrino energy is low. Finally, we obtain the approximation formula of the survival probability and the transition probability;

$$
\begin{aligned}
P_{\nu_e \to \nu_e} &= 1 - 4|U_{e3}|^2 \left(1 - |U_{e3}|^2\right) \sin^2\left(\frac{\Delta_{13}}{2}\right) \\
&\quad -4\frac{a}{\delta m^2_{13}} |U_{e3}|^2 \left(1 - 4|U_{e3}|^2 + 4|U_{e3}|^4\right) \sin^2\left(\frac{\Delta_{13}}{2}\right) \\
&\quad +2|U_{e3}|^2 \left[\left(1 + 2|U_{e3}|^4\right) \frac{aL}{2E} + |U_{e2}|^2 \Delta_{12}\right] \sin\Delta_{13}\,, \qquad \text{(38a)} \\
P_{\nu_e \to \nu_\alpha} &= 4|U_{e3}|^2 |U_{\alpha 3}|^2 \sin^2\left(\frac{\Delta_{13}}{2}\right) \\
&\quad +4|U_{e3}|^2 |U_{\alpha 3}|^2 \left[(1 - 2|U_{e3}|^2)\frac{2a}{\delta m^2_{13}} + \frac{J_{\rm MNS}}{|U_{e3}|^2 |U_{\alpha 3}|^2|} \Delta_{12}\right] \sin^2\left(\frac{\Delta_{13}}{2}\right) \\
&\quad +2|U_{e3}|^2 |U_{\alpha 3}|^2 \left[-(1 - 2|U_{e3}|^2)\frac{aL}{2E} + \frac{Re[U_{e2} U^*_{\alpha 3} U^*_{e3} U_{\alpha 3}]}{|U_{e3}|^2 |U_{\alpha 3}|^2|} \Delta_{12}\right] \sin\Delta_{13}\,, \qquad \text{(38b)} \\
P_{\nu_\alpha \to \nu_\alpha} &= 1 - 4|U_{\alpha 3}|^2 \left(1 - |U_{\alpha 3}|^2\right) \sin^2\left(\frac{\Delta_{13}}{2}\right) \\
&\quad +8|U_{\alpha 3}|^2 \left(1 - 2|U_{\alpha 3}|^2\right) |U_{e3}|^2 \frac{2a}{\delta m^2_{13}} \sin^2\left(\frac{\Delta_{13}}{2}\right) \\
&\quad + \quad 2|U_{\alpha 3}|^2 \left[\left(1 - 2|U_{\alpha 3}|^2\right) |U_{e3}|^2 \frac{aL}{2E} + |U_{\alpha 2}|^2 \Delta_{12}\right] \sin\Delta_{13}\,, \qquad \text{(38c)} \\
P_{\nu_\mu \to \nu_\tau} &= 4|U_{\mu 3}|^2 |U_{\tau 3}|^2 \sin^2\left(\frac{\Delta_{13}}{2}\right) \\
&\quad +4\left[-4|U_{e3}|^2 \frac{a}{\delta m^2_{13}} + \frac{J_{\rm MNS}}{|U_{\mu 3}|^2 |U_{\tau 3}|^2|} \Delta_{12}\right] \sin^2\left(\frac{\Delta_{13}}{2}\right)
\end{aligned}
$$

$$+\left[2|U_{e3}|^2\frac{aL}{2E}+\frac{Re[U_{\mu 2}U^*_{\tau 3}U^*_{\mu 3}U_{\tau 3}]}{|U_{\mu 3}|^2|U_{\tau 3}|^2|}\Delta_{12}\right]\sin^2\left(\frac{\Delta_{13}}{2}\right). \tag{38d}$$

Here we use the index α as non electron neutrino, ν_μ or ν_τ. $P_{\nu_\alpha\to\nu_e}$ and $P_{\nu_\tau\to\nu_\mu}$ can be obtained by changing the sign of the $J_{\rm MNS}$ term of eqs. (38b) and (38d), respectively. The first lines of each equation are the leading term, and the second and third line is correction from Δ_{12} and the matter effect. We find in eqs. (38a) and (38b) that the coefficients of the matter effect term are almost same as the leading term. When the $\frac{a}{\delta m^2_{13}}$ or $\frac{aL}{2E}$ is enough large, we should think of the contribution of the matter effect in the analysis for these modes. About the non ν_e mode, the matter effect terms are proportional to $|U_{e3}|^2$. Because CHOOZ experiment shows that $|U_{e3}|^2$ is very small, $|U_{e3}|^2 < 0.04$ for $|\delta m^2_{13}| = 2.5$ eV^2 [9], the correction of the matter effect for these oscillation modes is too small to detect. We can conclude from eq. (38) that we should perform the neutrino oscillation experiment for electron neutrino if we want to use the benefit of the matter effect.

4 Neutrino oscillation experiments

4.1 Atmospheric neutrino experiments and accelerator neutrino oscillation experiments

In this section, we review the various neutrino oscillation experiments, and our understanding about the neutrino oscillation parameters. First of all, we study the atmospheric neutrino oscillation experiments, and the accelerator neutrino oscillation experiments which measure the same parameter in the atmospheric neutrino oscillation experiment.

When the cosmic ray from the universe goes into the atmosphere, the cosmic ray interacts with the nucleons in the atmosphere, and then a lot of π's and K's are produced, so called secondary cosmic ray. These K's decay into μ and e and neutrinos. The summary of this decay process as follows;

$$\begin{aligned} p + N \to\ & \pi^+(K^+) + \ N' \\ & \downarrow \\ & \pi^+(K^+) \to \mu^+ + \nu_\mu \\ & \qquad \downarrow \\ & \qquad \mu^+ \to e^+ + \bar{\nu_\mu} + \nu_e \,. \end{aligned} \tag{39}$$

From eq. (39), we naively expect that the number of ν_μ and $\bar{\nu}_\mu$ is about twice that of ν_e and $\bar{\nu}_e$. The SK collaboration tried to measure the ratio of the muon neutrino and electron neutrino, $\nu_\mu + \bar{\nu}_\mu : \nu_e + \bar{\nu}_e$, and found that $\bar{\nu}_\mu : \nu_e + \bar{\nu}_e \sim 1.3 : 1$. Furthermore they measured the zenith angle dependence of the neutrino distribution. The zenith angle dependence can be interpreted as the traveling length dependence. The measured ν_e distribution is independent of the zenith angle, and they could not find the deficit of ν_e. For the ν_μ, they observe the reduction of the ν_μ and the distribution depends on the zenith angles [1]. This is the discovery of the neutrino oscillation.

Atmospheric neutrino experiments satisfied with the approximation condition for eq. (15), $\Delta_{13} \sim O(1) \gg \Delta_{12}$. Basically, the ν_μ survival probability is analyzed in the two flavor model. The present constraint of the atmospheric (ATM) oscillation parameter from the ATM neutrino oscillation experiments are [2],

$$\delta m^2_{\rm ATM} = |\delta m^2_{13}| = 2.1^{+1.3}_{-0.6} \times 10^{-3}{\rm eV}^2 \,, \tag{40a}$$

$$\sin^2 2\theta_{\rm ATM} = 4|U_{\mu 3}|^2 \left(1 - |U_{\mu 3}|^2\right) = 1.0_{-0.08} \,, \tag{40b}$$

at 90% CL. For the transition from ν_μ, most of all ν_μ become tau neutrino because the number of ν_e does not increase. SK collaboration reported that the τ neutrino appearance events is consistent of this picture at 2.4σ level [28].

The ATM parameters have been measured by the accelerator neutrino experiments, too. In the accelerator neutrino experiment, the large number of the charged π's are produced by accelerator at first. This high energy π mainly decays into μ and ν_μ. Finally, the survival rate of the produced ν_μ is measured at a far detector. The point of the accelerator long baseline experiment is that source of the neutrino can be controlled by human hand. The first accelerator neutrino experiments is KEK-to-Kamioka (K2K) experiment[3]. K2K had been running from 1999 to 2004. In K2K, the neutrinos were produced by KEKPS and shot at SK, which is 250 km away from KEK. The ATM parameter constraints from K2K experiments are

$$\delta m^2_{13} = 2.8^{+0.7}_{-0.9} \times 10^{-3}\mathrm{eV}^2\,, \tag{41}$$

$$\sin^2 2\theta_{\mathrm{ATM}} = 1.0_{-0.6}\,, \tag{42}$$

at 90% CL. The Main Injector Neutrino Oscillation Search (MINOS) experiment is the second accelerator neutrino oscillation experiment, which have been running since 2005[4]. The neutrino beam for the MINOS experiment is produced at the Fermi Laboratory, and the target far detector is placed in the Soudan iron mine in Minnesota. Baseline length is 735 km and the detector is a 5.4 kt iron detector, which can distinguish not only the flavor but also neutrino from the anti-neutrino. Present result of MINOS gives the more tight limit to the ATM parameter than that of K2K;

$$\delta m^2_{13} = 2.74^{+0.69}_{-0.33} \times 10^{-3}\mathrm{eV}^2\,, \tag{43}$$

$$\sin^2 2\theta_{\mathrm{ATM}} = 1.0_{-0.22}\,. \tag{44}$$

About the flavor transition, $\nu_\mu \to \nu_e$ oscillation have not been observed in both K2K and MINOS. The transition probability is roughly proportional to $|U_{e3}|^2$; see eq.(15b). Therefore the smallness of the transition probability can be interpreted as the smallness of $|U_{e3}|^2$. We will discuss about it in section 4.3.

4.2 Solar neutrino oscillation experiment

The soler neutrino problem was a difficult problem. First observation of the solar neutrino was performed in 1967 [5]. In this experiment, ν_e which comes from solar is captured by the ^{37}Cl,

$$\nu_e + {}^{37}Cl \to e^- + {}^{37}Ar\,. \tag{45}$$

However the number of observed neutrino were smaller than the expected number which is estimated from the standard solar model. After the Homestake experiment, the other solar neutrino experiments also reported the solar neutrino deficit.

After discovering the neutrino oscillation, the solar neutrino deficit is understand in the neutrino oscillation phenomena. The Sudbury Neutrino Oscillation (SNO) experiment confirmed that the origin of the solar neutrino is the neutrino oscillation [6]. In the SNO experiment, they checked both the charged current interaction, $\nu_e + d \to e^- + p + p$, and the neutral current interaction, $\nu + e^- \to \nu + e^-$. If the number of the neutral current event is same as the expected one but the charged current event is smaller than the expected one, then the ν_e is expected to transit the other neutrino flavor, ν_μ or ν_τ. The SNO experiment reported that they did not find the any deficit for the neutral current interaction, but the number of the ν_e is smaller than that of null oscillation as well as the other experiments.

Because the approximation condition for eq. (16) is satisfied in the solar neutrino experiment, the solar neutrino oscillation is also analyzed in the two flavor model.

$$P_{\nu_e \to \nu_e} = 1 - 4\sin^2\theta_{\rm SOL}\sin^2\left(\frac{\Delta_{12}}{2}\right), \tag{46}$$

$$\delta m^2_{\rm SOL} = \delta m^2_{12}, \tag{47}$$

$$\sin^2 2\theta_{\rm SOL} = 4|U_{e1}U_{e2}|^2. \tag{48}$$

$$(|U_{e1}|^2 = \sin^2\theta_{\rm SOL}, |U_{e2}|^2 = \cos^2\theta_{\rm SOL})$$

Here we ignore the small factor $|U_{e3}|^2$, which is less than 5% as we study in the next subsection. Furthermore, the neutrinos travels inside the sun, and then we should consider the matter effect inside the solar, MSW effect [26]. Though we can solve the degeneracy between $|U_{e1}|$ and $|U_{e2}|$ by using the matter effect, the several allowed regions in the $\delta m^2_{\rm SOL}$ - $\sin^2\theta_{\rm SOL}$ plane still remain.

Kamioka Liquid scintillator Anti-Neutrino Detector (KamLAND) experiment [7] was planed to eliminate the fake allowed regions. In KamLAND, the 1kt liquid scintillator is placed in Kamioka mine to observe the $\bar{\nu}_e$ from reactor power plants in Japan. Finally, the KamLAND experiment kill the fake allowed region. Present constraints on the SOL parameters from the solar neutrino oscillation experiments, and the KamLAND experiment are [8],

$$\delta m^2_{12} = (8.0 \pm 0.3) \times 10^{-5}{\rm eV}^2, \tag{49a}$$

$$\sin^2\theta_{\rm SOL} = 0.30 \pm 0.03 \tag{49b}$$

$$(\tan^2\theta_{\rm SOL} = 0.40).$$

4.3 Measurement of $|U_{e3}|$

We already studied that $|U_{e3}|$ is too small to observe the ν_μ to ν_e oscillation in the atmospheric neutrino oscillation experiments in section 4.1. The smallness of $|U_{e3}|$ was

	beginning of the running	planed sensitivity to $\sin^2 2\theta_{\rm RCT}$
Double-CHOOZ	2009	~ 0.03
Daya bay	2010	~ 0.01
RENO	2010	~ 0.02

Table 1: Planned reactor experiments and their sensitivity to $\sin^2 2\theta_{\rm RCT}$.

also checked by the CHOOZ [9] experiment and Palo Verde [10] experiments. These are the first generation reactor neutrino experiments. The neutrino energy from the power plant is about 3 MeV, and the baseline length is 1 km. From eqs. (44) and (49), we easily understand that the $\Delta_{13} \sim O(1)$ and $\Delta_{12} \ll 1$, and hence we can analyze the reactor experiments in the two flavor model like,

$$P_{\nu_e \to \nu_e} \approx 1 - 4\sin^2 2\theta_{\rm RCT} \sin^2 \frac{\Delta_{13}}{2}\,, \tag{50}$$

$$\sin^2 \theta_{\rm RCT} = |U_{e3}|\,. \tag{51}$$

However the CHOOZ experiment could not find any deficit of $\bar{\nu}_e$. The CHOOZ reactor experiment gives the most strong constraint on the value of $\sin^2 2\theta_{\rm RCT}$;

$$\begin{aligned} &\sin^2 2\theta_{\rm RCT} < 0.20 \quad \text{for} \quad |\delta m^2_{13}| = 2.0 \times 10^{-3}\text{eV}^2\,, \\ &\sin^2 2\theta_{\rm RCT} < 0.16 \quad \text{for} \quad |\delta m^2_{13}| = 2.5 \times 10^{-3}\text{eV}^2\,, \\ &\sin^2 2\theta_{\rm RCT} < 0.14 \quad \text{for} \quad |\delta m^2_{13}| = 3.0 \times 10^{-3}\text{eV}^2\,, \end{aligned} \tag{52}$$

at 90% CL.

The $\theta_{\rm RCT}$ is the last unmeasured mixing angle in the lepton-sector, therefore the measuring it is the prior task in the future neutrino oscillation experiment. We can classify the future neutrino experiment which measure $\theta_{\rm RCT}$ as reactor neutrino experiments with multi reactor [13, 14, 15] and the accelerator experiments with high intensity neutrino beam [11, 12]. The CHOOZ reactor experiments suffered from the not only the statistic error but also the systematic error, such as the error of the neutrino flux and the uncertainty of the cross sections. In the future reactor experiments, the multi neutrino detectors will be used in order to reduce the systematic error by using the event ratio among the each detectors. As of December 2007, the planed reactor experiment which will start till 2010 is Double-CHOOZ in French, Daya bay in China, and RENO in Korea. [13, 14, 15] as summarized in Table. 1. If $\sin^2 2\theta_{\rm RCT}$ is larger than 0.03, the all experiments detect the $\bar{\nu}_e$ deficits near the future.

Regarding as next generation accelerator neutrino experiments, their task is detecting the $\nu_\mu \to \nu_e$ oscillation, which is roughly proportional to $\sin^2 \theta_{\rm RCT}$. For detecting such small transition probability, the beam intensity should be more strong than K2K and

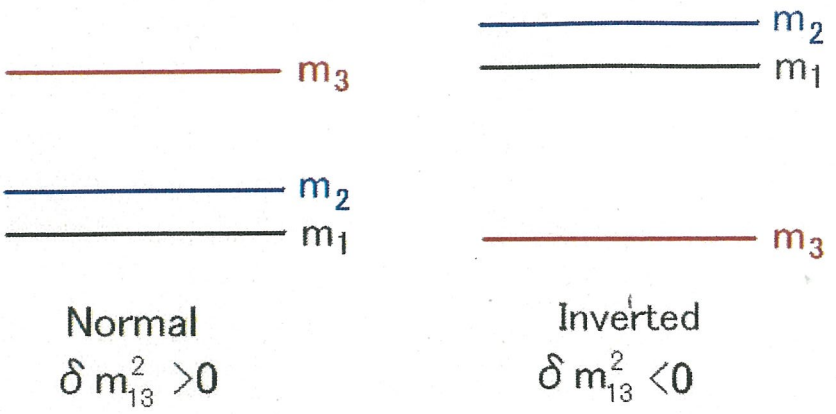

Figure 2: The picture of the neutrino mass hierarchy pattern. The left side is the case for δm^2_{13} is positive, so called the normal hierarchy. The right side is the case for δm^2_{13} is negative, the inverted hierarchy.

MINOS. Now there are two proposals which will run near the future, the T2K experiment, and the NOνA experiment [11, 12]. We will study the detail of T2K experiment in the next section.

4.4 How to constrain the sign of δm^2_{13} and δ ?

At the end of this section, we consider how to measure the least parameters, the sign of the δm^2_{13} and the CP phase, δ . This discussion is useful to find the physics potential of the T2KK experiment.

For the sign of the mass squared difference, δm^2_{13}, we shows the picture of the neutrino mass hierarchy pattern in Fig. 2. In Fig. 2 The left side is the case for δm^2_{13} is positive, which is called the normal hierarchy. The right side is the case for δm^2_{13} is negative, which is called the inverted hierarchy. As long as, we determine the sign of mass hierarchy pattern, we can not determine the which picture of the mass hierarchy in lepton sector is true.

In section 3, we learn that the matter effect is powerful tool to determine the mass hierarchy pattern. Since the atmospheric neutrinos which comes from the opposite of the earth go though the high density region, core of the earth, we naively wonder whether we can determine the sign of δm^2_{13} in the atmospheric experiment by using the matter effect ? But the answer is no. Let us check how large contribution of the matter effect

to ν_μ survival mode are, around the first oscillation maximum region, $\Delta_{13} \sim \pi$.

$$P_{\nu_\mu \to \nu_\mu} = 1 - 4\sin^2\theta_{\rm ATM}(1+A^\mu)\sin^2\left(\frac{\Delta_{13}}{2} + B^\mu\right) . \tag{53}$$

Here A^μ and B^μ is the first order corrections from the Δ_{12} and the matter effect, a to the oscillation amplitude and the oscillation phase, respectively. These term can be calculated from eq. (38c)

$$\begin{aligned} A^\mu &= -\frac{2a}{\Delta m^2_{13}} \frac{1-2\sin^2\theta_{\rm ATM}}{\cos^2\theta_{\rm ATM}} \sin^2\theta_{\rm RCT} \\ &\sim -0.005\left(1-2\sin^2\theta_{\rm ATM}\right)\frac{\pi}{\Delta_{13}}\frac{L}{295{\rm km}}\left(\frac{\sin^2 2\theta_{\rm RCT}}{0.10}\right) , \end{aligned} \tag{54a}$$

$$\begin{aligned} B^\mu &= \frac{aL}{4E}\frac{1-2\sin^2\theta_{\rm ATM}}{\cos^2\theta_{\rm ATM}}\sin^2\theta_{\rm RCT} \\ &-\frac{\Delta_{12}}{2}\left(\cos^2\theta_{\rm SOL} + \tan^2\theta_{\rm ATM}\sin^2\theta_{\rm SOL}\sin^2\theta_{\rm RCT} - \tan\theta_{\rm ATM}\sin 2\theta_{\rm SOL}\sin\theta_{\rm RCT}\cos\delta\right) \\ &\sim -\left[0.037 - 0.008\left(\frac{\sin^2 2\theta_{\rm RCT}}{0.10}\right)^{1/2}\cos\delta\right]\frac{|\Delta_{13}|}{\pi} . \end{aligned} \tag{54b}$$

From the first lines to second line in eqs. (54a) and (54b), we substitute the following number as the meaning value of the neutrino oscillation parameters;

$$\left.\begin{array}{l} |\delta m^2_{13}|^{\rm input} = 2.5\times 10^{-3}\ {\rm eV}^2 , \\ (\delta m^2_{12})^{\rm input} = 8.2\times 10^{-5}\ {\rm eV}^2 , \\ \sin^2\theta^{\rm input}_{\rm ATM} = 0.5 , \\ \sin^2 2\theta^{\rm input}_{\rm SOL} = 0.83 , \\ \rho^{\rm input} = 3.0{\rm g/cm}^2 . \end{array}\right\} \tag{55}$$

We find in eq. (54) that the matter effect term, a, is not only suppressed by the small value of $\sin^2 2\theta_{\rm RCT}$ but also $\left(1-2\sin^2\theta_{\rm ATM}\right)$, which is almost zero as long as $\sin^2 2\theta_{\rm ATM} \sim 1$. In other words, we can measure $\sin^2 2\theta_{\rm ATM}$ precisely. For the oscillation phase eq. (54b), the relative sign between Δ_{13} and B^e is sensitive to the mass hierarchy pattern, therefore terms proportional to Δ_{12} of B^e are sensitive the mass hierarchy pattern. However its effect can be renormalized to the measurement of $|\delta m^2_{13}|$ directly. Additionally, this effect is only 2%, so it is very difficult to detect it.

The next candidate to constrain the hierarchy pattern is the oscillation which is related to ν_e. As we studied in section 3, the oscillation mode which is affected by

the matter effect significantly is the ν_e survival mode or ν_e transition mode. Especially, solving the sign degeneracy of the δm^2_{13} by $\nu_\mu \to \nu_e$ transition mode is a realistic solution. The transition probability of the $\nu_\mu \to \nu_e$ mode can be expressed as

$$P_{\nu_\mu \to \nu_e} = 4\sin^2\theta_{\rm ATM}\sin^2\theta_{\rm RCT}\left\{(1+A^e)\sin^2\left(\frac{\Delta_{13}}{2}\right) + B^e\sin\Delta_{13}\right\} + C^e, \tag{56}$$

where A^e, B^e, and C^e are the correction terms as well as A^μ and B^μ in eq. (53). Because the leading term is order $\sin^2\theta_{\rm RCT}$, not only the linear terms of Δ_{12} and a but also the quadratic terms of them are required for the good approximation. We show the second order corrections to the S matrix in the Appendix. From the appendix, we can estimate the A^e, B^e, and C^e respectively;

$$\begin{aligned} A^e = {} & \frac{aL}{\Delta_{13}E}\cos 2\theta_{\rm RCT} - \frac{\Delta_{12}}{2}\frac{\sin 2\theta_{\rm SOL}}{\tan\theta_{\rm ATM}\sin\theta_{\rm RCT}}\sin\delta\left(1+\frac{aL}{2\Delta_{13}E}\right) \\ & + \frac{\Delta_{12}}{4}\left(\Delta_{12}+\frac{aL}{2E}\right)\left(\frac{\sin 2\theta_{\rm SOL}}{\tan\theta_{\rm ATM}\sin\theta_{\rm RCT}}\cos\delta - 2\sin^2\theta_{\rm SOL}\right) \\ & - \frac{1}{2}\left(\frac{aL}{2E}\right)^2 + \frac{3}{4}\left(\frac{aL}{\Delta_{13}E}\right)^2 \end{aligned} \tag{57a}$$

$$\begin{aligned} \sim {} & 0.11\frac{\pi}{\Delta_{13}}\frac{L}{295{\rm km}}\left(1-\frac{\sin^2 2\theta_{\rm RCT}}{2}\right) - 0.014\left(\frac{L}{295{\rm km}}\right)^2 + 0.0087\left(\frac{\pi}{\Delta_{13}}\frac{L}{295{\rm km}}\right)^2 \\ & - 0.29\left(\frac{0.10}{\sin^2 2\theta_{\rm RCT}}\right)^{1/2}\sin\delta\left(\frac{|\Delta_{13}|}{\pi} \pm 0.054\frac{L}{295{\rm km}}\right) \\ & + 0.015\left[\left(\frac{0.10}{\sin^2 2\theta_{\rm RCT}}\right)^{1/2}\cos\delta - 0.11\right]\left(\frac{|\Delta_{13}|}{\pi} + 1.7\frac{L}{295{\rm km}}\right)\frac{|\Delta_{13}|}{\pi}, \end{aligned} \tag{57b}$$

$$\begin{aligned} B^e = {} & -\frac{aL}{4E}\cos 2\theta_{\rm RCT} + \frac{\Delta_{12}}{4}\left(\frac{\sin 2\theta_{\rm SOL}}{\tan\theta_{\rm ATM}\sin\theta_{\rm RCT}}\cos\delta - 2\sin^2\theta_{\rm SOL}\right)\left(1+\frac{aL}{2\Delta_{13}E}\right) \\ & + \frac{\Delta_{12}}{8}\left(\Delta_{12}+\frac{aL}{2E}\right)\frac{\sin 2\theta_{\rm SOL}}{\tan\theta_{\rm ATM}\sin\theta_{\rm RCT}}\sin\delta - \frac{1}{\Delta_{13}}\left(\frac{aL}{2E}\right)^2 \end{aligned} \tag{57c}$$

$$\begin{aligned} \sim {} & -0.080\left(\frac{L}{295{\rm km}}\right)\left(1-\frac{\sin^2 2\theta_{\rm RCT}}{2}\right) - 0.0091\frac{\pi}{\Delta_{13}}\left(\frac{L}{295{\rm km}}\right)^2 \\ & + 0.15\left[\left(\frac{0.10}{\sin^2 2\theta_{\rm RCT}}\right)^{1/2}\cos\delta - 0.11\right]\left(\frac{|\Delta_{13}|}{\pi} \pm 0.054\frac{L}{295{\rm km}}\right) \\ & + 0.0072\left(\frac{0.10}{\sin^2 2\theta_{\rm RCT}}\right)^{1/2}\sin\delta\left(\frac{|\Delta_{13}|}{\pi} + 1.7\frac{L}{295{\rm km}}\right)\frac{|\Delta_{13}|}{\pi}, \end{aligned} \tag{57d}$$

$$C^e = \frac{\Delta_{12}^2}{4}\sin^2 2\theta_{\rm SOL}\cos^2\theta_{\rm ATM} - \frac{\Delta_{12}}{2}\frac{aL}{2E}\sin 2\theta_{\rm SOL}\sin 2\theta_{\rm ATM}\sin\theta_{\rm RCT}\cos\delta \tag{57e}$$

$$+\left(\frac{aL}{2E}\right)^2\sin^2\theta_{\rm RCT}\sin^2\theta_{\rm ATM}$$

$$\sim 0.0011\left(\frac{\Delta_{13}}{\pi}\right)^2 - 0.0013\frac{|\Delta_{13}|}{\pi}\frac{L}{295{\rm km}}\left(\frac{\sin^2 2\theta_{\rm RCT}}{0.10}\right)^{1/2}\cos\delta$$

$$+0.00036\left(\frac{L}{295{\rm km}}\right)^2\frac{\sin^2 2\theta_{\rm RCT}}{0.10}. \tag{57f}$$

Here $\pm$ in the first lines of eqs. (57b) and (57d) follows the sign of Δ_{13}. The first and second terms in eqs. (57a) and (57c) are linear, and the other terms including eq. (57e) are quadratic in Δ_{12} and a corrections. The quadratic terms can dominate the probability when $\sin^2 2\theta_{\rm RCT}$, and hence the leading term, is very small. The transition probability estimated from this approximation formula is great agreement that the one from the exact formula with 95% accuracy, when $\sin^2 2\theta_{\rm RCT} < 0.15$.

We find that the linear terms which are sensitive to the mass hierarchy pattern in eqs. (56) and (57) are the first term in eq. (57a), and the first term in eq. (57c). The first term of A^e in eq. (57b) gives about 10% to the leading term around the first oscillation maximum when $L = 1000$ km. Notice that this effect is observed as the effective amplitude, $\sin^2\theta_{\rm RCT}^{\rm effective} = \sin^2\theta_{\rm RCT}(1+A^e)$, as well as the case of B^μ. Therefore we need the comparison with the other neutrino oscillation experiment to observe the the matter effect term. For example, when there are a short baseline experiment and along baseline experiment, then the magnitudes of the first term in each experiment are different. The short baseline experiment measures almost bare $\sin^2\theta_{\rm RCT}$, and $\sin^2\theta_{\rm RCT}^{\rm effective}$ measured in the long baseline experiment is received the large correction from the matter effect. And hence if we check which amplitudes is larger, we can determine the neutrino mass hierarchy pattern. The important point is that, as long as we compare the first oscillation maximum at each detector, the second term in eq. (57a) does not disturb the comparison with the mass hierarchy determination, because the magnitude of this term is same as long as Δ_{13} is fixed.

As of the B^e, the sensitivity to the mass hierarchy comes from the $\sin\Delta_{13}$ in eq. (56). The problem is the second term in eq. (57c) is also sensitive to the mass hierarchy pattern for the same reason but there are another unconstrained sign, the sign of $\cos\delta$. When $\cos\delta$ dominates B^e, the fake hierarchy can reproduce the same B^e by taking the $\delta^{\rm fake} = \pi - \delta$. In order to conquer this difficulty, the baseline experiment of which baseline is very long is favored to make $\frac{aL}{2E}$ larger than the $\cos\delta$ term. Please notice that if we use the low energy neutrino, Δ_{12} becomes very large and hence the term of $\cos\delta$ is always

larger than the matter effect term. It is remarkable that the the matter effect in B^e dilutes (enhances) the the contribution of A^e when the $\sin\Delta_{13}$ is positive, (negative), $\Delta_{13} \sim \frac{\pi}{2}(\frac{3\pi}{2})$. In other words, the favored Δ_{13} region for determining the sign of Δ_{13} is between π and 2π.

The setting for the mass hierarchy is also very useful for the measurement of δ. The contribution of $\sin\delta$ is observed through the amplitude, the second term of eq. (57a). The correction from the $\sin\delta$ is about 30 % for $\sin^2 2\theta_{\rm RCT} = 0.10$ at $L = 295$ km, see eq. (57b). Since the contribution of $\sin\delta$ is included in A^e, the technique for separate A^e from $\sin^2\theta_{\rm RCT}$ is necessary. A popular technique is using both neutrino and anti-neutrino. The interesting point that the comparison with high energy neutrino experiment and the low energy experiment also solves the correlation ambiguity between $\sin^2\theta_{\rm RCT}$ and $\sin\delta$ due the different matter effect. This is a same technique for the mass hierarchy. We also need to measurement of $\cos\delta$ for distinguish $\sin\delta$ from the $\sin(\pi-\delta)$. From the above discussion, though we can observe this contribution around the $\Delta_{13} \sim \frac{\pi}{2}$, we are not possible to determine the sign of $\cos\delta$ as long as the mass hierarchy pattern is not constrained. As a result, the neutrino oscillation experiment for the mass hierarchy allows us the measurement of δ without invoking anti-neutrino beam.

We find from Fig. 14 that the 1.0° OAB in Korea still keeps the sensitivity to the neutrino mass hierarchy, where both a combination of 1.0° at $L = 1000$ km and 2.5° OAB at SK (Fig. 14 (a)) and that of 1.0° at $L = 1000$ km ~ 1150 km and the 3.0° OAB at SK (Fig. 14 (b)) distinguish the neutrino mass hierarchy nearly at 4-σ level in our simulation. This is because the CCQE cross section times the flux of 1.0° OAB extends to $\sim$ 1.7 GeV, see Fig. 4 (a) and (c), which barely overlaps with the broad peak region of the $\nu_\mu \to \nu_e$ oscillation probability shown in Fig. 4(d). From Fig. 5 (a) and (b), we find that the 1.0° OAB is observable only in the east coast of Korea ($L \sim 1000$ km) for the 2.5° OAB at SK, whereas for the 3.0° OAB at SK, it can be observed at various base-line lengths up to ~ 1150 km.

5 Tokai-to-Kamioka-and-Korea experiment

5.1 Tokai-to-Kamioka experiment

In this section, we eventually study the main theme of this thesis, the Tokai-to-Kamioka-and-Korea experiment. The idea of the T2KK experiment is based on making use of the lower side of T2K neutrino beam, which accidentally appears in Korea. At first, we review the setting of Tokai-to-Kamioka (T2K) experiment to learn the T2K neutrino beam in this sub section.

Tokai-to-Kamioka neutrino oscillation experiment is a next generation neutrino oscillation experiment, which will start in 2009 [11]. The machine which produce the neutrino beam for the T2K experiment is 50 GeV Proton accelerator which has been constructed in the J-PARC [16]. The expected Proton On Target (POT) in T2KK is 5×10^{21} for 5 years running, which is about 100 times as much as that of the K2K experiment. The far detector in T2K is the Super-Kamiokande (SK). The SK is a water Čerenkov detector, which can separate the ν_e appearance event from ν_μ appearance event by using Charged Current Quasi Elastic (CCQE) events. The fiducial volume of SK is 22.5 kt and the distance from the J-PARC is 295 km.

A purposes of the T2K experiment are the precise measurement of the ATM parameter. The expected errors of them are $\delta(|\delta m^2_{13}|) = 10^{-4}\mathrm{eV}^2$ and $\delta(\sin^2 2\theta_{\mathrm{ATM}}) = 0.01$. The more important task of the T2K experiment is observing the ν_e appearance events. The planed sensitivity for the $\sin^2\theta_{\mathrm{RCT}}$ is $\sin^2\theta_{\mathrm{RCT}} \sim 0.01$. In order to observe the signal of $\nu_\mu \to \nu_e$ clearly, the neutrino beam should satisfy the following conditions.

1. The neutrino energy near the oscillation maximum ($|\Delta_{13}| \sim \pi$) at $L = 295$km is expected to be around 0.5 GeV to 0.7 GeV according to the present experimental bound, eq. (40a). The ν_μ flux should hence be large in this energy region.

2. High energy neutrinos produce π^0's via neutral current, which become background to the ν_e Charged Current Quasi-Elastic (CCQE) events. Therefore, the flux of ν_μ beam should be small at high energies.

One of the neutrino beam which satisfies the above conditions is the off-axis beam. At the J-PARC, a lot of π's and K's are produced by the accelerator and then collected by the magnetic hones. Collected charged π will travel along the decay pipe, and finally decays into the μ and ν. In that time, the relation between the energy of pion, E_π, and that of the neutrino, E_ν, can be expressed as the mass of the π, m_π, and μ, m_μ, and the off-axis angle *theta*;

$$E_\nu = \frac{m_\pi^2 - m_\mu^2}{2(E_\pi - \sqrt{E_\pi^2 - m_\pi^2}\cos\theta)}. \tag{58}$$

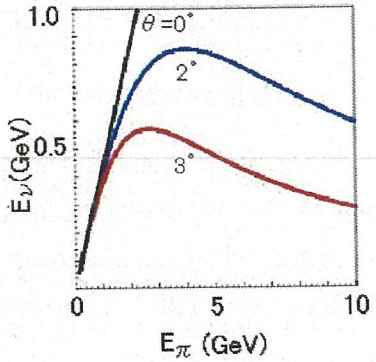

Figure 3: The correlation between E_π and E_ν. The degree close the line shows the off-axis angle.

We show the relation between E_π and E_ν as the function of θ in Fig. 3 In Fig. 3, we find that the neutrino traveling on axis is high energy if the source is high energy π. On the other hand, off-axis neutrino has the limit on the own energy and their neutrino energy tends to be from 0.6 GeV to 0.8 GeV for the 2° and from 0.3 GeV to 0.6 GeV for 3°. By using this kinematics, we can easily cut the high energy neutrino, and obtain the strong flux around the oscillation maximum.

Actually, the center of T2K neutrino beam is planed to aim the slightly off the SK. We show the flux of the T2K off-axis ν_μ beam [29] in Fig. 4 (a), for 10^{21} POT/yr at $L =$ 295 km for various off-axis angles between 0° and 3°. It is clearly seen that the flux peaks at 0.55 to 0.75 GeV at 2° to 3° off-axis angles. In Fig. 4(b) we show the cross section per nucleon of the ν_e and ν_μ CCQE events off the water target [3], and in Fig. 4(c), we show the product of the ν_e CCQE cross section and the ν_μ flux at 295 km for various off-axis angles. Fig. 4(b) shows that the CCQE cross sections grow quickly above the threshold, become $\sim 3.5 \times 10^{-39}$ cm^2 at $E_\nu \sim 0.6$ GeV, and stay approximately constant at $\sim 4.5 \times 10^{-39}$ cm^2 at $E_\nu \gtrsim 0.8$ GeV up to ~ 5 GeV where the flux diminishes. We also show the typical $\nu_\mu \to \nu_e$ transition probability at $L = 295$ km and that at $L = 1000$ km in Fig. 4(d), calculated in the oscillation parameter summarized in eq. (55) and $\sin^2 2\theta_{\rm RCT} = 0.10$, $\delta = 0°$, and $\rho = 2.8$g/cm^3 for $L = 295$ km, and $\rho = 3.0$g/cm^3 for $L = 1000$ km. From Fig. 4 (a), (c), and (d), we find that the 2.0° to 3.0° off-axis beam (OAB) has a strong flux peak where the oscillation maximum is expected at SK and no high energy tails. Actually, 2.0° to 3.0° OAB are planed to use in the T2K experiment.

5.2 Off-axis beam in Korea

We learn that the off-axis beam is useful for the T2K experiment. The interesting point is that not only the upper-side neutrino beam and the other side of the neutrino

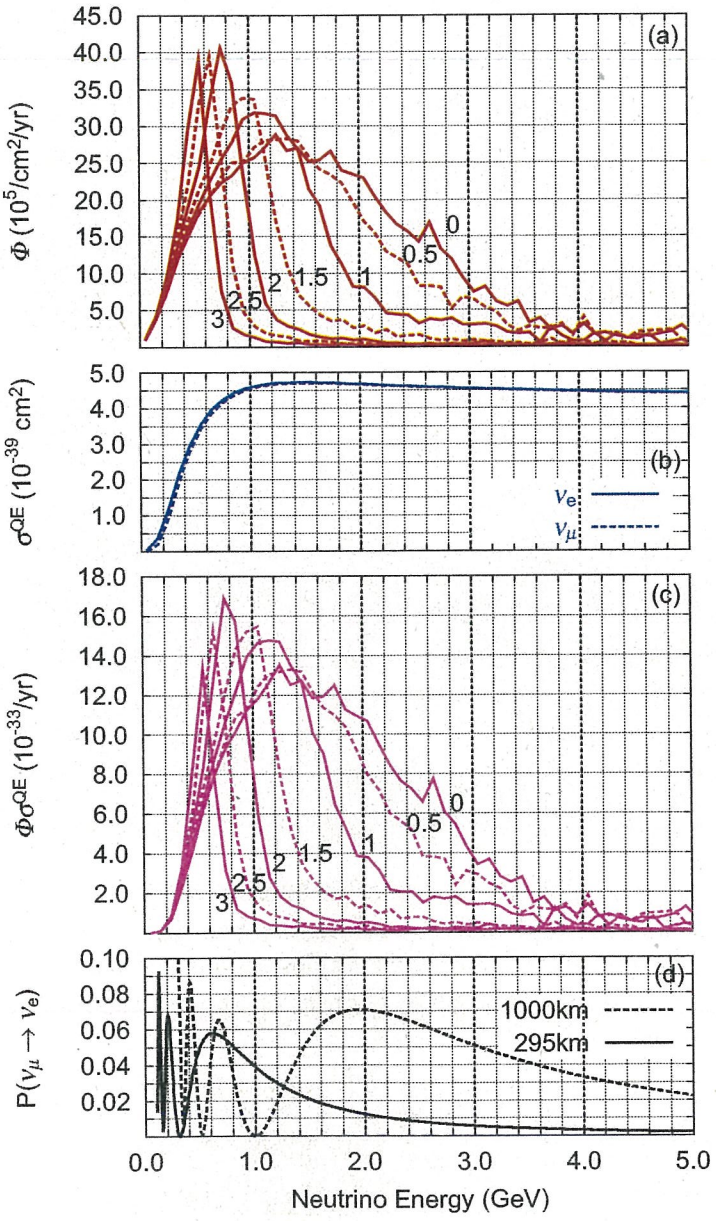

Figure 4: (a). The flux of the T2K ν_μ beam for 10^{21} POT/yr at $L = 295$ km for various off-axis angles between $0°$ and $3°$. (b). The cross section per nucleon of the Charged Current Quasi Elastic (CCQE) events for ν_e and ν_μ off the water target. (c). The flux at 295 km times ν_e CCQE cross section. (d). Probability of $\nu_\mu \rightarrow \nu_e$ transition at 295 km (solid line) and that at 1000 km (dashed line) calculated for $m_3^2 - m_1^2 = 2.5 \times 10^{-3}\text{eV}^2$, $m_2^2 - m_1^2 = 8.2 \times 10^{-5}\text{eV}^2$, $\sin^2 2\theta_{\text{ATM}} = 1.0$, $\sin^2 2\theta_{\text{SOL}} = 0.83$, $\sin^2 2\theta_{\text{RCT}} = 0.10$, $\delta = 0°$, and $\rho = 2.8\text{g/cm}^3$ for $L = 295$ km, and $\rho = 3.0\text{g/cm}^3$ for $L = 1000$ km.

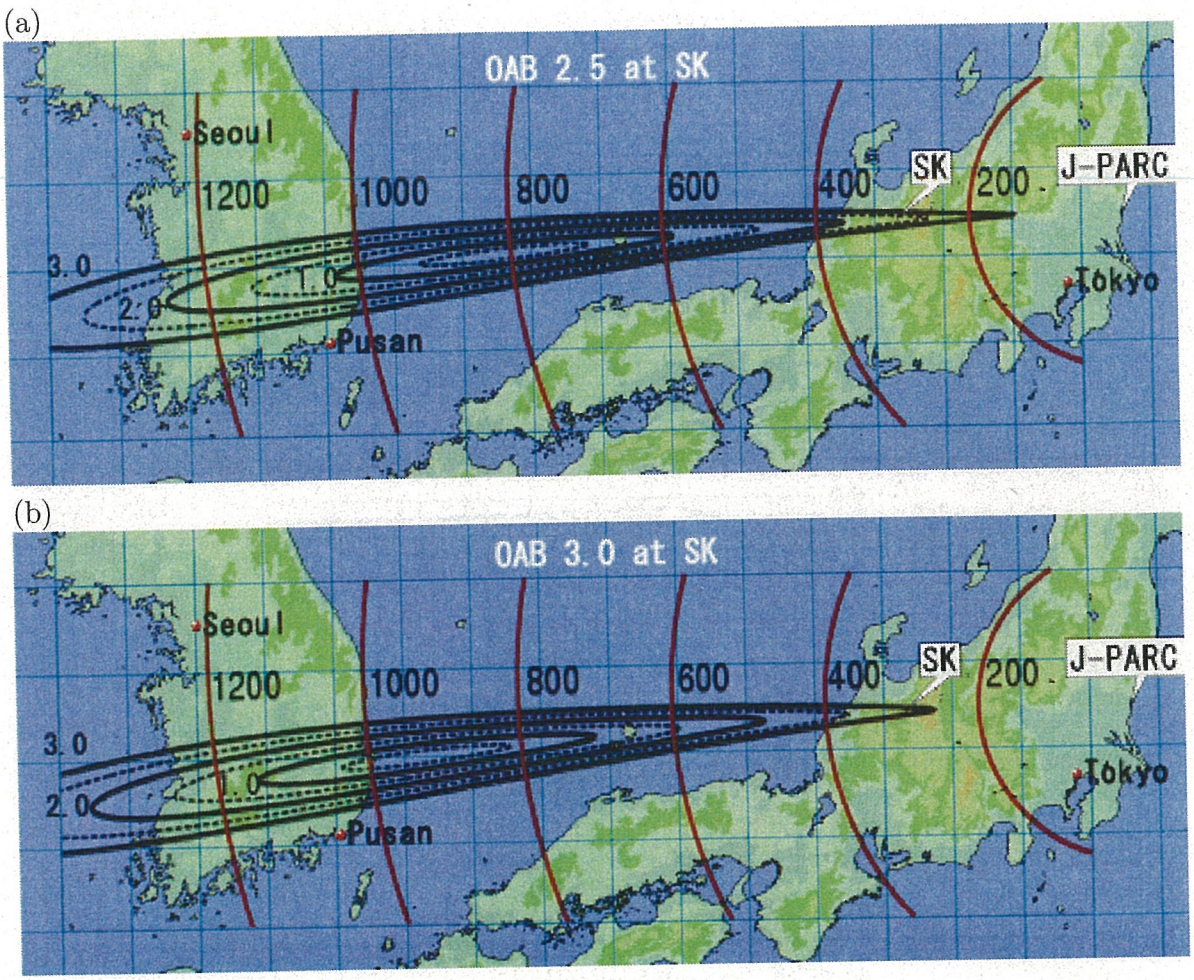

Figure 5: The off-axis angle of the neutrino beam from J-PARC on the sea level, when the beam center is 2.5° (a) and 3.0° (b) off at the SK site. The baseline lengths are shown by vertical contours, and the off-axis angles at the sea level are shown by elliptic contours between 0.5° and 3.0°. The SK is slightly off the corresponding contour because it is about 320 m above sea level.

beam will appear in various places during the T2K experimental period. We shows the off-axis angle in Japan, Japan sea (East sea), and Korea in Fig. 5 We show in Fig. 5 the off-axis angle of the ν_μ beam at the sea level for the 2.5° off-axis beam (a) and 3.0° off-axis beam (b) at SK. The baseline lengths are shown by vertical contours, and the off-axis angles at the sea level are shown by elliptic contours between 0.5° and 3.0°. The SK is slightly off the corresponding contour because it is about 320 m above sea level. In Fig. 5, the center of the neutrino beam appears the middle (the west side) of the Japan sea (East) sea. So at least we can not use the center of the T2K neutrino beam.

The interesting region in Fig. 5 is Korea. It seems that we have so many freedom of the combination of the off-axis angles in Korea. It means that there are many possibility of the neutrino oscillation experiment by using T2K off-axis beam appearing in Korea.

(a) 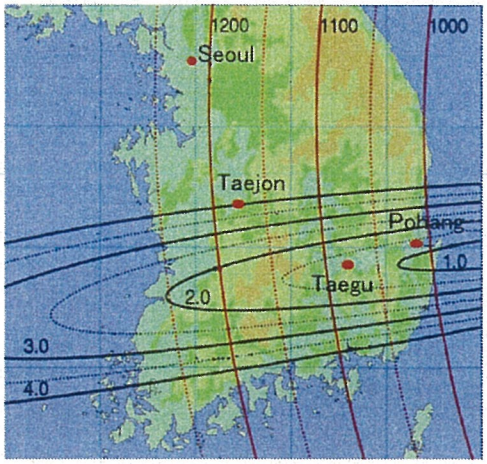

(b) 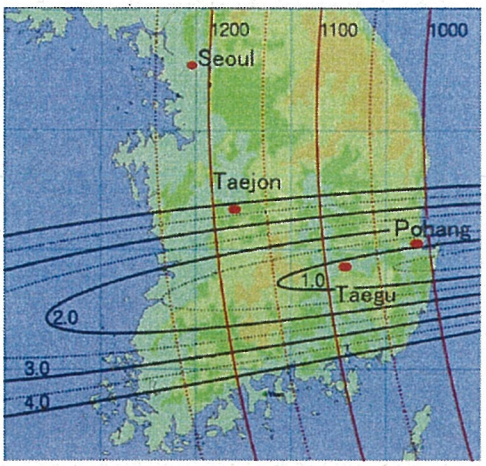

Figure 6: The same figure as Fig. 5 but focus on the South Korea. The left side is for OAB 2.5° at SK and the right side is for OAB 3° at SK

We shows the more detail of the appearing off-axis angle in Korea in Fig. 6. Fig. 6 shows that the beam close the center $\sim 0.5°$ cannot reach the east coast of Korea when 2.5° off-axis beam reach SK. Similarly, the smaller off-axis beam cannot reach the west side of Korea. If we want longer baseline experiment, we must give up the small off-axis beam.

We again check the correlation between the neutrino energy and the off-axis angle. Fig. 4 shows that the 0.5° and 1.0° off-axis beam covers the oscillation maximum region of the $\nu_\mu \to \nu_e$ oscillation. Using the small off-axis beam means that we can perform the experiments which observe the first oscillation maximum at each site. We also find that 2° to 3° off-axis beam covers the second oscillation maximum. In such case, we can observe the contribution of Δ_{12} more clearly.

5.3 Solving the degeneracy in T2KK

As we have already learned in section 4.4, the comparison of the two long baseline experiment is a great tool for the degeneracy problem. But we naively wonder which the small or large off-axis beam is attractive for the degeneracy problem in Korea. The favored oscillation phase in order to use the benefits of the matter effect is $\pi < \Delta_{13} < 2\pi$; see section 4.4. In the words of the energy, the neutrino energy 1.0 GeV to 2.0 GeV is favored energy region at $L \sim 1000$ km. We find that the off-axis beams which cover the favored region are 0.5° and 1.0° off-axis beam. We would like to check that the matter effect are the very powerful tool in the T2KK experiment.

Since the matter effect term in eq. (57a) is proportional to the neutrino energy, measuring the first oscillation maximum at Korea corresponds to the measuring the difference of the correction from the matter effect at each site. When we choose the small off-axis beam, the baselines length determined almost uniquely, $L \sim 1000$ km; see

Fig. 6, and hence the first term in eq. (57b) becomes about 30%, and the difference of the amplitude of the $\nu_\mu \to \nu_e$ oscillation at each site is about 20%. It seems that enough large to detect the matter effect. Now let us briefly estimate the significance of this matter effect. Let us examine this observation semi-quantitatively by using the approximate formulae in eqs. (56) - (57). The difference between the $\nu_\mu \to \nu_e$ oscillation amplitude at a far detector and that at a near detector is

$$\Delta P_{\nu_\mu \to \nu_e}(\Delta_{13}) = P_{\nu_\mu \to \nu_e}(L_{\rm far}; \Delta_{13}) - P_{\nu_\mu \to \nu_e}(L_{\rm near}; \Delta_{13}) \ . \tag{59}$$

The error of the $\Delta P_{\nu_\mu \to \nu_e}(\Delta_{13})$ can be estimated as

$$\begin{aligned} \left[\delta\left(\Delta P_{\nu_\mu \to \nu_e}(\Delta_{13})\right)\right]^2 &= \left[\delta P_{\nu_\mu \to \nu_e}(L_{\rm near})\right]^2 + \left[\delta P_{\nu_\mu \to \nu_e}(L_{\rm far})\right]^2 \\ &= \left(\frac{P_{\nu_\mu \to \nu_e}(L_{\rm near})}{\sqrt{N_e^{\rm near}}}\right)^2 + \left(\frac{P_{\nu_\mu \to \nu_e}(L_{\rm far})}{\sqrt{N_e^{\rm far}}}\right)^2 \ . \end{aligned} \tag{60}$$

Here N_e is the number of ν_e appearance events. The ratio between $N_e^{\rm far}$ and $N_e^{\rm near}$ at the maximum value of the oscillation probability, $\Delta_{13} = +\pi$, can be expressed as

$$\frac{N_e^{\rm far}}{N_e^{\rm near}} = \frac{V_{\rm far}}{V_{\rm near}} \frac{\Phi_{\rm far}(E_\nu \text{ at } \Delta_{13} = \pi, L_{\rm far})}{\Phi_{\rm near}(E_\nu \text{ at } \Delta_{13} = \pi, L_{\rm near})} , \tag{61}$$

where V denotes the fiducial volume of the detector and $\Phi(E_\nu,\ L)$ is the neutrino beam flux at L, which is proportional to $(1/L)^2$. The cross section ratio at different energies drops out, because the neutrino cross section of CCQE events is almost constant in the 0.7 - 5 GeV region; see Fig. 4(b). We therefore need to estimate the number of ν_e CCQE events near the oscillation maximum at SK, $N_{\rm near}$. We show in Fig. 7, typical numbers of expected CCQE events for the μ events (a) and the e events (b), for the 3.0° OAB at SK. The open squares show the expected numbers of events in a 200 MeV wide E_ν bin, after 5 years (5×10^{21} POT), at $\sin^2 2\theta_{\rm RCT} = 0.1$ and $\delta = 0°$ for the normal hierarchy, just as in Fig. 4 (d). From the two bins around $E_\nu = 0.6$ GeV in Fig. 7(b), we may estimate $N_{\rm near} \sim 130$.

The difference between the maximum value of the oscillation probability, $\Delta P_{\nu_\mu \to \nu_e}$, for the normal hierarchy ($\Delta_{13} = +\pi$) and that for the inverted hierarchy ($\Delta_{13} = -\pi$) can be expressed as

$$\left[\Delta P_{\nu_\mu \to \nu_e}(+\pi) - \Delta P_{\nu_\mu \to \nu_e}(-\pi)\right] \sim 0.01 \left(\frac{\sin^2 2\theta_{\rm RCT}}{0.10}\right)\left(\frac{L_{\rm far}}{295{\rm km}} - 1\right)$$

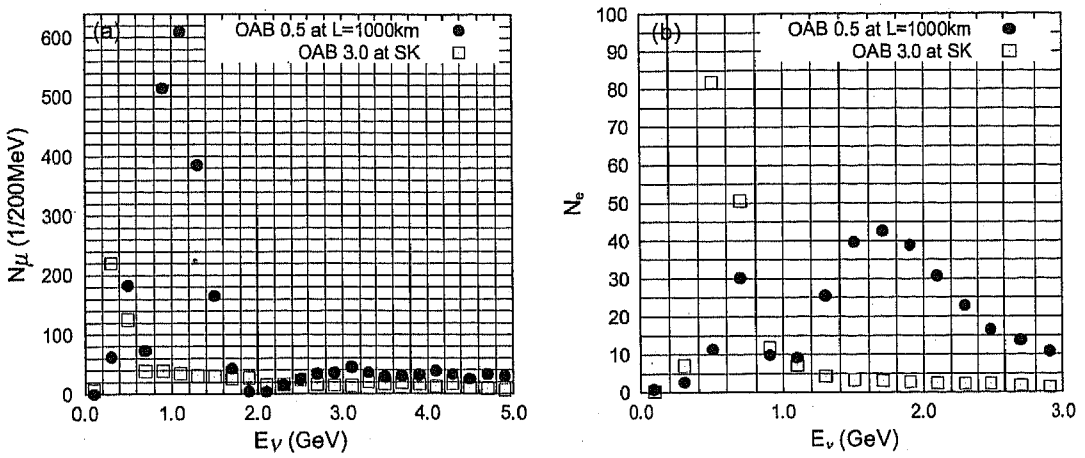

Figure 7: The typical numbers of the μ events (a), and those of the e events (b), for the exposure time of 5 years (5×10^{21} POT), for the 3.0° OAB at SK (open square), and for the 0.5° OAB at $L = 1000$ km with a 100 kt water Čerenkov detector (solid circles). The input parameters are the same as those of Fig. 4 (d) [19].

where we set $L_{\rm near} = 295$ km and used the approximation of eqs. (56) and (57b). The difference grows linearly with the distance, $L_{\rm far}$, as long as the oscillation maximum is covered by the flux. The significance of excluding the fake hierarchy can then be estimated as

$$\frac{\Delta P_{\nu_\mu\to\nu_e}(+\pi) - \Delta P_{\nu_\mu\to\nu_e}(-\pi)}{\delta(\Delta P_{\nu_\mu\to\nu_e}(+\pi))}$$

$$= 2.3\left(\frac{\sin^2 2\theta_{\rm RCT}}{0.10}\right)^{1/2}\left(\frac{L_{\rm far}}{295{\rm km}} - 1\right)\left[1 + 0.225\left(\frac{L_{\rm far}}{295{\rm km}}\right)^2\frac{100{\rm kt}}{V_{\rm far}}\right]^{-1/2}. \quad (62)$$

We find from this very rough estimation that we need 100 kt to exclude the fake hierarchy at the 3-σ level, which is confirmed in the following numerical studies.

The term of the matter effect term of B^e in eq. (57c) is also significantly large in Korea. In order to the understand the contribution of B^e more clearly, let composite eq. (56) as

$$P_{\nu_\mu\to\nu_e} \approx 4\sin^2\theta_{\rm ATM}\sin^2\theta_{\rm RCT}\,(1 + A^e)\sin^2\left(\frac{\Delta_{13}}{2} + B^e\right) + C^e, \quad (63)$$

This formula is appropriate when $|A^e| < 0.5$. In this formula, B^e can be interpreted as the phase shift term. At Kamioka, $L = 295$ km, the magnitude of term is 0.08 and the that of the $\cos\delta$ term is 0.15 for $\sin^2 2\theta_{\rm RCT} = 0.10$ around the oscillation maximum; see eq. (57d). At Korea around the $\Delta_{13} \sim \frac{3\pi}{2}$, the magnitude of the $\cos\delta$ term is fixed at 0.21 but the matter effect term is 3 times of that at SK, about 0.24. Then the relative

sign degeneracy between B^e and Δ_{13} due to the $\cos\delta$ around 0.5 GeV region. For the case $\sin^2 2\theta_{\rm RCT} \sim 0.05$, the term of $\cos\delta$ becomes larger than the matter effect term.

Once the sign of $\cos\delta$ is constrained, we can determine the neutrino mass hierarchy uniquely. The important points that longer baseline helps us also the measurement of $|\cos\delta|$. This is because the contribution of the $\cos\delta$ can be observed as the phase shift, shown in eq. (63), and the resolution of the oscillation phase $\delta(E/L)$, becomes good as long as the bin width is fixed. The difference of amplitudes at each site due to the matter effect tells us the not only the sign of δm^2_{13} but also the size of the $\sin^2 2\theta_{\rm RCT}$ because the difference is proportional to $\sin^2\theta_{\rm RCT}$. Then we can constraint the value of the $\sin\delta$. Fortunately this is enough large to distinguish the non CP violating case from the maximal CP violating case, which differences about 30% for $\sin^2 2\theta_{\rm RCT} = 0.10$; see eq. (57b). We also confirmed that we can determine the δ uniquely in the T2KK experiment, at the next section.

6 Physics potential of T2KK

6.1 χ^2 analysis

In this section, we study the physics potential of the T2KK experiments by the numerical calculation. Before we show the result of our calculation. We would like to introduce our analysis method in this sub section.

In our case study, we consider a 100 kt level detector because of the requirement from the rough estimation in the previous section. We adopt a Water Čerenkov detector because it allows us to distinguish clearly the $e^{\pm}$ events from $\mu^{\pm}$ events. We use the CCQE events in our analysis, because it allows us to kinetically reconstruct the neutrino energy event by event. The Fermi-motion of the target nucleon dominates is the origin which blur the neutrino energy reconstruction. Because the uncertainty of the Fermi-motion is about 80 MeV, we take the width of the energy bin as $\delta E_\nu = 200$ MeV for $E_\nu > 400$ MeV, in the following analysis.

The event numbers of ν_β form ν_α flux (Φ_{ν_α}) which is delivered by J-PARC [29] in the i-th energy bin, $E_\nu^i = 200\text{MeV} \times (i+1) < E_\nu < E_\nu^i + \delta E_\nu$, are then calculated as

$$N_\beta^i(\nu_\alpha) = M N_A \int_{E_\nu^i}^{E_\nu^i + \delta E_\nu} \Phi_{\nu_\alpha}(E)\; P_{\nu_\alpha \to \nu_\beta}(E)\; \sigma_\beta^{QE}(E)\; dE\,, \tag{64}$$

where $P_{\nu_\alpha \to \nu_\beta}$ is the neutrino oscillation probability including the matter effect, M is the detector mass, $N_A = 6.017 \times 10^{23}$ is the Avogadro constant, and σ_α^{QE} is the CCQE cross section per nucleon in water [3]. All the primary as well as secondary fluxes used in our analysis are obtained from the website [29]. As we mentioned in the previous, the fiducial volume of Super-Kamiokande is 22.5 kt, and that of the detector in Korea is 100 kt. The detection efficiencies of both detectors for both ν_μ and ν_e CCQE events are set at 100% for brevity. We calculate the survival and the transition probability exactly by the numerical calculation. We also include the contribution from the secondary neutrino flux ($\nu_e\,, \bar{\nu}_e\,, \bar{\nu}_\mu$), because they are also sensitive the oscillation parameter. Finally the e-like and μ-like events for the i-th bin are obtained as

$$N_\alpha^i = N_\alpha^i(\nu_\mu) + \sum_{\nu_\beta = \nu_e\,, \bar{\nu}_e\,, \bar{\nu}_\mu} N_\alpha^i(\nu_\beta)\,, \qquad (\alpha = e\,, \mu)\,. \tag{65}$$

The second term in eq.(65) corresponds to the contribution from the secondary neutrino flux. In our analysis, we calculate $N_{\mu,e}^i$ by we assume that the mean value summarized in eq. (55). Our results are not sensitive to the small change in the input values in eq.(55) For the density along the Tokai-to-Kamioka baseline, we adopt $\rho^{\text{input}} = 2.8\ \text{g/cm}^3$, which

is shown in T2K LOT [11]. Since the Tokai-to-Korea baseline go through deeper region than the Tokai-to-Kamioka- baseline, we take the slightly larger value, 3.0 g/cm^3 as the mean value of the density along the Tokai-to-Korea baseline. We will show that rough estimation is not so bad in section 7. We examine various input values of $\sin^2 2\theta_{\rm RCT}$, δ , and the sign of $m_3^2 - m_1^2$. Since our concern is the possibility to distinguish the neutrino mass hierarchy and to constrain the CP phase uniquely, we study how the above 'data' can constrain the model parameters by using the χ^2 function

$$\Delta\chi^2 = \chi^2_{\rm SK} + \chi^2_{\rm Kr} + \chi^2_{\rm sys} + \chi^2_{\rm para}\,. \tag{66}$$

Here the first two terms, $\chi^2_{\rm SK}$ and $\chi^2_{\rm Kr}$, measure the parameter dependence of the fit to the SK and the Korean detector data,

$$\chi^2_{\rm SK,Kr} = \sum_i \left\{ \left(\frac{(N_e^i)^{\rm fit} - N_e^i}{\sqrt{N_e^i}} \right)^2 + \left(\frac{(N_\mu^i)^{\rm fit} - N_\mu^i}{\sqrt{N_\mu^i}} \right)^2 \right\}, \tag{67}$$

where the summation is over all bins from 0.4 GeV up to 5.0 GeV for N_μ, 1.2 GeV for N_e at SK, and 2.8GeV for N_e at Korea. These upper bounds are chosen such that most of the bins used in our analysis contain more than 10 events. Here $N^i_{\mu,e}$ is the calculated number of events in the i-th bin, and its square root gives the statistical error. $N_i^{\rm fit}$ is calculated by allowing the model parameters to vary freely and by allowing for systematic errors. In our analysis, we consider 4 types of systematic errors. The first ones are for the overall normalization of each neutrino flux, for which we assign 3% errors,

$$f_{\nu_\beta} = 1 \pm 0.03\,, \tag{68}$$

for $\nu_\beta = \nu_e,\ \bar{\nu}_e, \nu_\mu,\ \bar{\nu}_\mu$, which are taken common for T2K and the Tokai-to-Korea experiments. The second systematic error is for the uncertainty in the matter density, for which we allow 3% overall uncertainty along the baseline, independently for T2K ($f_\rho^{\rm SK}$) and the Tokai-to-Korea experiment ($f_\rho^{\rm Kr}$):

$$\rho_i^{\rm fit} = f_\rho^i\, \rho_i^{\rm true} \qquad (i = {\rm SK},\ {\rm Kr})\,. \tag{69}$$

The third uncertainty is for the CCQE cross section,

$$\sigma_\alpha^{\rm QE,\ fit} = f_\alpha^{\rm QE}\, \sigma_\alpha^{\rm QE,\ true}\,. \tag{70}$$

Since ν_e and ν_μ QE cross sections are expected to be very similar theoretically, we assign a common overall error of 3% for ν_e and ν_μ ($f_e^{\rm QE} = f_\mu^{\rm QE} \equiv f_\ell^{\rm QE}$), and an independent 3% error for $\bar{\nu}_e$ and $\bar{\nu}_\mu$ QE cross sections ($f_{\bar{e}}^{\rm QE} = f_{\bar{\mu}}^{\rm QE} \equiv f_{\bar{\ell}}^{\rm QE}$). The last one is the uncertainty

of the fiducial volume, for which we assign 3% error independently for T2K ($f_{\rm V}^{\rm SK}$) and the Tokai-to-Korea experiment ($f_{\rm V}^{\rm Kr}$). $N_\alpha^{i,\rm fit}$ is then calculated as

$$N_\alpha^{i,\rm fit}(\nu_\beta) = f_{\nu_\beta}\, f_\alpha^{\rm QE}\, f_{\rm V}^{\rm SK,Kr}\, N_\alpha^i(\nu_\beta)\,, \tag{71}$$

and $\chi^2_{\rm sys}$ has four terms;

$$\chi^2_{\rm sys} = \sum_{\alpha=e,\bar{e},\mu,\bar{\mu}} \left(\frac{f_{\nu_\alpha}-1}{0.03}\right)^2 + \sum_{\alpha=l,\bar{l}} \left(\frac{f_\alpha^{\rm QE}-1}{0.03}\right)^2 + \sum_{i={\rm SK,\ Kr}} \left\{ \left(\frac{f_\rho^i-1}{0.03}\right)^2 + \left(\frac{f_{\rm V}^i-1}{0.03}\right)^2 \right\}. \tag{72}$$

In short, we assign 3% errors for the normalization of each neutrino flux, the ν_e and $\bar{\nu}_e$ CCQE cross sections, the effective matter density along the base line, and for the fiducial volume of SK and the Korean detector. Finally, $\chi^2_{\rm para}$ accounts for the present constraints on the SOL oscillation parameters, summarized in eq. (49):

$$\chi^2_{\rm para} = \left(\frac{(\delta m^2_{12})^{\rm fit} - (\delta m^2_{12})^{\rm input}}{0.6\times 10^{-5}}\right)^2 + \left(\frac{\sin^2 2\theta_{\rm SOL}^{\rm fit} - \sin^2 2\theta_{\rm SOL}^{\rm input}}{0.07}\right)^2 . \tag{73}$$

In total, our $\Delta\chi^2$ function depends on 16 parameters, the 6 model parameters and the 10 normalization factors.

6.2 Determination of the mass hierarchy

In this subsection, we study the capability of determining the sign of δm^2_{13} in the T2KK experiment. First of all, we investigate the favored the combination of the off-axis angle at Kamioka, that in Korea, and the baseline length for the Tokai-to-Korea baseline to determine the mass hierarchy pattern. This is most important point, because the we can not measure the δ uniquely without constraint on the mass hierarchy pattern.

For this purpose, we first calculate the expected number of the $\nu_\mu \to \nu_e$ CCQE events at both detectors by assuming either normal or inverted hierarchy, and then examine if the resulting 'data' can be fitted for the opposite hierarchy by adjusting the model parameters.

We show in Fig. 8 the minimum $\Delta\chi^2$ expected at the T2KK two detector experiment after 5 years of running (5×10^{21}POT), as functions of the off-axis angle and the baseline length of the far-detector site from J-PARC at Tokai, when the normal hierarchy ($m_3^2 - m_1^2 > 0$) is assumed in generating the events, and the inverted hierarchy ($m_3^2 - m_1^2 <$

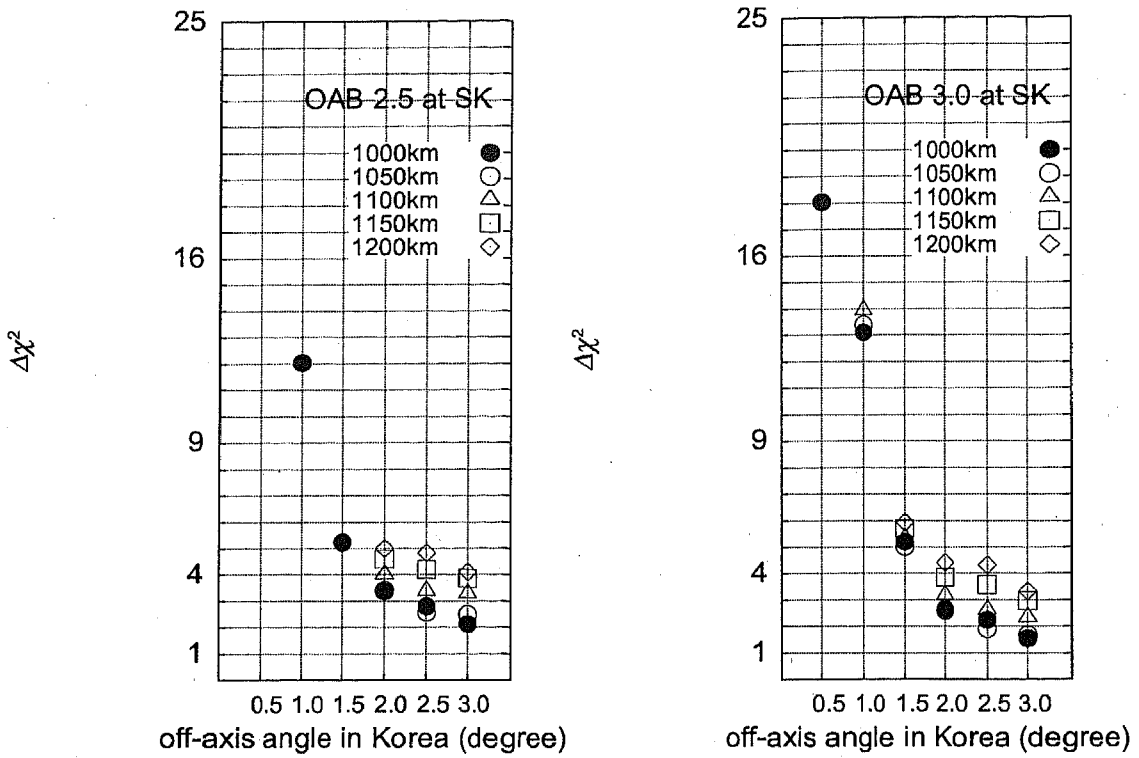

Figure 8: Minimum $\Delta\chi^2$ of the T2KK two detector experiment after 5 years of running (5×10^{21} POT) as functions of the off-axis angle and the base-line length of the far-detector from J-PARC at Tokai, when the normal hierarchy ($m_3^2 - m_1^2 > 0$) is assumed in generating the events, and the inverted hierarchy ($m_3^2 - m_1^2 < 0$) is assumed in the fit. The left-hand figure (a) is for the 2.5° OAB at SK, and the right-hand one (b) is for the 3.0° OAB beam at SK. The input parameters are the same as those of Fig. 4 (d); in particular, $\sin^2 2\theta_{\rm RCT}^{\rm input} = 0.10$ and $\delta^{\rm input} = 0°$.

0) is assumed in the fit. The left-hand figure (a) is for the 2.5° OAB at SK, and the right-hand one (b) is for the 3.0° OAB beam at SK. The input parameters are choose as in eq. (55), $\sin^2 2\theta_{\rm RCT}^{\rm input} = 0.10$ and $\delta^{\rm input} = 0°$. The four symbols, solid circle, open circle, triangle, and square are for L = 1000km, 1050km, 1100km, and 1150km, respectively. There are no data points at 0.5° in Fig. 8(a) for the 2.5° OAB at SK, because the 0.5° off-axis beam does not reach Korea: see Fig. 5(a). It is clearly seen from Fig. 14 that the best combination of off-axis angles are 3° for SK and 0.5° for the Korean detector at $L = 1000$ km. The 0.5° off-axis beam has strong flux up to ~ 2.2 GeV, which overlaps significantly with the broad peak of the $\nu_\mu \to \nu_e$ oscillation at $L = 1000$ km; see Fig. 4 (a), (c) and (d). Because the number of the ν_e CCQE events is large enough around the oscillation maximum for $\sin^2 2\theta_{\rm RCT} \sim 0.1$, both at SK and at the far detector in Korea, we are able to measure the difference in the magnitude of the $\nu_\mu \to \nu_e$ probability at two vastly different baselines, and can hence distinguish between the normal hierarchy

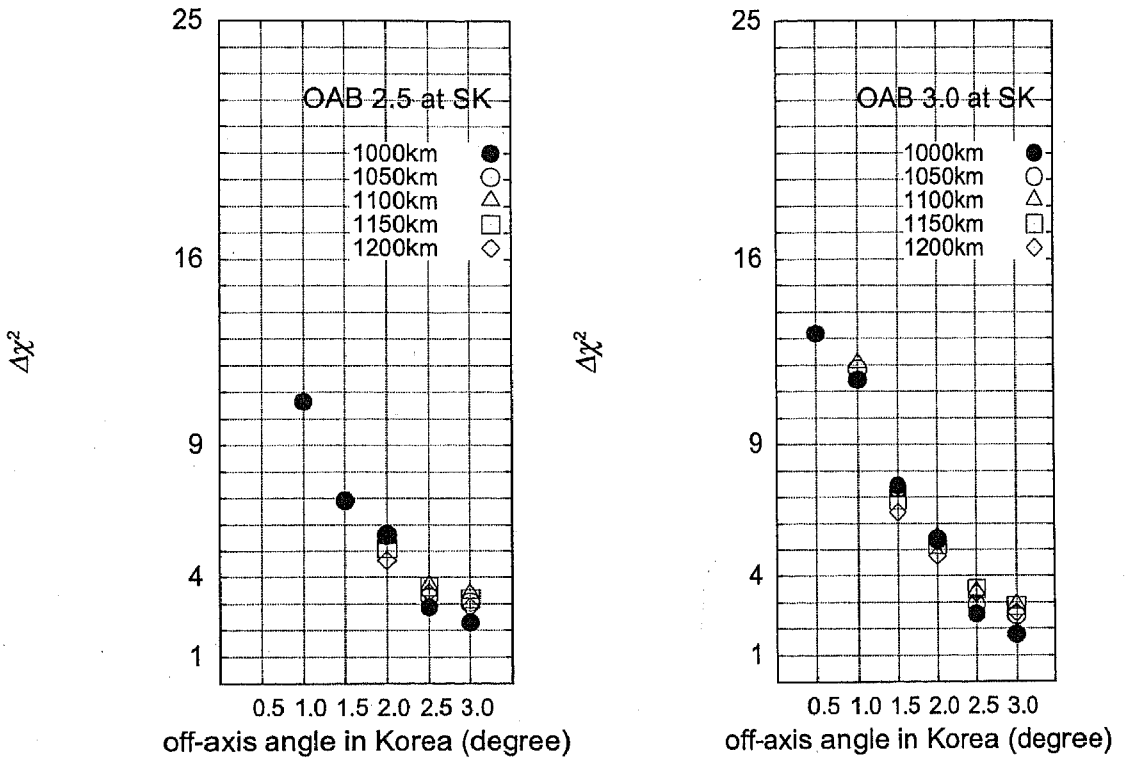

Figure 9: The same as Fig. 8, but when the input data is calculated for the inverted hierarchy ($m_3^2 - m_1^2 < 0$) and the fit is performed by assuming the normal hierarchy ($m_3^2 - m_1^2 > 0$). All the other parameters are the same as those in Fig. 14.

and the inverted hierarchy. We can reject the fake hierarchy at 4.1-σ level in our simple simulation with this combination of 3.0° at SK and 0.5° at $L = 1000$ km. We find from Fig. 8 that the 1.0° OAB in Korea still keeps the sensitivity to the neutrino mass hierarchy, where both a combination of 1.0° at $L = 1000$ km and 2.5° OAB at SK (Fig. 8 (a)) and that of 1.0° at $L = 1000$ km ~ 1150 km and the 3.0° OAB at SK (Fig. 8 (b)) distinguish the neutrino mass hierarchy at about 3.5-σ level in our simulation. This is because the CCQE cross section times the flux of 1.0° OAB extends to ~ 1.7 GeV, see Fig. 4 (a) and (c), which barely overlaps with the broad peak region of the $\nu_\mu \to \nu_e$ oscillation probability shown in Fig. 4(d). From Fig. 5 (a) and (b), we find that the 1.0° OAB is observable only in the east coast of Korea ($L \sim 1000$ km) for the 2.5° OAB at SK, whereas for the 3.0° OAB at SK, it can be observed at various base-line lengths up to ~ 1150 km. When we compare the data points for the same off-axis angle but the different baseline length, the $\Delta\chi^2$ for the further points tends to be large. This is effect of the $\frac{aL}{2W}$ in eq. (57d), which grows with the baseline length, L. The other combinations, OAB $\geq$ 2.0, have little hope to constraint the neutrino mass hierarchy pattern.

Fig. 9 is the same as Fig. 8, but when the input data is calculated for the inverted

hierarchy and the fit is performed by assuming the normal hierarchy. The favored combination is same as the case for the normal hierarchy, 3.0° at SK, and 0.5° at $L \sim 1000$ km in Korea, but the value of minimum $\Delta\chi^2$ drops from 18.0 to 13.8. This deficit comes from the statistic error. At Korea, the number of ν_e appearance signal is strongly suppressed by the matter effect term. Then the statistic errors is large. Especially, the signal for the 0.5° off-axis beam is strongly suppressed because the main flux of the 0.5° is from 1.5 GeV to 2.0 GeV region. For the 1.0° case, the decreases of the minimum $\Delta\chi^2$ is not so large, because of lower energy flux. But it is remarkable that still the data points of which off-axis angle in Korea is smaller than 0.5 keeps 3-σ significance. We may conclude that a far detector that observes the T2KK off-axis beam have the capability of the neutrino mass hierarchy pattern.

Because we find from Fig. 8 and Fig. 9 that a combination of 0.5° OAB at $L \sim 1000$ km and the 3.0° OAB at SK has a significantly better capability of determining the neutrino mass hierarchy, we study in the following physics potential of this preferred T2KK set up in more detail. In particular, we investigate the whole un-explored parameter space of the three neutrino model.

First in Fig. 10, we summarize our findings on the capability of the T2KK experiment to determine the neutrino mass hierarchy in the whole space of $\sin^2 2\theta_{\rm RCT}$ and δ . Fig. 10(a) shows our result when the mass hierarchy is normal ($m_3^2 - m_1^2 > 0$), and (b) when it is inverted ($m_3^2 - m_1^2 < 0$). In each figure the input data are calculated for the model parameters at various $\sin^2 2\theta_{\rm RCT}^{\rm input}$ and $\delta^{\rm input}$ points, and the fit has been performed by surveying the whole parameter space, but under the opposite mass hierarchy. The resulting values of the minimum $\Delta\chi^2$ are shown as contours for 2, 3, 4, and 5-σ. The wrong mass hierarchy can be excluded with the corresponding confidence level if the true $\sin^2 2\theta_{\rm RCT}$ value lies in the right-hand side of each contour along the true value of δ ($\delta^{\rm input}$). In particular, the minimum $\Delta\chi^2$ values of 18 for the point ($\sin^2 2\theta_{\rm RCT}^{\rm input}$, $\delta^{\rm input}$) = (0.10, 0°) in Fig. 10(a) corresponds to the highest point in Fig. 8(b), and the corresponding value of 14 in Fig. 10(b) is the highest point in Fig. 15(b). We find that the wrong hierarchy can be excluded at the 3-σ level if $\sin^2 2\theta_{\rm RCT}^{\rm input} > 0.055$ (0.09) if the hierarchy is normal (inverted).

It is remarkable that the $\delta = 0°$ case chosen to plot Fig. 8 and Fig. 9 turns out to be the case when it is most difficult to determine the neutrino mass hierarchy. If $\delta = 180°$, the wrong hierarchy can be excluded at the 3-σ level for $\sin^2 2\theta_{\rm RCT}^{\rm input} \gtrsim 0.025$ for the normal hierarchy (Fig. 10(a)) or $\sin^2 2\theta_{\rm RCT}^{\rm input} \gtrsim 0.03$ for the inverted hierarchy (Fig. 9(b)). The origin of the δ dependence is the difference of the oscillation phase at the far detector in Korea. From eqs. (57d) and (63), the difference of the oscillation phase

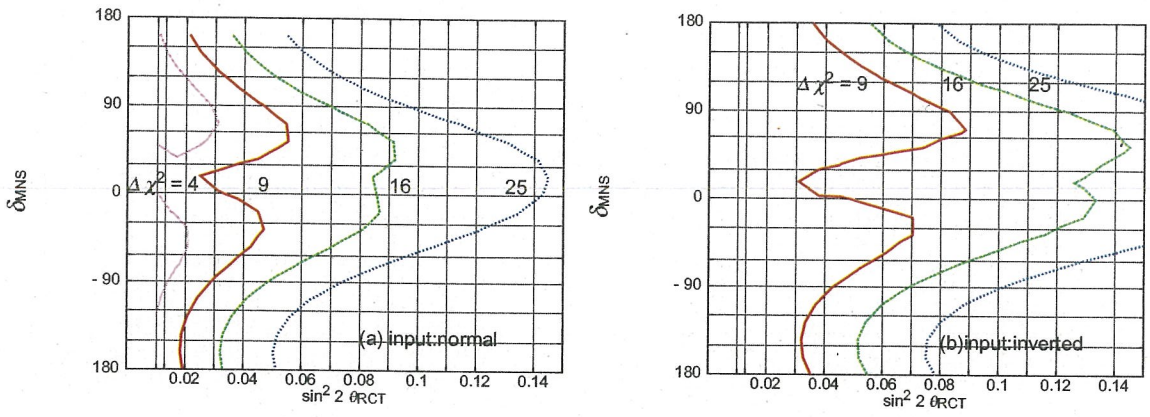

Figure 10: Capability of the T2KK two-detector experiment to determine the neutrino mass hierarchy, (a) when the mass hierarchy is normal ($m_3^2 - m_1^2 > 0$), and (b) when it is inverted ($m_3^2 - m_1^2 < 0$). The numerical results are obtained for a combination of 3.0°OAB at SK and 0.5°off-axis at $L = 1000$km with a 100 kt water Čerenkov detector, after 5 years of running (5×10^{21} POT). In each figure the input data are calculated for the model parameters at various $\sin^2 2\theta_{\rm RCT}^{\rm input}$ and $\delta^{\rm input}$, and the fit has been performed by surveying the whole parameter space with the opposite mass hierarchy. The resulting values of minimum $\Delta\chi^2$ are shown as contours for 2, 3, 4, and 5σ. The wrong hierarchy can be excluded with the corresponding confidence level if the true $\sin^2 2\theta_{\rm RCT}$ and δ values lie in the right-hand side of each contour. The model parameters are set at $(m_3^2 - m_1^2)^{\rm input} = 2.5 \times 10^{-3}{\rm eV}^2$ (a), $-2.5 \times 10^{-3}{\rm eV}^2$ (b), $(m_2^2 - m_1^2)^{\rm input} = 8.2 \times 10^{-5}{\rm eV}^2$, $\sin^2 2\theta_{\rm ATM}^{\rm input} = 1.0$, $\sin^2 2\theta_{\rm SOL}^{\rm input} = 0.83$, $\rho^{\rm input} = 2.8{\rm g/cm}^3$ for SK, and $\rho^{\rm input} = 3.0{\rm g/cm}^3$ for $L = 1000$km.

near the oscillation maximum, $|\Delta_{13}| = \pi$, between the input and the fit is expressed as,

$$\left|\frac{\Delta_{13}}{2} + B^e_{\rm input}\right| - \left|-\frac{\Delta_{13}}{2} + B^e_{\rm fit}\right|$$

$$\sim \pm 0.15 \left\{ \cos\delta^{\rm input} \left(\frac{0.10}{\sin^2 2\theta_{\rm RCT}^{\rm input}} \right)^{1/2} + \cos\delta^{\rm fit} \left(\frac{0.10}{\sin^2 2\theta_{\rm RCT}^{\rm fit}} \right)^{1/2} \right\} \left(\frac{|\Delta_{13}|}{\pi} \right)$$

$$\mp 0.58 \left(\frac{L}{1000{\rm km}} \right) . \qquad (74)$$

The upper sign is for the normal hierarchy, and the lower sign is for the inverted hierarchy. The phase-shift difference depends on both $\cos\delta^{\rm input}$ and $\cos\delta^{\rm fit}$. As explained in section 3, below eq. (62), when $\cos\delta^{\rm input} \sim 1$ ($\delta^{\rm input} \sim 0°$) the phase shift is smaller than that with the other $\delta^{\rm input}$ at $L = 1000$ km. Therefore the fitted value of $\cos\delta$ ($\cos\delta^{\rm fit}$) also tends to be large and has the opposite sign for the fake hierarchy. If $\cos\delta^{\rm input} \sim -1$, it is not possible to compensate for the phase-shift difference of eq. (74) even by choosing $\cos\delta^{\rm fit} = 1$, and the significantly higher minimum $\Delta\chi^2$ value results in Fig. 10(a) and (b). In general, $\cos\delta^{\rm fit} > 0$ is favored even when $\cos\delta^{\rm input} < 0$ in order to minimize the

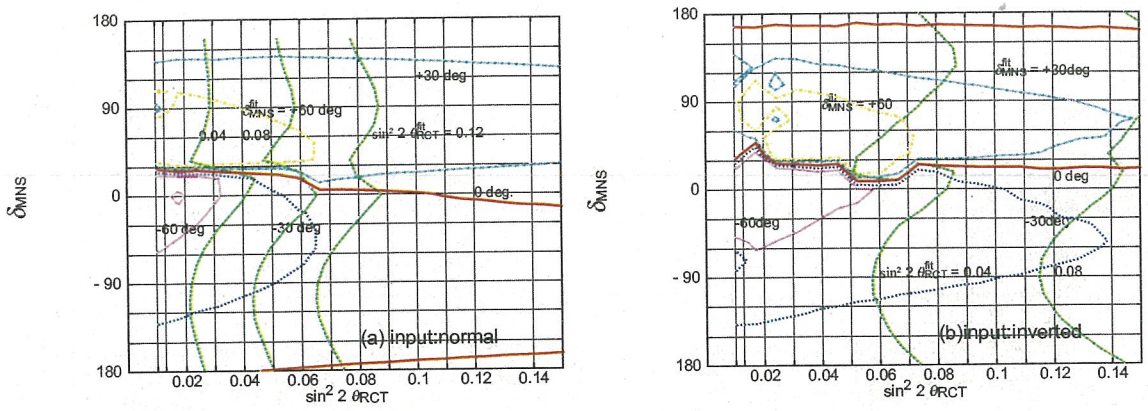

Figure 11: The values of the fit parameters, $\sin^2 2\theta^{\rm fit}_{\rm RCT}$ and $\delta^{\rm fit}$, at the minimum $\Delta\chi^2$ point of the analysis of Fig. 10 are shown. The results for the normal hierarchy (a) and those for the inverted hierarchy (b) are shown correspondingly to the fit of Fig. 10 (a) and Fig. 10 (b), respectively. The vertical lines are the $\sin^2 2\theta^{\rm fit}_{\rm RCT}$ contours. The thinner contours give the $\delta^{\rm fit}$ values.

phase-shift difference of eq. (74). This is clearly seen in Fig. 11, where we show the values of the best fit parameters, $\sin^2 2\theta^{\rm fit}_{\rm RCT}$ and $\delta^{\rm fit}$, at the minimum $\Delta\chi^2$ point of the analysis of Fig. 10. The results for the normal hierarchy (a) and those for the inverted hierarchy (b), are shown correspondingly to the fit of Fig. 10(a) and Fig. 10(b), respectively. The thick vertical lines are the $\sin^2 2\theta^{\rm fit}_{\rm RCT}$ contours. The thinner contours give the $\delta^{\rm fit}$ values. We find that the value of $\delta^{\rm fit}$ around 0° is almost always favored as expected.

Here let us try to explain more detailed features of Fig. 10 and Fig. 11 by separating the parameter space of $\sin^2 2\theta^{\rm input}_{\rm RCT}$ and $\delta^{\rm input}$ into 4 regions.

1. small $\sin^2 2\theta^{\rm input}_{\rm RCT}$ region ($\sin^2 2\theta^{\rm input}_{\rm RCT} < 0.04$) at any $\delta^{\rm input}$: In this region the phase difference eq. (74) is mainly controlled by the $\cos\delta$ terms, because of the $1/\sqrt{\sin^2 2\theta_{\rm RCT}}$ enhancement over the matter effect term. It is hence relatively easy to make the difference small by adjusting $\cos\delta^{\rm fit} + \cos\delta^{\rm input} \sim 0$. The hierarchy is determined essentially by the difference of the $\nu_\mu \to \nu_e$ oscillation amplitude only.

2. $\sin^2 2\theta^{\rm input}_{\rm RCT} \gtrsim 0.04$ at $\delta^{\rm input} \sim 180^\circ$: Although the effect of $\cos\delta^{\rm input} \sim -1$ is canceled by choosing $\cos\delta^{\rm fit} \sim +1$, the difference from the matter effect term in eq. (74) cannot be canceled. Therefore in this region the hierarchy is determined by the differences of both the amplitude and the oscillation phase.

3. $\sin^2 2\theta^{\rm input}_{\rm RCT} \gtrsim 0.04$ at $\delta^{\rm input} \sim \pm 90^\circ$: In eq. (74), the difference is controlled by the matter effect term and the $\cos\delta^{\rm fit}$ term because $\cos\delta^{\rm input} \sim 0$. In this region, we can make the phase-shift difference small by choosing $\cos\delta^{\rm fit} > 0$.

4. $\sin^2 2\theta_{\rm RCT}^{\rm input} \sim 0.04$ to 0.08 at $\delta^{\rm input} \sim 0°$: In this region the phase-shift difference eq. (74) at $|\Delta_{13}| \sim \pi$ can be made small at $\cos\delta^{\rm fit} \sim 1$, but the difference at $|\Delta_{13}| \sim 2\pi$ becomes large. Because the flux of 0.5° off-axis beam is strong at lower energies where $\pi < |\Delta_{13}| < 2\pi$, the growth of the phase-shift difference eq. (74) at larger $|\Delta_{13}|$ cannot be compensated. This explains why the minimum $\Delta\chi^2$ value in this region is larger than the one for the case 3.

The systematics of the oscillation phase is rather complicated, but its effect turns out to be significant in determining the neutrino mass hierarchy.

We also investigate the sensitivity of the mass hierarchy pattern for the combination of 2.5° OAB at SK, 1.0° OAB at Korea, and L for the Tokai-to-Korea baseline is 1000 km, and the result is shown in Fig. 12. We find that we can constrain the sign of Δ_{13} at

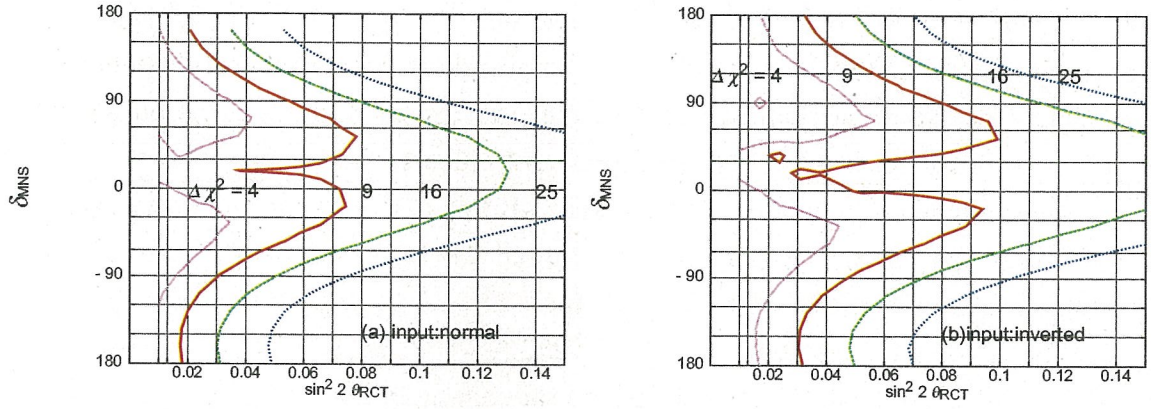

Figure 12: The same figure as Fig. 10 but the off-axis angle at SK is 2.5°, that at Korea is 1°, and the distance from J-PARC to the detector placed in Korea is 1000 km.

3-σ level when $\sin^2 2\theta_{\rm RCT} > 0.077(0.1)$ for the normal (inverted) hierarchy, respectively. If we want the same capability of the best combination, 0.5° at $L \sim 1000$ km, and 3° at SK, we need about 120 kt level water Čerenkov detector in Korea. In Fig. 12 that the CP dependence of the capability of determining the mass hierarchy is rather stronger than the that shown in Fig. 12. The flux of 1.0° OAB covers lower energy than that of 0.5°, then the magnitude of Δ_{12} becomes large, and finally the CP dependent terms in eqs. (57b) and (57d).

Before closing this subsection, let us briefly study the value of $\sin^2 2\theta_{\rm RCT}^{\rm fit}$ in Fig. 11. In Fig. 11(a), $\sin^2 2\theta_{\rm RCT}^{\rm fit}$ is larger than $\sin^2 2\theta_{\rm RCT}^{\rm input}$, whereas in Fig. 11(b), $\sin^2 2\theta_{\rm RCT}^{\rm fit}$ is smaller than $\sin^2 2\theta_{\rm RCT}^{\rm input}$. This is because the same oscillation amplitude can be obtained by choosing $\sin^2 2\theta_{\rm RCT}^{\rm fit} > \sin^2 2\theta_{\rm RCT}^{\rm input}$ when the hierarchy is normal but it is assumed to be inverted in the fit, and *vice versa* for the opposite case. A bad point for the inverted case is that the small $\sin^2 2\theta_{\rm RCT}^{\rm fit}$ enhances the contribution of the CP phase. As results

of this smallness, the phase difference in eq. (56) can be canceled by $\cos\delta^{\rm fit}$. Therefore, constraining the neutrino mass hierarchy suffers the slightly larger statistical error and the cancellation of the phase difference for the inverted case.

6.3 Measurement of CP phase

In this section we investigate the measurement of $\sin^2 2\theta_{\rm RCT}$ and δ for our preferred combination of the 3.0° OAB at SK and 0.5° OAB at $L = 1000$ km. This combination of the T2KK experiment allows us to measure the $\nu_\mu \to \nu_e$ oscillation around the oscillation maximum at two base-line lengths, which can be parametrized as in eq. (56), in terms of the amplitude shift eq. (57b) and the phase shift eq. (57d). Once the neutrino mass hierarchy is determined as explained in the previous section, the terms proportional to $|\Delta_{13}|/\pi$ in the amplitude shift eq. (57b) measure $\sin\delta$, and those in the phase shift eq. (57d) measure $\cos\delta$. In the T2KK two detector system, both $\sin^2 2\theta_{\rm RCT}$ and $\sin\delta$ can be determined uniquely because the amplitude shift eq. (57b) has significantly different matter effect contributions between SK and the far detector. The phase shift measurement of the term eq. (57d) constrains $\cos\delta$ independent of $\sin\delta$.

We also examine the capability of the Tokai-to-Korea LBL experiments for measuring the CP phase. We show in Fig. 13 regions allowed by this experiment in the plane of $\sin^2 2\theta_{\rm RCT}$ and δ. The mean values of the inputs are calculated for the parameters of eq. (55). In each figure, the input points $(\sin^2 2\theta_{\rm rct}^{\rm true}, \delta^{\rm true})$ are shown by solid-circles for $\sin^2 2\theta_{\rm rct}^{\rm true} = 0.10$, and 0.06. The regions where the minimum $\Delta\chi^2$ is less than 1, 4, 9 are depicted by solid, dashed and dotted boundaries, respectively. Even though we allow the sign of $m_3^2 - m_1^2$ to vary in the fit, no solution with the inverted hierarchy that satisfy $\Delta\chi^2_{\rm min} < 9$ appear in the figure.

From these figures, we learn that δ can be constrained to $\pm 30°$ at 1σ level, when $\sin^2 2\theta_{\rm rct}^{\rm true} > 0.06$. It is remarkable that we can constrain both $\sin\delta$ and $\cos\delta$ without using anti-neutrino experiments. It is remarkable that the error of δ is almost independent of $\sin^2 2\theta_{\rm RCT}^{\rm input}$ at 0.06 and 0.1, for all the four input values of $\delta^{\rm input}$, 0°, $\pm 90°$, and 180°. This is remarkable because the event number N_e is proportional to $\sin^2 2\theta_{\rm RCT}$ according to eq. (56), and hence the statistical error of the measurement of the amplitude and the phase should be proportional to $1/\sqrt{N_e}$, or $1/\sqrt{\sin^2\theta_{\rm RCT}}$. This increase in the error for small $\sin^2 2\theta_{\rm RCT}^{\rm input}$ values is canceled by the increased sensitivities of both the amplitude and the phase shift to $\sin\delta$ and $\cos\delta$, respectively, which are both proportional to $1/\sqrt{\sin^2\theta_{\rm RCT}}$. The two effects cancel rather accurately, and we find that the error of δ is almost independent of the input values of $\sin^2 2\theta_{\rm RCT}$ and δ.

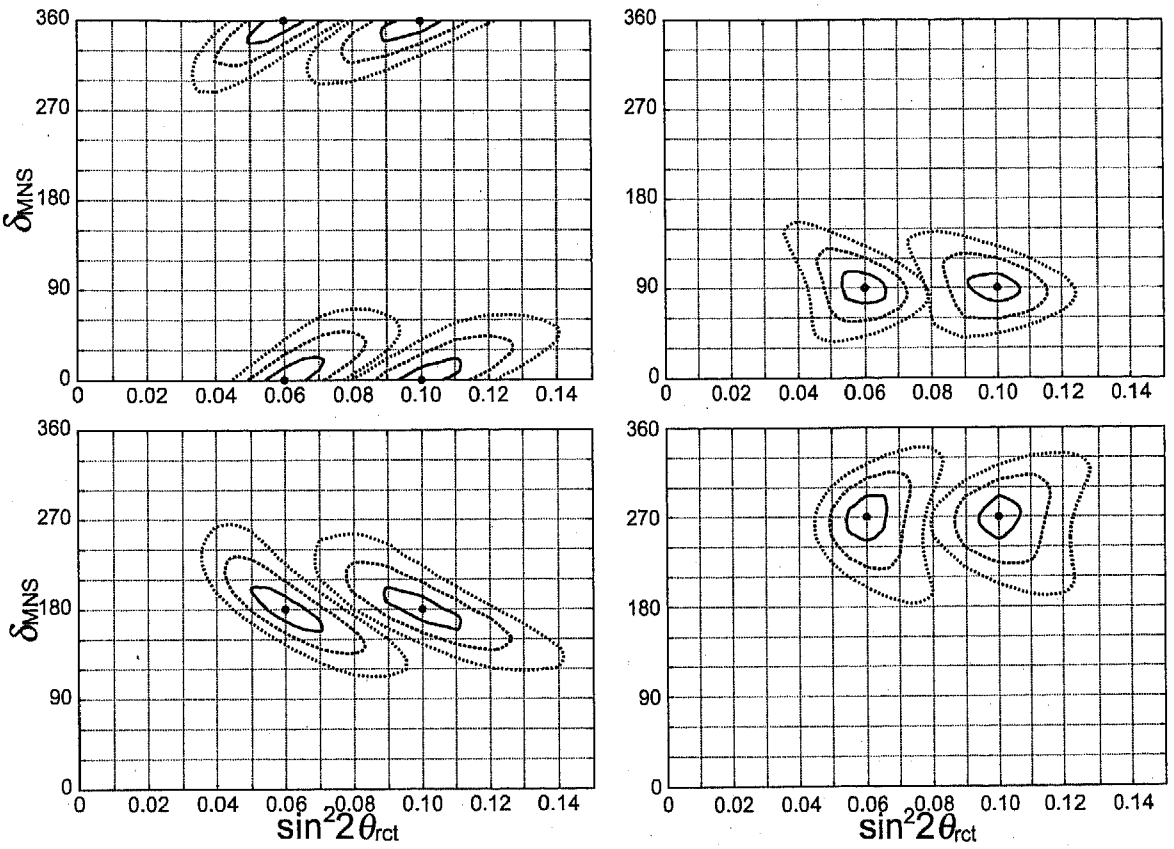

Figure 13: Allowed region in the plane of $\sin^2 2\theta_{\rm rct}^{\rm fit}$ and $\delta^{\rm fit}$, when the event numbers at SK and Korea are calculated for the parameters of eq. (55). In each figure, the input points ($\sin^2 2\theta_{\rm rct}^{\rm true}$, $\delta^{\rm true}$) are shown by solid-circles, and the regions where the minimum $\Delta\chi^2$ is less than 1, 4, 9 are depicted by solid, dashed and dotted boundaries, respectively.

7 Effect of the future reactor experiment

7.1 The effect of the constraint on $\sin^2 2\theta_{\rm RCT}$ in T2KK

In the previous section, we learn that the T2KK have the capability of solving the degeneracy problem. However, Fig. 11 shows that the $\sin^2 2\theta^{\rm fit}_{\rm RCT}$ is different from the $\sin^2 2\theta^{\rm input}_{\rm RCT}$. This fact encourages the more combining analysis, the T2KK experiment and the future neutrino oscillation experiment, such as Double CHOOZ, Daya bay, Reno and so on. So let me consider what happen if we combine the result of T2KK and the future reactor oscillation experiments.

The most affected part is the determination of the amplitude of the $\nu_\mu \to \nu_e$ oscillation. In the previous discussions, we learn that there is a huge difference of the ν_e signals between the normal hierarchy and the inverted hierarchy at Korea. Then $\sin^2\theta^{\rm fit}_{\rm RCT}$ tends to recover this difference, but finally $\sin^2\theta^{\rm fit}_{\rm RCT}$ produces the another difference in Korea. In other words, the role of SK is a stopper for $\sin^2\theta^{\rm fit}_{\rm RCT}$. If the value of $\sin^2\theta^{\rm fit}_{\rm RCT}$ is constrained by the reactor experiments strongly, the large difference between the signals and estimated signal from fitting parameter at Korea survives, and then fake hierarchy is excluded more strongly. This fact does not mean that SK is not necessary for the T2KK with reactor experiment. The another role of SK is constraining $\delta^{\rm fit}$. In A^e the term of $\sin\delta$ is comparable the matter effect term in Korea, So $\delta^{\rm fit}$ can make the contribution of the matter effect term weak by the $\sin\delta$ term of A^e; see eq. (57b). But if $\delta^{\rm fit}$ is fitted like the above case, $\sin\delta^{\rm fit}$ produces the difference of the event number at SK, because the magnitude of the matter effect terms is smaller than the $\sin\delta$ term at SK in eq. (57b).

For the B^e, the related part of $\sin^2 2\theta_{\rm RCT}$ is the term of $\cos\delta$, which is proportional to $1/\sqrt{\sin^2 2\theta_{\rm RCT}}$; see eq. (57d). We can find in Fig. 11 that $\sin^2 2\theta^{\rm fit}_{\rm RCT}$ tends different of $\sin^2 2\theta^{\rm input}_{\rm RCT}$ by factor 2. For the normal hierarchy case, the magnitude of the $cos\theta^{\rm fit}_{\rm RCT}$ term in eq. (74) is small, then we can use the phase difference. As we learn in the previous section, for the inverted hierarchy case too small $\sin^2 2\theta^{\rm fit}_{\rm RCT}$ enhances the power of $\cos\delta^{\rm fit}$ and then difference of the oscillation phase is diluted. If we use the strong constraint for $\sin^2 2\theta_{\rm RCT}$, it is very difficult that $\sin^2 2\theta^{\rm fit}_{\rm RCT}$ takes small value, then the case for the inverted hierarchy case also receive the benefits of the B^e.

The measurement of the CP phase are not so affected from the reactor experiments. About the measurement of CP phase, the effect of constrain of $\sin^2 2\theta_{\rm RCT}$ does not significantly improve the error of δ , because the contribution from the CP phase in the χ^2 function is independent of the value of $\sin^2 2\theta_{\rm RCT}$, as we check in the section 6.3. For the $\sin^2 2\theta_{\rm RCT}$ measurements, once we constrain the mass hierarchy pattern, the freedom of $\sin^2 2\theta_{\rm RCT}$ is strongly constrained by the difference of the magnitude of the $\nu_\mu \to \nu_e$ transition probability. Then the large difference allows us to measure the $\sin^2 2\theta_{\rm RCT}$ pre-

cisely. Fig. 13 shows that the error of $\sin^2 2\theta_{\rm RCT}$ is already 0.01 by only T2KK. But the expected error the future reactor experiment is almost same size as the sensitivity to $\sin^2 2\theta_{\rm RCT}$, which is about 0.01. Therefore we can expected more strong constraint of $\sin^2 2\theta_{\rm RCT}$ by the combination of the T2KK and the reactor experiments. We can conclude that the constraint from the reactor neutrino experiment seems very powerful for determining the mass hierarchy, especially for the inverted hierarchy. However the measurement of the δ not expected to be much improved by the combining analysis. Finally, the combining analysis gives more tiny constraint on $\sin^2 2\theta_{\rm RCT}$. We will check the power of the reactor experiment by the numerical calculation in the next and the after next sub sections.

7.2 Mass hierarchy

In this sub section, we would like to check the power of the future reactor experiment. Here we assume that the $\sin^2 2\theta_{\rm RCT}$ will be constrained by the reactor experiment till the end of T2KK experiment, and the error of $\sin^2 2\theta_{\rm RCT}$ is 0.01 for any $\sin^2 2\theta_{\rm RCT}$. Then it constraints can be added into the χ^2 function. The new $\chi^2_{\rm para}$ can be written as,

$$\chi^2_{\rm para} = \left(\frac{(\delta m^2_{12})^{\rm fit} - (\delta m^2_{12})^{\rm input}}{0.6\times 10^{-5}}\right)^2 + \left(\frac{\sin^2 2\theta^{\rm fit}_{\rm SOL} - \sin^2 2\theta^{\rm input}_{\rm SOL}}{0.07}\right)^2 + \left(\frac{\sin^2 2\theta^{\rm fit}_{\rm RCT} - \sin^2 2\theta^{\rm input}_{\rm RCT}}{0.01}\right)^2 . \quad (75)$$

The first second terms are same as eq. (73). The last is the new term which comes from the reactor experiments.

By using the new $\chi^2_{\rm para}$, we again investigate the best combination of the off-axis-angles and the baseline length for the Tokai-to-Korea baselines. We show the same figures in Figs.14 and 15 as Fig. 8 Fig. 9 but including the the constraint on the $\sin^2 2\theta_{\rm RCT}$ from the future reacotr experiment, $\Delta(\sin^2 2\theta_{\rm RCT}) = 0.01$ into the $\Delta\chi^2$ function. We find that the most of all data point improve from the Fig. 8 and Fig. 9. The best combinations of the off-axis angle and the baseline length at Korea are not changed by this analysis, the values of minimum $\Delta\chi^2$ is increased from 18 to 23 in Fig. 14, and the 16 to 22 in Fig. 15. The data points for the inverted hierarchy, Fig. 15, are much improved than that for the normal hierarchy case. From the discussion in the previous sub section, we expected that the origin of the large imporvement comes from the B^e. To make the origin of the improvement clear, we also check the sensitivity of the mass hierarchy pattern and the fitting parameters for the minimum $\Delta\chi^2$ points. We show the

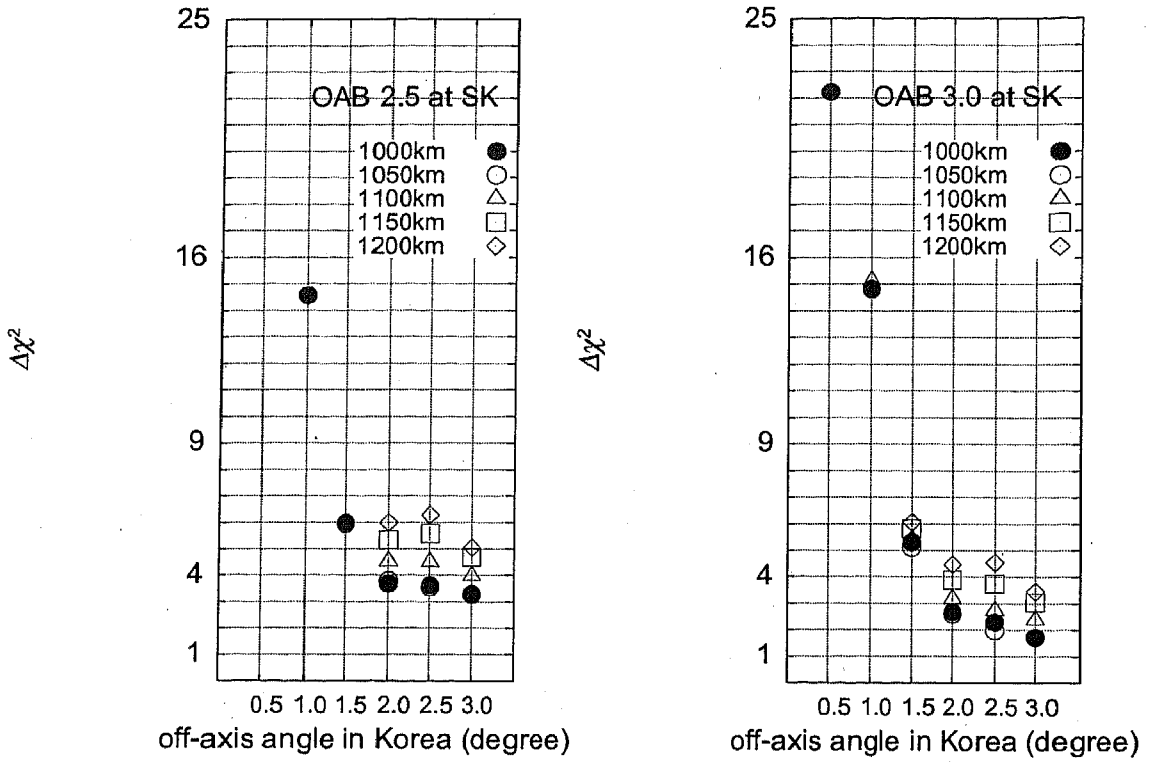

Figure 14: The same figure as Fig. 8 but the constraint on the $\sin^2 2\theta_{\rm RCT}$ from the future reactor experiment, $\Delta(\sin^2 2\theta_{\rm RCT}) = 0.01$ is included the $\Delta\chi^2$ function. The signal is calculated by the normal hierarchy but the fitting parameter is assumed in the inverted hierarchy.

sensitivity of the capability of determining the mass hierarchy by the T2KK with the reactor experiments in Fig. 16, which is the same figure as Fig. 10. We find that the limit of $\sin^2 2\theta_{\rm RCT}$ for determining the neutrino mass hierarchy for any δ is improved, from 0.06 to 0.45 for the normal hierachy, and 0.09 to 0.55 for the inverted hierarchy. The remarkable point that the the fake hierachy obtaion the capability as much as that for the normal hierarchy, and the CP dependence in Fig. 16(b) is weaker than that shown in Fig. 16(b). From the above facts that we conlude that the constraining $\sin^2 2\theta_{\rm RCT}$ by the future neutrino oscillation experiments is very powerful tool for determining the neutrino mass hierarchy.

The best combination for 2.5° OAB SK is also improved. We show the sensitivity to the sign of Δ_{13} for the combination the OAB 2.5° at SK and 1° at $L = 10000$ km in Fig. 17. We find that the even for this combination, the sign of δm^2_{13} can be constrained at 3-σ*level* for $\sin^2 2\theta_{\rm RCT} > 0.07$.

At the final of this subsection, we check how important SK is in the combining analysis by the changing the volume ratio between near and far. We show in Fig. 18 the

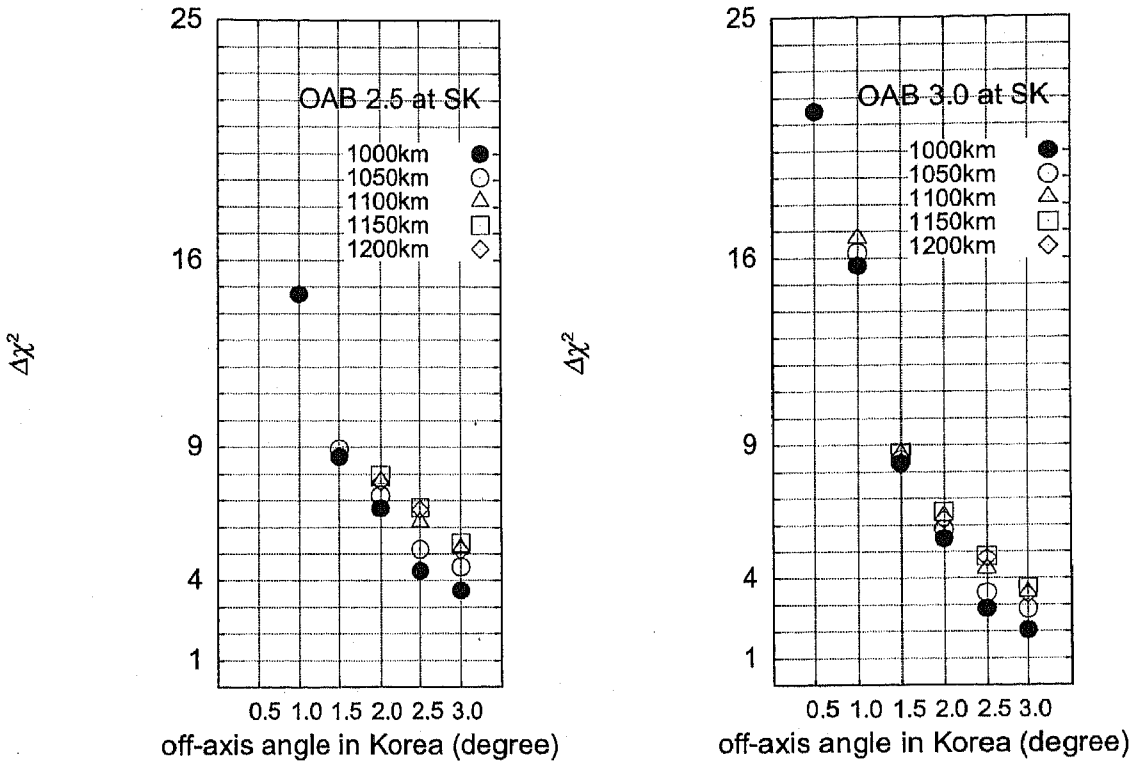

Figure 15: The same figure as Fig. 9 but the constraint on the $\sin^2 2\theta_{\rm RCT}$ from the future reactor experiment, $\Delta(\sin^2 2\theta_{\rm RCT}) = 0.01$ is included into the $\Delta\chi^2$ function. The signal is calculated by the inverted hierarchy but the fitting parameter is assumed in the normal hierarchy.

minimum $\Delta\chi^2$ as functions of the volume ratio of the near (Kamioka) and far (Korea) detectors while keeping the total volume at 600 kt for 5×10^{21} POT. We assume the normal hierarchy for the input and the inverted hierarchy in the fit. We examine 8 cases, for $\sin^2 2\theta_{\rm RCT}^{\rm input} = 0.1$ (solid lines) and $\sin^2 2\theta_{\rm RCT}^{\rm input} = 0.06$ (dotted lines), and for $\delta^{\rm input}$ $= 0°$ (a), $90°$ (b), $180°$ (c), and $-90°$(d). It is clearly seen from Fig. 18 that a 600 kt detector in Kamioka alone cannot resolve the mass hierarchy at all, because there is a little difference in $\nu_\mu \to \nu_e$ transition probability between the normal hierarchy and the inverted hierarchy. On the other hand, in the case of only a Korean detector with 600 kt, the minimum $\Delta\chi^2$ value is not much smaller than the best case. This is because the constraint of $\sin^2 2\theta_{\rm RCT}$ from the future reactor neutrino experiment replaces the role of the near detector which measures the $\nu_\mu \to \nu_e$ transition at low energies where the matter effect is small. We find that the minimum $\Delta\chi^2$ value of 23.5 in Fig. 18(a) at the volume ratio of 1:5 ($\approx 22.5 : 100$) is about 4.5 times as large as the minimum $\Delta\chi^2$ value in Fig. 14(b), confirming the dominance of the statistical error in our analysis. If we request that the minimum $\Delta\chi^2$ should be at least 80% of its optimal value, then the

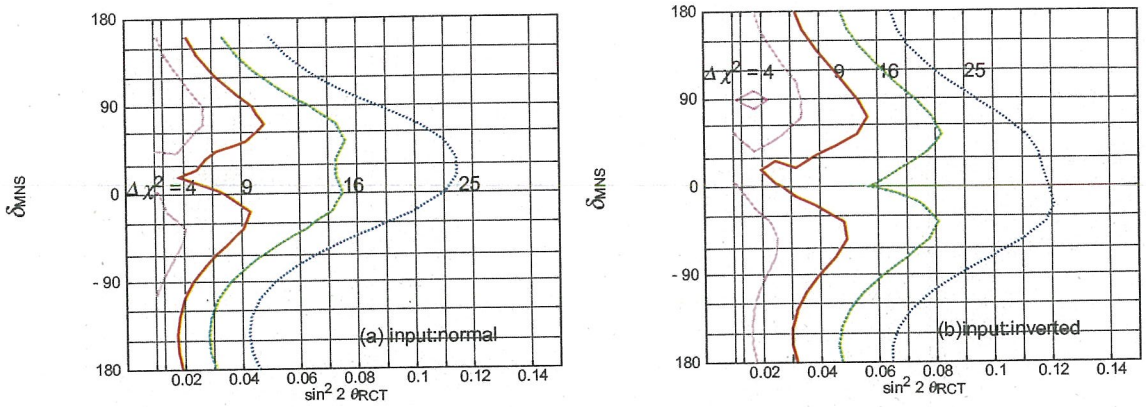

Figure 16: The same figure as Fig. 10 but the constraint from the reactor experiment is included

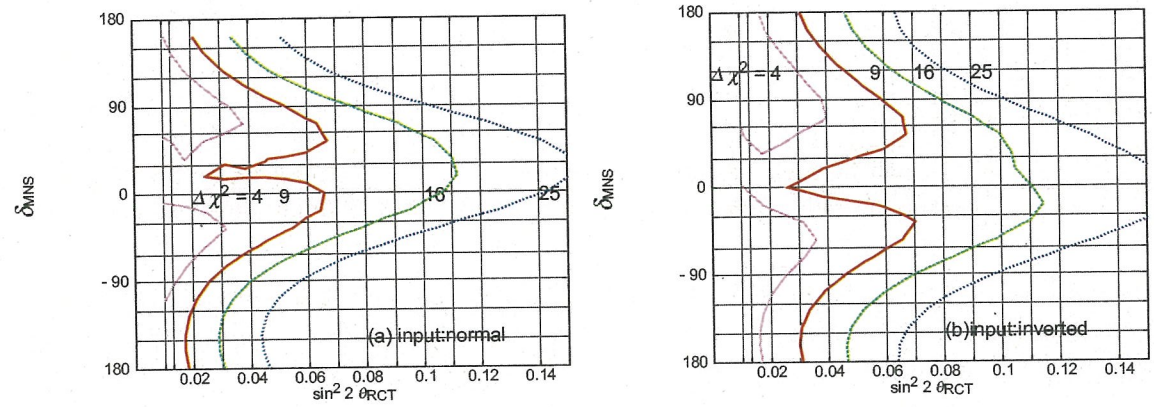

Figure 17: The same figure as Fig. 12 but the constraint from the reactor experiment is included

near-to-far volume ratio should be between 0.5 : 5.5 and 2.5 : 3.5. More volumes should be given to the far detector than to the near detector.

7.3 CP phase

In this subsection, we study the how much the constraint on $\sin^2 2\theta_{\rm RCT}$ improves the measurement of CP phase and $\sin^2 2\theta_{\rm RCT}$. We show in Fig. 19 and Fig. 20 regions allowed by this experiment in the plane of $\sin^2 2\theta_{\rm RCT}$ and δ. The mean values of the input data are calculated for the parameters of eq. (55). In each figure, input points $(\sin^2 2\theta_{\rm RCT}^{\rm input}, \delta^{\rm input})$ are shown by solid-circles for $\sin^2 2\theta_{\rm RCT}^{\rm input}$ between 0.02 and 0.1, with an interval of 0.02, and for four values of $\delta^{\rm input}$; 0°(a), 90°(b), 180°(c), and −90°(d). The regions where the minimum $\Delta\chi^2$ value is less than 1, 4, 9 are depicted by solid, dashed, and dotted boundaries, respectively. Fig. 19 is for the normal hierarchy, and Fig. 20 is for the inverted hierarchy. From these figures, we find that δ can be constrained to $\pm 30°$ at

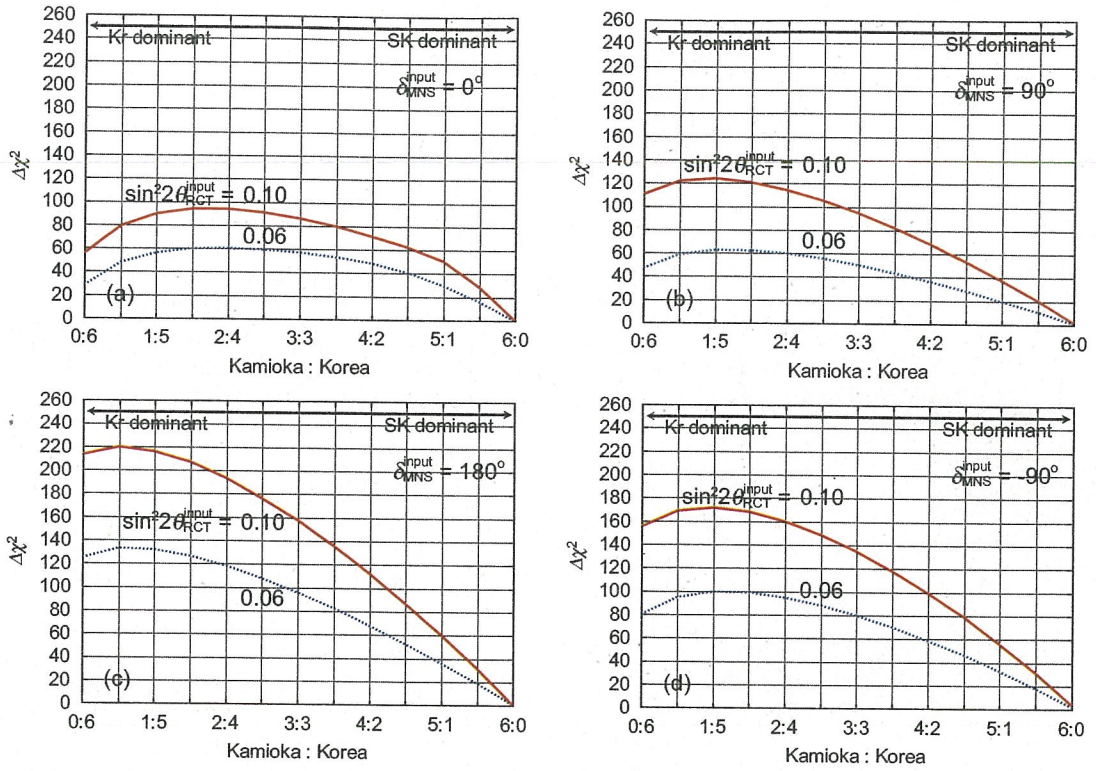

Figure 18: Optimal ratio of the fiducial volumes of two detectors, one at Kamioka ($L = 295$ km) and the other at $L = 1000$ km in Korea, for determining the neutrino mass hierarchy. The input data are calculated for the normal hierarchy at $\delta m^2_{13} = 2.5\times10^{-3}\text{eV}^2$ and the minimum $\Delta\chi^2$ of the fit with the wrong hierarchy is shown for $\sin^2 2\theta^{\text{input}}_{\text{RCT}} = 0.10$ (solid lines) and 0.06 (dotted lines) and for $\delta^{\text{input}} = 0°$ (a), 90° (b), 180° (c), and 270° (d), when the sum of the fiducial volumes is fixed at 600 kt. The other parameters are same as those in Fig. 4 (d), and the results are calculated for 5×10^{21}POT.

1-σ level, when $\sin^2 2\theta^{\text{input}}_{\text{RCT}} \gtrsim 0.02$ as long as the neutrino mass hierarchy is determined.

As shown in Fig. 16(a) and (b), the mass hierarchy cannot be determined at 3-σ level ($\Delta\chi^2 > 9$) when $\sin^2 2\theta^{\text{input}}_{\text{RCT}}$ is too small. In case of the input parameters of Fig. 19 for the normal hierarchy, this is the case for $\sin^2 2\theta^{\text{input}}_{\text{RCT}} = 0.02$ at $\delta^{\text{input}} = 0°$ (a), $\sin^2 2\theta^{\text{input}}_{\text{RCT}} = 0.02$ and 0.04 at $\delta^{\text{input}} = 90°$ (b), and $\sin^2 2\theta^{\text{input}}_{\text{RCT}} = 0.02$ at $\delta^{\text{input}} = -90°$(d). For those input points, there appear an additional allowed region whose center (local minimum of $\Delta\chi^2$) is shown by a solid square. No extra allowed region appears for $\delta = 180°$ in Fig. 19(c), in accordance with the result of Fig. 16(a). In case of Fig. 20 for the inverted hierarchy, the local minimum appears for $\sin^2 2\theta^{\text{input}}_{\text{RCT}} = 0.02$ at $\delta^{\text{input}} = 0°$ (a), $\sin^2 2\theta^{\text{input}}_{\text{RCT}} = 0.02$ and 0.04 at $\delta^{\text{input}} = 90°$ (b), $\sin^2 2\theta^{\text{input}}_{\text{RCT}} = 0.02$ at $\delta^{\text{input}} = 180°$ (c), and $\sin^2 2\theta^{\text{input}}_{\text{RCT}} = 0.02$ at $\delta^{\text{input}} = -90°$(d).

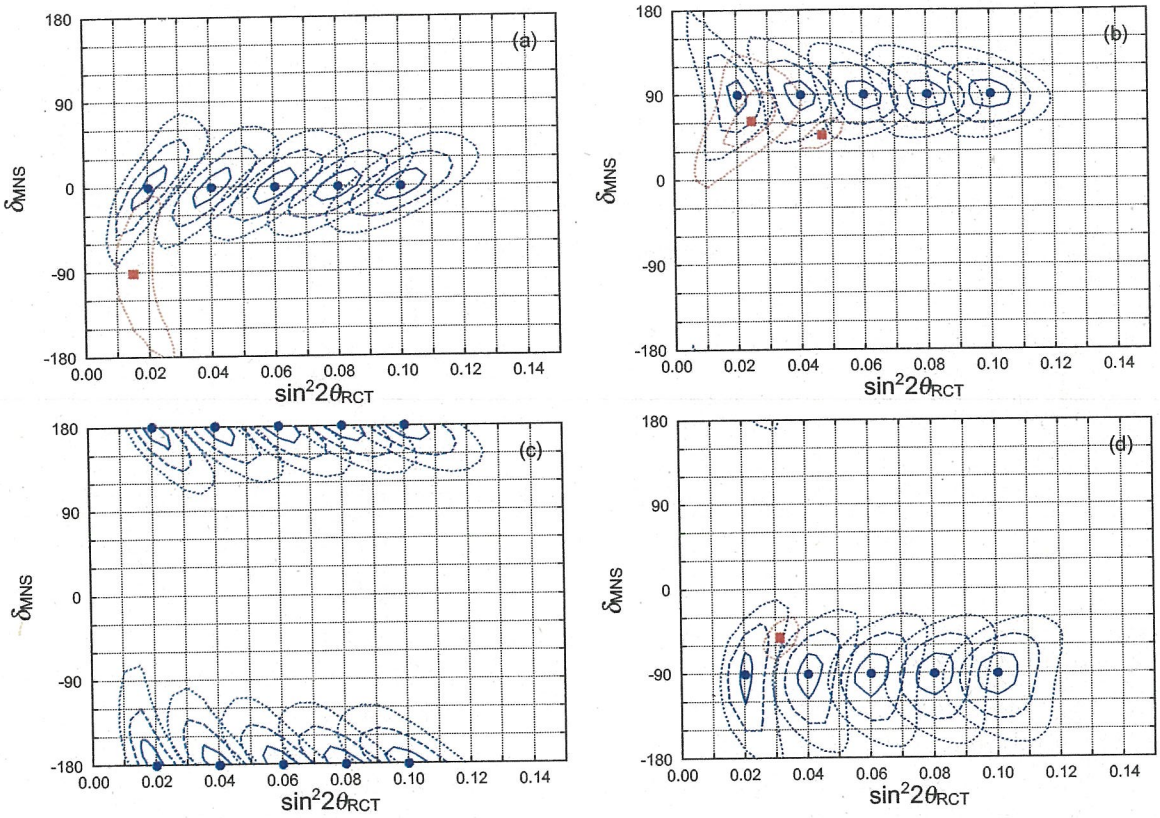

Figure 19: Capability of the T2KK two detector experiment with the future reactor experiment for measuring $\sin^2 2\theta_{\rm RCT}$ and δ . Allowed regions in the plane of $\sin^2 2\theta_{\rm RCT}$ and δ are shown for a combination of 3.0°OAB at SK and 0.5°at $L = 1000$km with a 100 kt water Čerenkov detector after 5 years of running (5×10^{21} POT). The input values of $\sin^2 2\theta_{\rm RCT}$ are 0.02, 0.04, 0.06, 0.08 and 0.10 for $\delta = 0°$(a), 90°(b), 180°(c), and $-90°$(d). The normal hierarchy is assumed at $m_3^2 - m_1^2 = 2.5 \times 10^{-3}{\rm eV}^2$, and the other parameters are the same as those in Fig. 16. The input points are shown as solid blobs, where $\Delta\chi^2 = 0$ by definition. The 1-, 2-, and 3-σ contours are then shown by solid, dashed, and dotted lines, respectively. For the input values of $(\sin^2 2\theta_{\rm RCT}^{\rm input}, \delta^{\rm input}) = (0.02, 0°)$ (a), (0.02, 90°) and (0.04, 90°) (b) and (0.02, $-90°$) (d), there appear additional allowed regions when the mass hierarchy is chosen with the wrong sign in the fit, where the local minimal $\Delta\chi^2$ point is depicted by a solid square.

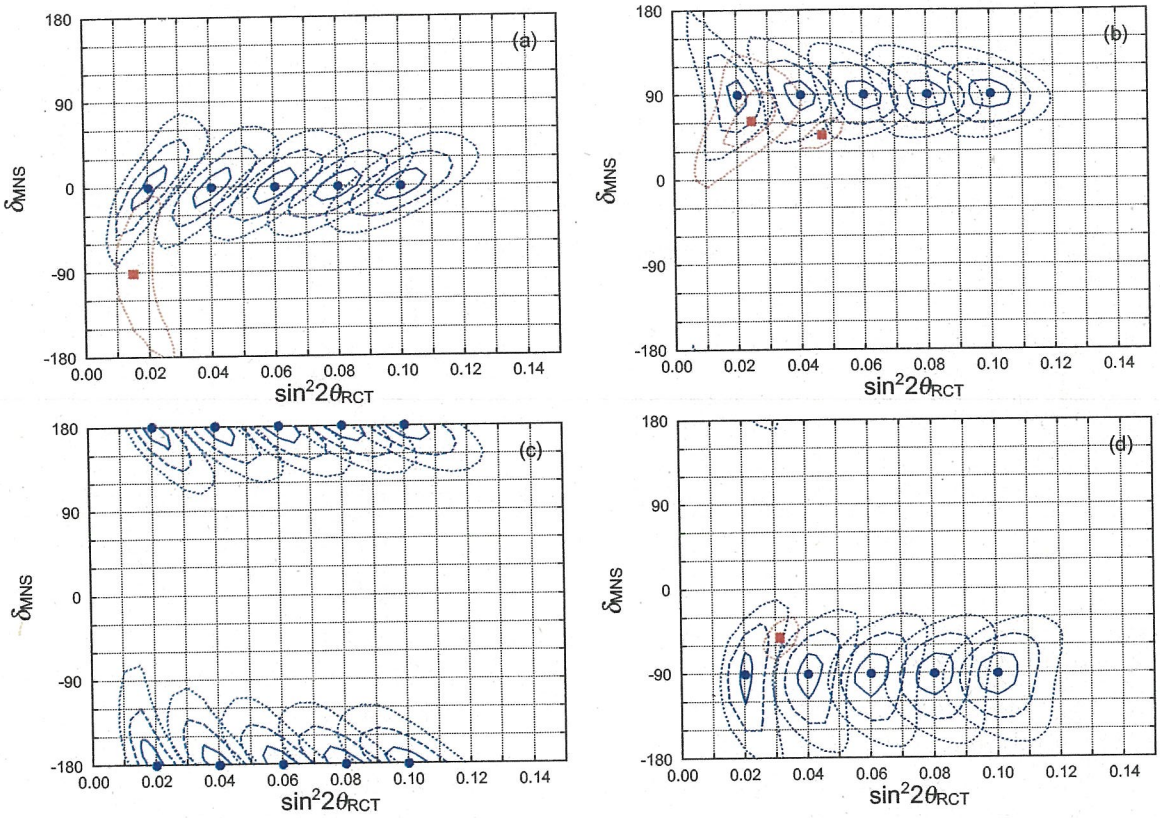

Figure 19: Capability of the T2KK two detector experiment with the future reactor experiment for measuring $\sin^2 2\theta_{\rm RCT}$ and δ . Allowed regions in the plane of $\sin^2 2\theta_{\rm RCT}$ and δ are shown for a combination of 3.0°OAB at SK and 0.5°at $L = 1000$km with a 100 kt water Čerenkov detector after 5 years of running (5×10^{21} POT). The input values of $\sin^2 2\theta_{\rm RCT}$ are 0.02, 0.04, 0.06, 0.08 and 0.10 for $\delta = 0°$(a), 90°(b), 180°(c), and $-90°$(d). The normal hierarchy is assumed at $m_3^2 - m_1^2 = 2.5 \times 10^{-3}{\rm eV}^2$, and the other parameters are the same as those in Fig. 16. The input points are shown as solid blobs, where $\Delta\chi^2 = 0$ by definition. The 1-, 2-, and 3-σ contours are then shown by solid, dashed, and dotted lines, respectively. For the input values of $(\sin^2 2\theta_{\rm RCT}^{\rm input}, \delta^{\rm input}) = (0.02, 0°)$ (a), (0.02, 90°) and (0.04, 90°) (b) and (0.02, $-90°$) (d), there appear additional allowed regions when the mass hierarchy is chosen with the wrong sign in the fit, where the local minimal $\Delta\chi^2$ point is depicted by a solid square.

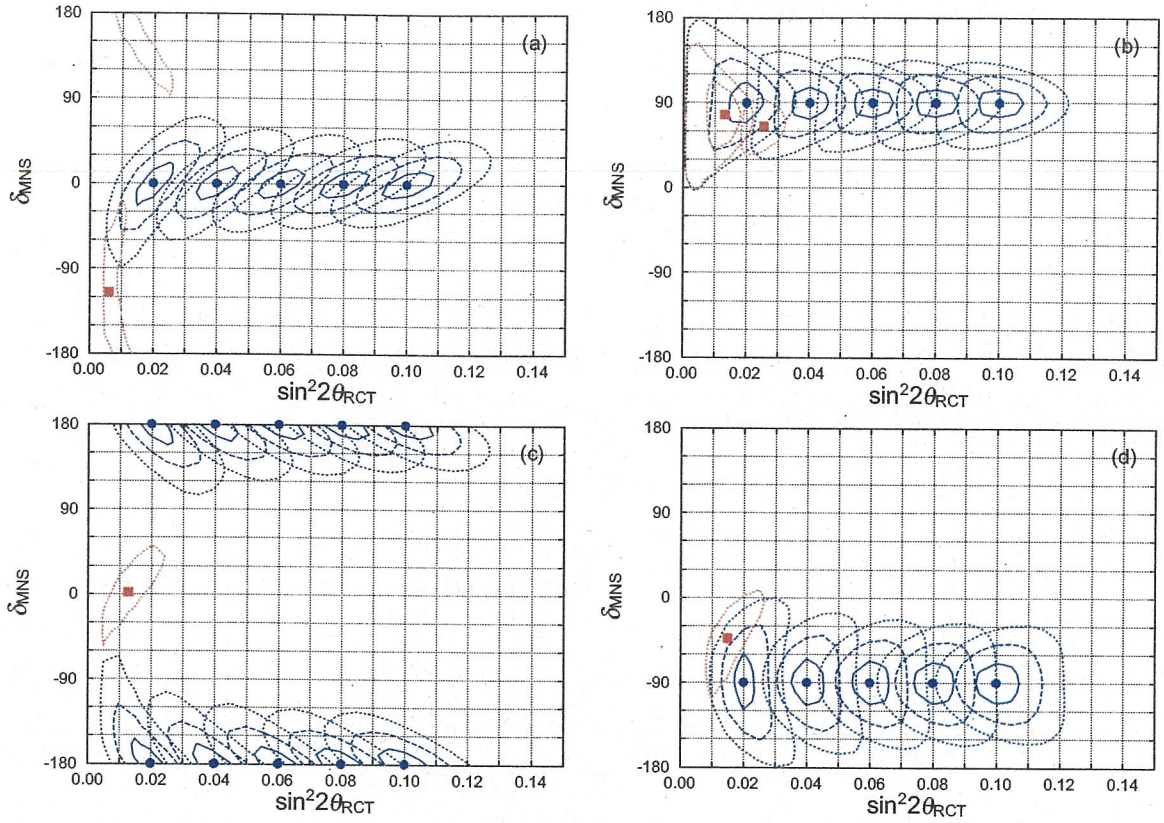

Figure 20: The same as Fig. 19, but when the events are calculated for the inverted hierarchy, *i.e.*, $m_3^2 - m_1^2 = -2.5 \times 10^{-3}\text{eV}^2$. Just like in Fig. 19, additional allowed regions, when the wrong sign of the $m_3^2 - m_1^2$ is chosen in the fit, appear for all the δ^{input} cases at $\sin^2 2\theta_{\text{RCT}}^{\text{input}} = 0.02$, and for $\delta^{\text{input}} = 90^\circ$ (b) at $\sin^2 2\theta_{\text{RCT}}^{\text{input}} = 0.04$.

8 Earth Matter Effect in T2KK

8.1 The effect of the matter density distribution

We saw the importance of the matter effect in the actual analysis. But in the previous analysis, we assume the the matter profile along the baseline is constant and we put the mean value and its error of the matter density along the baseline by hands. Actually, the matter profile along the baseline is complicated and its error seems to be larger than 3%. In this section, we study the earth matter effect in the T2KK experiment. At first, we study the correction of the matter density distribution to the $\nu_\mu \to \nu_e$ oscillation.

Now we consider that the matter profile along the baseline is not constant. In this case, it is too difficult to solve the schorödinger equations analytically. We use again the approximation formula to understand the effect of the matter density distribution. We can start the discussion from eq. (32), because this formulation is correct for any $a(x)$. In eq. (32), the integration of $a(x)$ is necessary, and to treat this integration analytically,

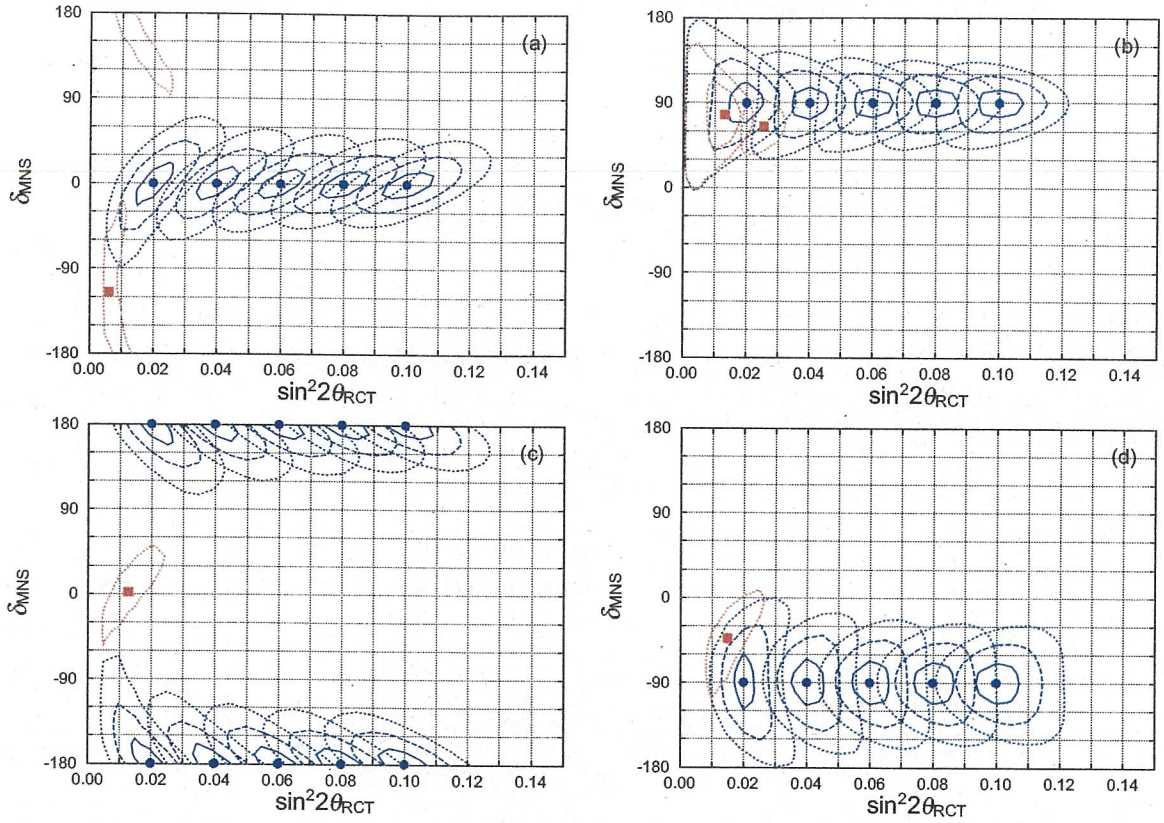

Figure 20: The same as Fig. 19, but when the events are calculated for the inverted hierarchy, *i.e.*, $m_3^2 - m_1^2 = -2.5 \times 10^{-3}\text{eV}^2$. Just like in Fig. 19, additional allowed regions, when the wrong sign of the $m_3^2 - m_1^2$ is chosen in the fit, appear for all the δ^{input} cases at $\sin^2 2\theta_{\text{RCT}}^{\text{input}} = 0.02$, and for $\delta^{\text{input}} = 90^\circ$ (b) at $\sin^2 2\theta_{\text{RCT}}^{\text{input}} = 0.04$.

8 Earth Matter Effect in T2KK

8.1 The effect of the matter density distribution

We saw the importance of the matter effect in the actual analysis. But in the previous analysis, we assume the the matter profile along the baseline is constant and we put the mean value and its error of the matter density along the baseline by hands. Actually, the matter profile along the baseline is complicated and its error seems to be larger than 3%. In this section, we study the earth matter effect in the T2KK experiment. At first, we study the correction of the matter density distribution to the $\nu_\mu \to \nu_e$ oscillation.

Now we consider that the matter profile along the baseline is not constant. In this case, it is too difficult to solve the schorödinger equations analytically. We use again the approximation formula to understand the effect of the matter density distribution. We can start the discussion from eq. (32), because this formulation is correct for any $a(x)$. In eq. (32), the integration of $a(x)$ is necessary, and to treat this integration analytically,

we adopts the Fourier expansion to $a(x)$.

$$a(x) = \sum_{n=-\infty}^{\infty} a_n e^{-i\frac{2n\pi x}{L}}$$

$$= a_0 \left\{ 1 + 2\sum_{k=1}^{\infty} \left[Re\,(r_k) \cos\left(\frac{2\pi kx}{L}\right) + Im\,(r_k) \sin\left(\frac{2\pi kx}{L}\right) \right] \right\} . \tag{76}$$

Here a_0 gives the average matter effect, $Re(r_k)$ terms give fluctuations which are symetric about the center of the baseline, and $Im(r_k)$ terms give asymmetric fluctuations. We can separate the Fourier modes from the constant mode in H_1.

$$H_1 = \bar{H}_1 + \delta H_1 , \tag{77}$$

$$\bar{H}_1 = \frac{1}{2E} U \begin{pmatrix} 0 & 0 & 0 \\ 0 & \delta m^2_{12} & 0 \\ 0 & 0 & 0 \end{pmatrix} U^\dagger + \frac{1}{2E} \begin{pmatrix} a_0 & 0 & 0 \\ 0 & 0 & 0 \\ 0 & 0 & 0 \end{pmatrix} , \tag{78}$$

$$\delta H_1 = \sum_{n=1}^{\infty} \frac{a_0}{E} \left[Re\,(r_k) \cos\left(\frac{2\pi nx}{L}\right) + Im\,(r_k) \sin\left(\frac{2\pi nx}{L}\right) \right] \begin{pmatrix} 1 & 0 & 0 \\ 0 & 0 & 0 \\ 0 & 0 & 0 \end{pmatrix} . \tag{79}$$

Because the $\bar{H}_1$ is constant along the baseline, we can identified as the $\bar{H}_1$ is the H_1 which we treated in the previous sections. The first order concretions of the Fourier modes to the time evolution operator can be obtained as,

$$\delta S_1(L)_{\beta\alpha} = -i \langle \nu_\beta | \left(\int_0^L dx e^{iH_0(x-L)} \delta H_1(x) e^{-iH_0 x} \right) | \nu_\alpha \rangle$$

$$= \sum_{n\neq 0} \left[U_{\beta 3} U^*_{e3} \delta_{\alpha e} f_- + \delta_{\beta e} U_{e3} U^*_{\alpha 3} f_+ - U_{\beta 3} U^*_{\alpha 3} |U_{e3}|^2 (f_- + f_+) \right]$$

$$\times \left(e^{-i\Delta_{13}} - 1 \right) \frac{a_n L}{2\Delta_{13} E} , \tag{80}$$

$$f_\pm \equiv \left(1 \pm \frac{\Delta_{13}}{2\pi n} \right)^{-1} . \tag{81}$$

Notice that there is no $\frac{a_k L}{2E}$ term in eq. (90). Such term ordinary comes from the integration of the constant but now such term is dropped by the factor $e^{-i\frac{2\pi n}{L}x}$. Since we interested in the matter effect term in $\nu_\mu \to \nu_\mu$ survival mode and the $\nu_\mu \to \nu_e$ transition mode, we substitute the flavor index into α, and β. Then we find that

$$\delta S_1(L)_{\mu\mu} = -4 \frac{a_0}{\delta m^2_{13}} |U_{e3}|^2 \sum_1^\infty (r_k) \frac{\Delta^2_{13}}{\Delta^2_{13} - 4k^2\pi^2} \left(1 - e^{-i\Delta_{13}} \right) , \tag{82a}$$

$$\delta S_1(L)_{e\mu} = U_{e3}U^*_{\mu 3}\frac{a_0}{\delta m^2_{13}}\left(\sum_1^\infty Re(r_k)\frac{\Delta^2_{13}}{\Delta^2_{13}-4k^2\pi^2} - i\sum_1^\infty Im(r_k)\frac{k\pi\Delta_{13}}{\Delta^2_{13}-4k^2\pi^2}\right)$$

$$\times\left(1-e^{-i\Delta_{13}}\right). \tag{82b}$$

We find in eq. (82) that the Fourier modes of the matter effect is suppressed by the Fourier coefficient, $1/(\Delta^2_{13}-4k^2\pi^2)$. So the terms for large k mode are strongly suppressed in the neutrino oscillation experiment [30]. Rough characteristic of the matter profile along the baseline is more important in the neutrino oscillation. We also find that this suppression factor has the singular point around $\Delta_{13}\sim\pi$. However around Δ_{13} , δS_1 term becomes 0 due to the oscillation factor. We find that the $\delta S_{\beta\alpha}$ is almost same as the leading term of S matrix; see eq. (36). The difference is the factor comes from the matter effect. So when we calculate the transition probability, the term of $Im(r_k)$ can not coupled to the other imaginary part, and hence the imaginary part of Fourier modes does not appear in the first order collection.

Finally we obtain the correction terms from the Fourier mode. For the ν_μ mode,

$$P_{\nu_\mu\to\nu_\mu} = 1-\sin^2 2\theta_{\rm ATM}\left(1+A^\mu+\delta A^\mu\right)\sin^2\left(\frac{\Delta_{13}}{2}+B^\mu\right),$$

$$\delta A^\mu = -\frac{a}{\delta m^2_{13}}|U_{e3}|^2\sum_1^\infty(r_k)\frac{\Delta^2_{13}}{\Delta^2_{13}-4k^2\pi^2}\frac{1-2|U_{\mu 3}|^2}{1-|U_{\mu 3}|^2}, \tag{83}$$

where A^μ and B^μ are the contribution from the average matter effect and the Δ_{12}, which are same as in eq. (53). As well as δA^μ, δA^μ is almost zero as long as the $\theta_{\rm ATM}$ is the maximal mixing. Therefore the ν_μ survival mode is affected by not only the constant but also the density distribution effect.

Regarding as the $\nu_\mu\to\nu_e$ transition mode, the

$$P_{\nu_\mu\to\nu_e} = 4\sin^2\theta_{\rm ATM}\sin^2\theta_{\rm RCT}\left\{\left(1+A^e+\delta A^e\right)\sin^2\left(\frac{\Delta_{13}}{2}\right)+B^e\sin\Delta_{13}\right\}+C^e,$$

$$\delta A^e = \frac{4a_0}{\delta m^2_{13}}\left(Re(r_k)\frac{\Delta^2_{13}}{\Delta^2_{13}-4k^2\pi^2}\right). \tag{84}$$

Here we find that the correction from the Fourier mode only appear the correction to the amplitude. The interesting point that this term is also sensitive to the mass hierarchy pattern. But the sign of δA^e depends on the oscillation phase, and sign of r_k. Sometimes this term helps us to determine the neutrino mass hierarchy, but sometimes they absorb the contribution of the matter effect of A^e. Studying both the magnitude and sign of Rer_k are important.

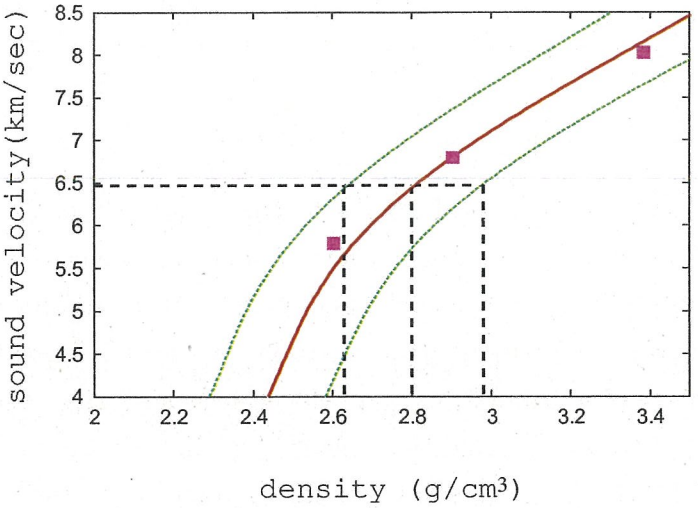

Figure 21: The relation between densities and sound velocities shown in Ref. [31]. The solid line is mean value of the density, and the dotted lines of both sides shows the error of the estimated density. Dashed lines shows how to estimate the density and its error when $V_p = 6.5$ km/sec. Three points shows the reference points shown in Preliminarily Reference Earth Model (PREM) [32].

8.2 Earth matter profile in T2KK

In this section we examine the matter profile along the baseline of Tokai-to-Kamioka and Tokai-to-Korea, and then estimate the average and the Fourier modes of the matter effects along the baselines. Fortunately, there are many measurement of the crustal structure around the T2K and the Tokai-to-Korea baselines by using the seismic wave reflection. We can estimate the depth of the boundaries of each layer from the reflection points and the average matter density from the velocity of the seismic wave. Most of works in geophysics show only the seismic wave velocity and not shows the their estimation of the mean value of the density for each layer. In this section, we use one of the density-velocity relation to estimate the matter density from the velocity measured by geophysicists [31]. We show the density-velocity relation shown in Ref. [31]. The solid line shows the relation between sound velocity and density, which can be expressed as

$$\rho = -0.00283V_p^4 + 0.0704V_p^3 - 0.598V_p^2 + 2.23V_p - 0.7\,. \tag{85}$$

Here V_p is the sound velocity inside the matter. The dashed lines of both sides show the error of the estimated density. The error of the estimated density is about 6%, which is expected to becomes smaller by combining the other kind of measurements, gravity anomaly magnetic anomaly, actually digging the crust and so on. Dashed lines show how to estimate the density and its error when $V_p = 6.5$ km/sec. Three points show the reference points shown in Preliminarily Reference Earth Model (PREM) [32], which is often

used to estimate average density along the baseline for various LBL experiments. These points are enough close the mean value of the densities so the difference is negligibly small.

At first, we check the matter profile for the T2K experiment. We show the Tokai-to-Kamioka baselines and the matter profile along the T2K baseline in Fig. 22. The upper figure in Fig. 22 shows the Tokai-to-Kamioka baselines. The scale on the baseline shows the distance from J-PARC. The each interval is 50 km. The shadow region is Fossa Magna region [33]. There is a border between two continental plate, North America Plate and Eurasia Plate. In this region, the sediment layer is deeper than the usual. On the other hand, the lower one shows the cross section view of the T2K experiment. The horizontal line shows the distance from the J-PARC and the vertical axis means the depth from the sea level. The number of each region means the average density. The unit is g/cm^3. In this figure, the thickness of the sediment layer except for Fossa Magna region is assumed 1km and we refer the geological map to identify the kind of rock [34]. At the Fossa Magna, the sediment layer is down to 6 km [33]. The most of sediment layer is composed by milestones, sand stone,and so on [34]. Ref. [33] shows that the density of such sediment layer is 2.5g/cm^3. On the other hand, the sediment layer near the Kamioka, $L > 230$ km, is composed by the granite, which composes the upper crust. The mean value of the granite is about 2.8g/cm^3

Now we can estimate the average density and the Fourier modes of the density along the baseline. When we average out the matter density along the baseline shown in Fig. 22, the average density is 2.6 g/cm^3. The possible source of the error is the systematic error of eq. (85) and the uncertainty of the boundary of each layer. In T2K case, the uncertainty of the boundary between sediment and the crust is estimated $\pm 300m$. Fortunately, the region which the neutrino goes through for longest time is Fossa Magna, and the uncertainty of boundary has no meanings near the Kamioka. So the error of the average density from the boundary uncertainty is 0.05%. It concludes that the most serious error to the average density is the error of the model, which is about 6%. We show the Fourier coefficient of the matter density profile along the Tokai-to-Kamioka baseline in Fig. 23. Black circle and white square shows the magnitude of the real and imaginary part of the Fourier mode, respectively. Fig. 23 shows that the magnitude of the each Fourier modes is less than 0.05g/cm^3. It is corresponds to $r_k < 0.02$. Because the corrections from the matter effect around the oscillation maximum to the $\nu_\mu \to \nu_e$ oscillation is about 10% in T2K experiment; see eq. (57b), the corrections of r_k is almost zero. In order to check the actual effect of the Fourier mode to the oscillation, we show the $\nu_\mu \to \nu_e$ transition probability at Kamioka around the oscillation maximum region for various δ and the matter density profile in Table. 2. The matter profile and the value of the Fourier mode

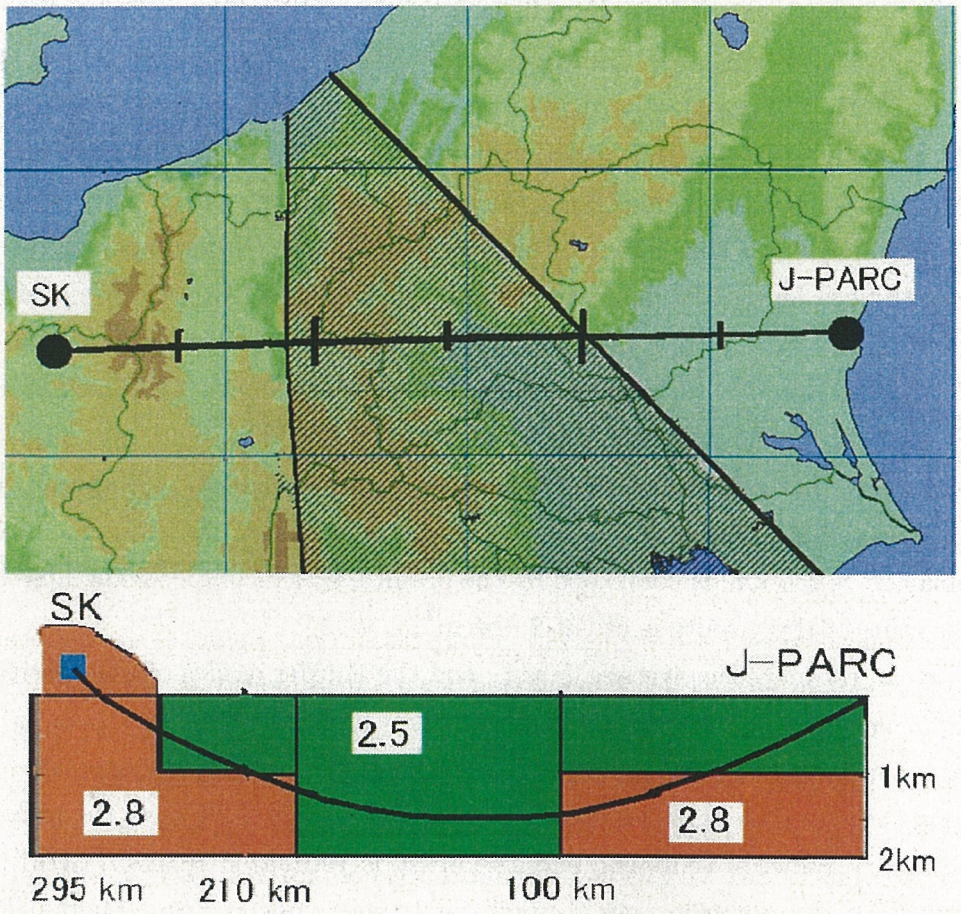

Figure 22: Upper: The Tokai-to-Kamioka baselines. The scale on the baseline shows the distance from J-PARC. The each interval corresponds to 50 km. The shadow region is Fossa Magna region [33]. Lower: The cross section view of the T2K experiment. The horizontal line shows the distance from the J-PARC and the vertical axis means the depth from the sea level. The number of each region means the average density. The unit is g/cm^3.

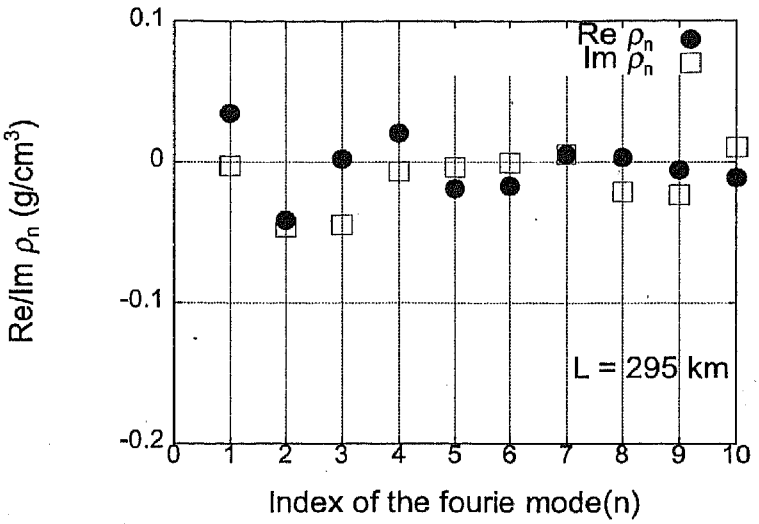

Figure 23: The Fourier mode of the matter density profile along the Tokai-to-Kamioka baseline. Black circle and white square shows the magnitude of the real and imaginary part of the Fourier mode, respectively.

of the density along the baseline are shown in Fig. 22 and Fig. 23, respectively. The transition probability shown in the table is calculated by the Runge-Kutta method. In the calculation, $\sin^2 2\theta_{\rm RCT} = 0.10$ and the normal hierarchy is assumed. In Table. 2,

$P_{\nu_\mu \to \nu_e}$	$\delta = 0°$	$90°$	$180°$	$-90°$
(1) Full matter effect	5.7643×10^{-2}	4.1063×10^{-2}	5.9300×10^{-2}	7.4114×10^{-2}
(2) Average matter effect only	5.7670×10^{-2}	4.1086×10^{-2}	5.9336×10^{-2}	7.4154×10^{-2}
(3) (2) + First Fourier mode	5.7633×10^{-2}	4.1054×10^{-2}	5.9285×10^{-2}	7.4101×10^{-2}
(4) (3) + Second Fourier mode	5.7642×10^{-2}	4.1062×10^{-2}	5.9296×10^{-2}	7.4114×10^{-2}

Table 2: The $\nu_\mu \to \nu_e$ transition probability at Kamioka around the oscillation maximum region for various δ and the matter density profile. The matter profile and the value of the Fourier mode of the density along the baseline are shown in Fig. 22 and Fig. 23, respectively. The transition probability shown in the table is calculated by the Runge-Kutta method. In the calculation, $\sin^2 2\theta_{\rm RCT} = 0.10$ and the normal hierarchy is assumed.

the difference between the transition probabilities for (1), full matter effect, and those for (2), average matter effect only, is less than 0.1 %. We also find in Table. 2 that the summation of the Fourier mode is enough up to the second Fourier mode in the T2K experiment.

Secondly, let us check the Tokai-to-Korea baseline. Because Tokai-to-Korea baselines go through deeper than one for T2K, the depth of the boundary between each layer is important for the matter profile. We show the cross section view along the baseline of Tokai-to-Korea in Fig. 24. The surface map (up) of the planned Tokai-to-Kamioka-and-

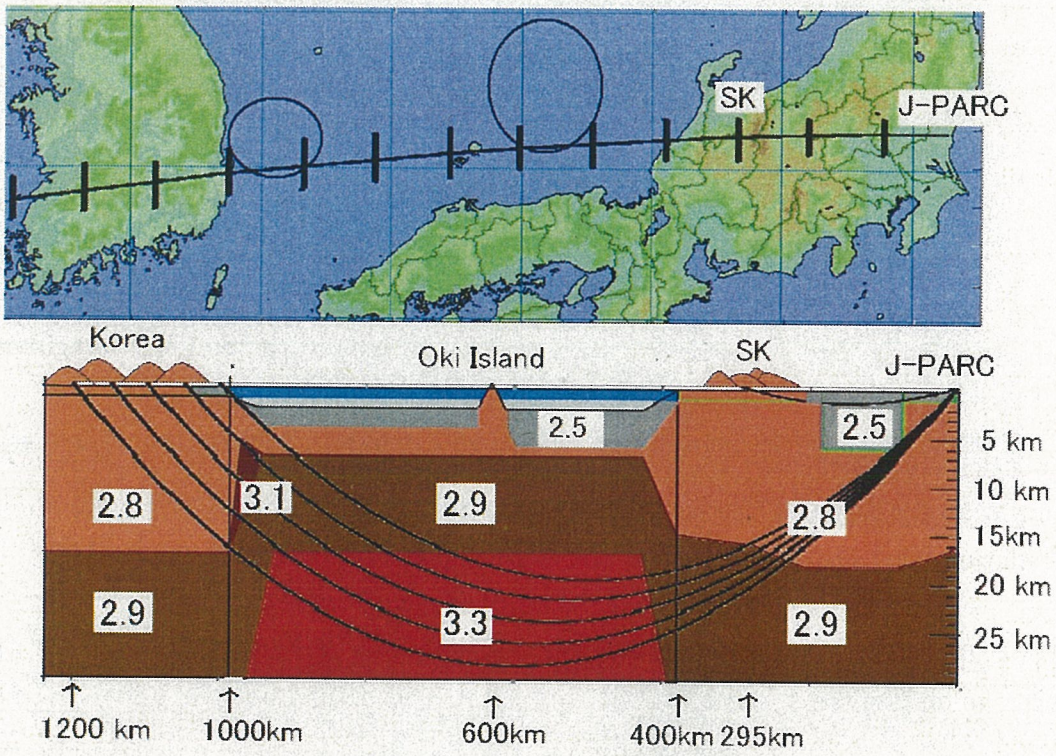

Figure 24: The surface map (up) of the planned Tokai-to-Kamioka-and-Korea (T2KK) experiment and the cross section view (bottom) and the surface map (bottom). The center of the neutrino beam line is shown in up figure. The distance from J-PARC is shown by the scale, of which interval is 100 km. The two circles shows the regions which is studied by geophysicists , Yamato basin (east side) and Tsushima/Ulleung basin (west side) [37, 38] In the bottom figure, each line corresponds to the baseline for $L = 1000$, 1050, 1100, 1150 and 1200 km, the numbers represents the average matter density, in units of g/cm^3, the horizontal axis shows the distance along the baseline from J-PARC.

Baseline length	The moho discontinuity under the sea		
L (km)	16 km	17km	18 km
1000	2.94	2.96	2.98
1100	2.99	3.01	3.02
1200	3.03	3.03	3.03

Table 3: Averaged density for each baseline length with various position of the mantle. Unit is g/cm^3

Korea (T2KK) experiment and the cross section view (bottom) and the surface map (bottom). The center of the neutrino beam line is shown in up figure. The distance from J-PARC is shown by the scale, of which interval is 100 km. The two circles shows the region which is studied by geophysicists [37, 38] In the bottom figure, each line corresponds to the baseline for $L = 1000$, 1050, 1100, 1150 and 1200 km, the numbers represents the average matter density, in units of g/cm^3, the horizontal axis shows the distance along the baseline from J-PARC. In order to make this figure, we use the actual measurement of the Conrad discontinuity, boundary between upper and lower crust, and Moho discontinuity, boundary between the crust and the mantle, under the Japan and the Korea [35, 36]. Regarding as the matter profile under the Japan sea (east sea), two measurements shown in Fig. 24 suggest that the depth of the Conrad discontinuity and the Moho discontinuity are about 7 km and 17 km, respectively at both Yamato basin, east side Circe, and Tsushima (Ulleung) basin, Western side circle [37, 38]. So we assume that the depth of each boundary is 7 km and 17 km, respectively. At the edge of the sea, we connect the boundary at the sea to the that at Japan or Korea directly. The depth ambiguity of Conrad line is ± 1 km for the Japan and the ± 2 km for the others at $3_{\cdot}-\sigma$ level. About the Conrad discontinuity, the ambiguity of the depth is ± 1 km.

Let us estimate the average matter density along each baseline. Since the traveling length though the mantle and crust depends on the location of those, the error of the averaged matter density comes from the errors of the boundary, especially that of the moho discontinuity below the sea. We show the averaged matter density for the various mantle positions in Table. 3. Because the longer baseline go through the mantle and crust longer time, the averaged density for the longer baseline gets slightly larger value. The error of averaged densities from the uncertainty of the boundaries are less than 1%. So the uncertainty of the average density for Tokai-to-Korea baseline is dominated by the model ambiguity as well as the that for Tokai-to-Kamioka baseline.

We also check the fluctuation of the matter density for the Tokai-to-Korea baseline,. We show the value of Fourier mode of the density in Figs. 25. Fig. 25 shows the real and the imaginary part of Fourier coefficient of the density. Black circle and white square

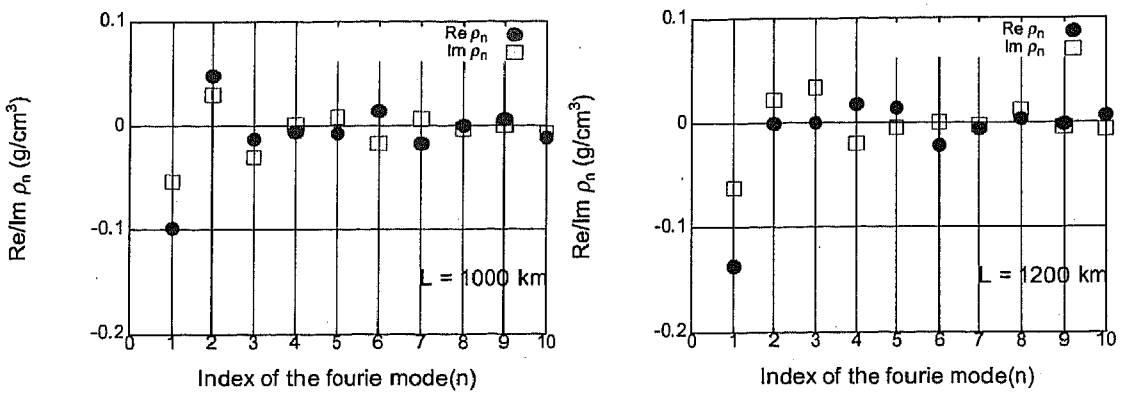

Figure 25: The Fourier coefficient of the density fluctuation along the baseline. Black circle and white square shows the magnitude of the real and imaginary part of the Fourier mode, respectively. Each figure shows the value for the $L = 1000$ km (left side), and 1200 km (right side).

shows the magnitude of the real and imaginary part of the Fourier mode, respectively. Each figure is for the $L = 1000$ km (left side), and 1200 km (right side). We find in Fig. 25 that the Fourier coefficient of which magnitude is larger than 0.1 g/cm^3 is only real part of the first mode. This is because the density fluctuation is almost same as a cosine function. So the $Re(r_1)$ dominates the corrections from the Fourier modes in eq. (57b). When we input the real part of ρ_1 into eq. (57b), the term of $Re(r_1)$ in eq. (57b) becomes about $+0.02$ at $\Delta_{13} \sim \pi$, and then this term gives about 1% corrections to the leading term. We also find that the contribution of r_1 term enhances the amplitude of the average matter effect around the first oscillation maximum region, $|\Delta_{13}| \sim \pi$, because the negative sign of $Re(r_1)$ is absorbed by the factor $\Delta_{13}^2 - 4\pi^2 k^2$ in eq. (57b). It means that the fluctuation of the matter effect helps to determine the neutrino mass hierarchy in T2KK. Let us check the magnitude of the correction of the Fourier modes.

$P_{\nu_\mu \to \nu_e}$	$\delta = 0°$	$90°$	$180°$	$-90°$
(1) Full matter effect	7.0956×10^{-2}	5.3280×10^{-2}	7.7906×10^{-2}	9.2444×10^{-2}
(2) Average matter effect only	7.0601×10^{-2}	5.2949×10^{-2}	7.7408×10^{-2}	9.1937×10^{-2}
(3) (2) + First Fourier mode	7.0985×10^{-2}	5.3321×10^{-2}	7.7983×10^{-2}	9.2493×10^{-2}
(4) (3) + Second Fourier mode	7.0941×10^{-2}	5.3252×10^{-2}	7.7923×10^{-2}	9.2433×10^{-2}

Table 4: The $\nu_\mu \to \nu_e$ transition probability at $L = 1000$ km in Korea around the oscillation maximum region for various δ and the matter density profile. The matter profile and the value of the Fourier mode of the density along the baseline are shown in Fig. 24 and 25, respectively. The transition probability shown in the table is calculated by the Runge-Kutta method. In the calculation, $\sin^2 2\theta_{\rm RCT} = 0.10$ and the normal hierarchy is assumed.

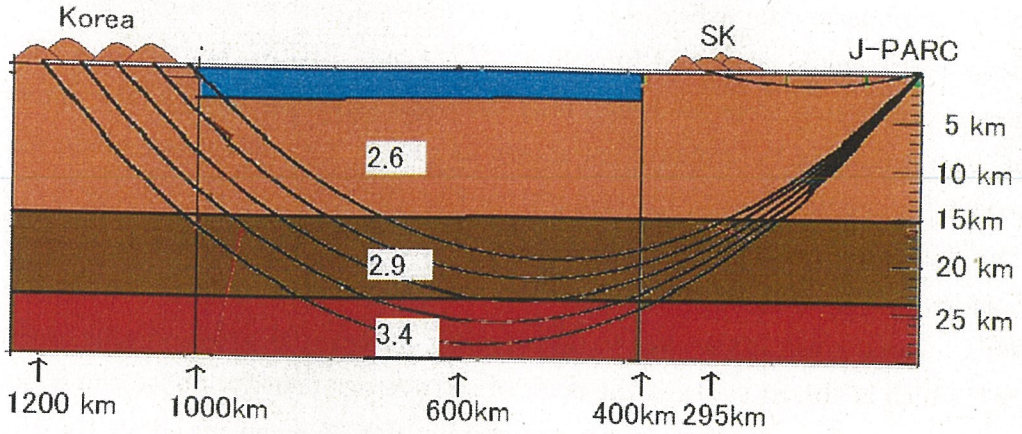

Figure 26: The cross section view of the T2KK experiment along the baselines which is estimated from PREM.

L	$\bar{\rho}$(this work)	$\bar{\rho}$(PREM)	$Re\rho_1$ (this work)	$Re\rho_1$ (PREM)
295 km	2.61	2.60	+0.034	0
1000 km	2.96	2.71	-0.098	- 0.040
1100 km	3.02	2.83	-0.124	-0.037
1200 km	3.04	2.98	-0.137	-0.033

Table 5: Average density and the real part of ρ_1 estimated from Figs. 22, 24, and PREM [32] for each baseline-length. Unit is g/cm^3

We show the same table as Table. 2 but the case for Tokai-to-Korea baseline with 1000 km baseline length in Table. 4. We confirm that the First Fourier mode enhances the $\nu_\mu \to \nu_e$ oscillation and its correction is about 1%, which is about 3% to the correction from the average matter effect. Notice that the correction of the first Fourier mode is about a half of the error of the correction from the average matter effect and hence the contribution of the first Fourier mode cannot be negligible. Therefore, in T2KK, the careful study about the matter profile along the baseline is important not only to reduce the error of the averaged matter density but also to constrain the Fourier coefficient.

Before closing this section, we compare our result and the PREM. In PREM, the earth is assumed as symmetric ball, and then the depth of the boundaries is same for everywhere. In Fig. 26, we show the cross section view of the T2KK experiment along the baselines which is estimated from PREM. Although original PREM paper assumed that the sea covers the earth everywhere down to 3 km from the sea level, we assume that the layer down to 15 km is upper crust. The large differences between our cross sections, Figs. 22 and 24, and Fig. 26 are that the T2K baseline go through only the upper crust, and moho-discontinuity in PREM is deeper than that under the sea. In

Table. 5, we summaries the average density and the real part of ρ_1 along the baseline for each baselines length estimated from Figs. 22, 24, and PREM. For the $L = 295$ km, the neutrino is expected to go thorough only the upper crust, so the average density is 2.6g/cm^3, the density of the upper-crust shown in PREM, and all Fourier mode is zero. Comparing with average density estimated from Fig. 22, both average density is almost same. For the Tokai-to-Korea case, all average density estimated from Fig. 24 is larger than those estimated from PREM. Especially, the difference of average density for the $L \sim 1000$ km case, which is the case to detect the T2K beam at small off-axis angles, is $0.2\ \text{g/cm}^3$, which is almost same as the error of the average density. So we can conclude that we tends to undervalue the physics potential of T2KK when we adopt the PREM model.

8.3 χ^2 analysis

In this subsection, we study the contribution of the earth matter effect, especially the error of the matter density, the Fourier mode, and the mean value of average density.

First of all, we explain how to treat the earth matter effect in our numerical calculation. Basically, we use same method in section 7. The first different point is how to calculate the transition probability and the survival probability including the contribution of the matter profile. In this paper, we calculate the transition and the survival probability for the average matter profile exactly by the numerical calculations, after the we add the correction from the Fourier mode, δA^e in eq. (84). As we learn that only the real part of the first Fourier mode gives the non-negligible effect so we only add the Constitution from the first Fourier mode in out estimation. We adapt 2.6 g/cm^3 as the average value for the Tokai-to-Kamioka baseline, and the 3.0 g/cm^3 for the Tokai-to-Korea baseline. As the Fourier modes, we take $Re(\rho_1)^{\text{SK}} = +0.05\text{g/cm}^3$, and $Re(\rho_1)^{\text{Korea}} = -0.1\text{g/cm}^3$. Since the origin of the density is common for both average and the Fourier mode, the uncertainty of the model which estimates the density from the sound velocity, we assign the common 6% normalzation factor for each baseline,

$$\begin{aligned}(\rho_{\text{SK,Kr}})^{\text{fit}} &= (1 + f_\rho^{\text{SK,Kr}})(\rho_{\text{SK,Kr}})^{\text{input}}, \\ (Re(\rho_{\text{SK,Kr}})_1)^{\text{fit}} &= (1 + f_\rho^{\text{SK,Kr}})((Re(\rho_{\text{SK,Kr}})_1)^{\text{input}}.\end{aligned} \tag{86}$$

So we change the denominator of the f_ρ term in eq. (72).

Let us check the best place to determine the neutrino mass hierarchy pattern. We show the result of our numerical calculation Fig. 27. Fig. 27 is the same figure as Fig. 14 but including the earth matter effect.

We find that the best combination to determine the neutrino mass hierarchy is OAB 3° at SK and OAB 0.5° at $L = 1000$ km in Korea. The value of minimum $\Delta\chi^2$ is

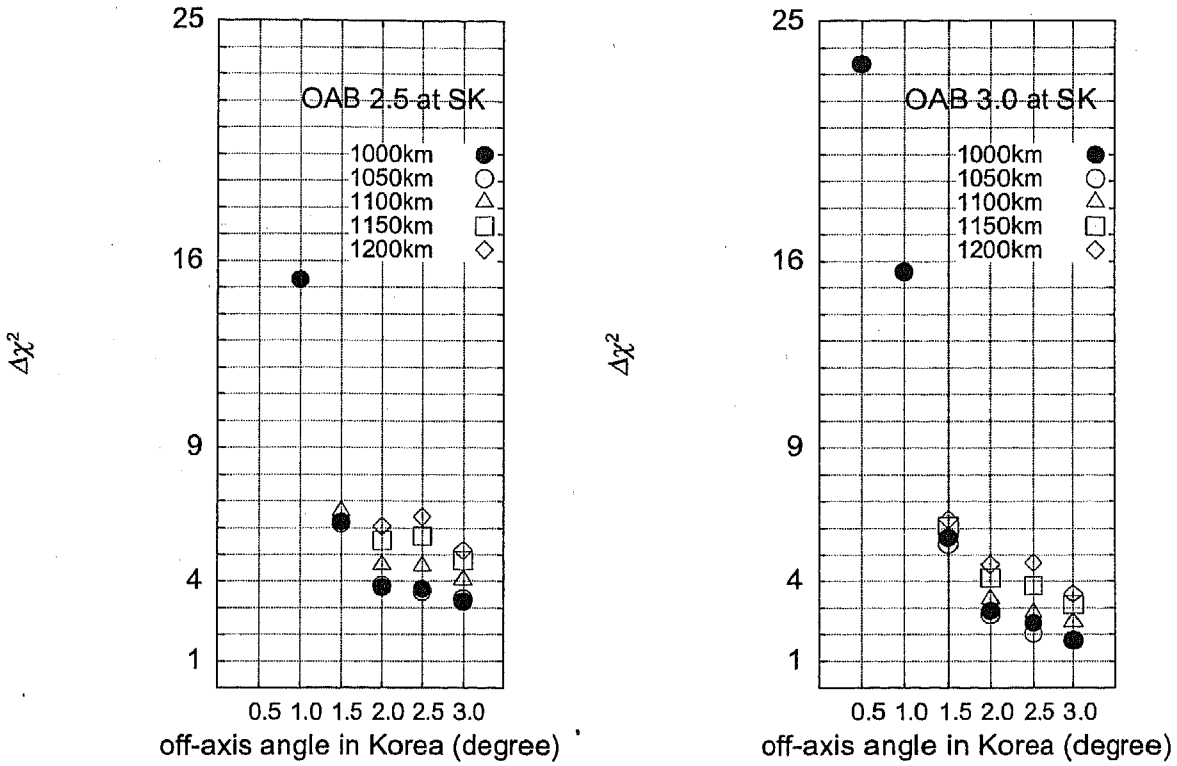

Figure 27: The same figure Fig. 14, but the earth matter effect considered, especially we include the real part of the first Fourier mode of the matter profile estimated in section 8.2, the average matter density is 2.6 g/cm^3 for the Tokai-to-Kamioka baseline, and 3.0 g/cm^3 for the Tokai-to-Korea baseline. The error of the average density is 6%

about 23.5. This is because the 0.5° OAB has the strongest flux around the oscillation maximum region in Korea [20].

Fig. 14, shows the value $\delta\chi^2$ as 22.2 for the same combination. Although the error of matter density becomes larger by 3%, $\rho_{\rm SK}$ gets slightly smaller than our previous analysis, $\rho_{\rm SK} = 2.8 \rightarrow 2.6{\rm g/cm}^3$, the difference of the matter effect between SK and Korea becomes little bit larger, and the sensitivity to the mass hierarchy pattern becomes better. Then larger systematic error is canceled by the smaller $\rho_{\rm SK}$. Both contribution changes the value of $\Delta\chi^2$ for the best combination by about 0.5 in the case of our analysis. Furthermore the contribution from $Re(r_1)$ increases the value of $\delta\chi^2$ by about 1. As we check the previous section, $Re(r_1)$ add the 3% correction to the average matter effect in Korea. Because $\chi^2_{\rm Kr}$ is roughly proportional to the the square of the matter effect corrections and, and $\Delta\chi^2$ is mainly controlled by $\chi^2_{\rm Kr}$, the value of $\Delta\chi^2$ increase by 6%.

Notice that the error of average density is only changing the $(N^e)^{\rm fit}$, and then the contribution of the error becomes a half to the $\Delta\chi^2$. Therefore the mean value of the average density along the baseline is more important than the error of the average

density. For example, if we use the average densities and the Fourier modes estimated from PREM shown in Table. 5, the matter effect contribution to the amplitude becomes smaller by about 10% (average: 6.7% and the Fourier mode: 3%), and hence the value of $\Delta\chi^2$ becomes about 80%. Actually the value of $\Delta\chi^2$ for the best combination becomes smaller by about 19%, 23.5 to 19.1. Therefore not only the off-axis combination but also the average density and the magnitude of the Fourier modes along the Tokai-to-Korea baseline should be considered when we choose the place to construct the detector in Korea.

9 Summary

In this doctor thesis, we study the physics potential of the Tokai-to-Kamioka-and-Korea (T2KK) experiment. The T2KK is a possibility of the extension the Tokai-to-Kamioka (T2K) neutrino oscillation experiment. In the T2K experiment, the off-axis beam, of which the center go though underground beneath the Super-Kamiokande, in order to detect the $\nu_\mu \to \nu_e$ transition clearly. During the T2K experimental period the lower side of the T2K off-axis beam will appear in Korea. The range of the off-axis angle is between 0.5° (1.0°) 3° when 3° (2.5°) off-axis beam is measured at SK; see Fig. 5. If we place the neutrino detector in Korea during the T2K experimental period, we can perform the two detector system.

We learn that the two detector long baseline experiment is a powerful tool to determine the neutrino mass hierarchy pattern in section 4.4, and the matter effect is key of the two detector system. The first merit of the matter effect is that the matter effect enhances (suppresses) the magnitude of the $\nu_\mu \to \nu_e$ transition probability for normal (inverted) hierarchy, respectively, and its effect becomes large at far detector as long as we measure the first oscillation maximum. Therefore by comparing the two amplitude and check the sign of the difference, we can constrain the mass hierarchy pattern. Another merit is solving the sign degeneracy between $\cos\delta$ and $\sin\Delta_{13}$ in the $\nu_\mu \to \nu_e$ mode. For the short baseline experiments, the coefficient of $\sin\Delta_{13}$ term is dominated by $\cos\delta$, then we can not constrain the sign of Δ_{13} from this contribution. For the very long baselines experiments, the matter effect term dominates the coefficient of $\sin\Delta_{13}$, the this contribution becomes powerful tool to determine the neutrino mass hierarchy. In the T2KK the we can measure the first oscillation maximum at each detector if we detect 0.5° or 1° off-axis beam in Korea, then we use the first merit of the matter effect. Additionally, the distance from the J-PARC to Korea, about 1000 km allowed that the matter effect term dominates the coefficient of the $\sin\Delta_{13}$ term.

We check the the capability of the determining the neutrino mass hierarchy in the T2KK experiment. We assume the the near detector is Super-Kamiokande and the 100 kt Water Čerenkov detector in Korea. At first we investigate the favored combination of the off-axis angles at each site and the baseline length in Korea. We find that the combination of 0.5° off-axis beam at $L = 1000$ km, 3° off-axis beam at SK is the best to determine the neutrino mass hierarchy, which can be constrained at 3-σ level when $\sin^2 2\theta_{\rm RCT} > 0.055(0.090)$ for the normal (inverted) hierarchy respectively. We find that the combination of 1° off-axis beam at $L = 1000$ km, 2.5° off-axis beam at SK keeps the enough capability. The limit of $\sin^2 2\theta_{\rm RCT}$ to constrain the mass hierarchy pattern in this combination is 0.07 for the normal hierarchy and 0.10 for the inverted hierarchy.

Once the hierarchy pattern is constrained, we can measure well the $\cos\delta$, and the setting of the T2KK two detector system is useful to measure the $\sin\delta$. Because the difference of the corrections from the matter effect to the $\nu_\mu \to \nu_e$ oscillation amplitude solve the degeneracy between $\sin^2 2\theta_{\rm RCT}$ and $\sin\delta$. We confirm that the above best combination can measure the δ uniquely. The error of δ is $\pm 30^\circ$ at 1-σ level.

The planned future neutrino oscillation experiment enhance the physics potential of T2KK. Especially, capability of determining the neutrino mass hierarchy pattern for the inverted hierarchy is much improved by using the constraint on $\sin^2 2\theta_{\rm RCT}$ from the reactor experiment. If we Cobain the result of the reactor experiment and one of the T2KK, we can determine the neutrino mass hierarchy for any δ and the hierarchy pattern when $\sin^2 2\theta_{\rm RCT} > 0.055$ for the 0.5° off-axis beam at $L = 1000$ km, 3° off-axis beam at SK.

Because the matter effect plays the important role in the T2KK. We examine the earth matter effect by using recent geophysics studies. The origin of the error of the matter density is mainly the uncertainty model which converts from the sound velocity to average matter density. The average matter density along the baseline is 2.6 g/cm^3 for the Tokai-to-Kamioka baseline and about 3.0 g/cm^3 for the Tokai-to-Korea baseline; see Table.3. About the effect of the density distribution, we can analyzed this effect by the Fourier expansion. We find that real part of the first Fourier mode gives the non-negligibly corrections in the T2KK. Finally, we find that T2KK is the statistical dominant experiment so the value of the minimum $\Delta\chi^2$ is not so improved when we improve the error of the average density from 6% to 3%, and the mean value of the average matter density is important to determine where we place the detector in Korea.

In this paper, we find that the T2KK experiment is a very powerful experiment to constraint the unmeasured oscillation parameter. If $\sin^2 2\theta_{\rm RCT} > 0.05$, the future neutrino oscillation experiments are expected to be successful in the measurement of $\sin^2 2\theta_{\rm RCT}$ near the future. In that case, the preparation for the T2KK should be started to realize the measurements of all remained oscillation parameters.

Acknowledgments

First of all, I would like to grateful thank my supervisor, K. Hagiwara and my collaborator N. Okamura. I thank our colleagues Y. Hayato, A.K. Ichikawa, T. Ishii, I. Kato, T. Kobayashi T. Nakaya, K. Nakamura and K. Nishikawa, from whom we learn about the K2K and T2K experiments. I thank N. Isezaki and M. Komazawa for teaching the geophysics in Japan (East) sea. I am also grateful to M. Aoki, V. Barger, P. Huber, M. Koike, and S. Sugiyama for useful discussions and comments. I thank the Phenomenology Institute at the University of Wisconsin for hospitality. I thank to K. Amano, K. Amikura, S. Hashimoto, S. Iwata, S. Miyamoto, S. Nakanishi, A. Okui, Y. Uchida, and M. Taka-

matsu, who gave an impetus to me during my Ph. D period. The numerical calculations were carried out on Altix3700 BX2 at YITP in Kyoto University.

A The approximation formula of the time eveolution matrix

In this appendix, we would like to show the approximation formula of the time-evolution operator.

First of all, the leading order is can be calculated as,

$$\begin{aligned} S_0(L)_{\beta\alpha} &= U_{\beta 1}U^*_{\alpha 1} + U_{\beta 2}U^*_{\alpha 2} + U_{\beta 1}U^*_{\alpha 1} \\ &= U_{\beta 3}U^*_{\alpha 3}\left(e^{-i\Delta_{13}} - 1\right). \end{aligned} \tag{87}$$

S_1, NLO, can be divided into two part, the contributions from $\bar{V}$ and δV. We obtain the both expressions by integrating eq. (35)

$$S_1(L)_{\beta\alpha} = S_1^{(1)}(L)_{\beta\alpha} + S_1^{(2)}(L)_{\beta\alpha}, \tag{88}$$

$$\begin{aligned} S_1^{(1)}(L)_{\beta\alpha} &= -i\left\langle \nu_\beta \right| \left(\int_0^L dx e^{iH^0(x-L)} \bar{V}(x) e^{-iH^0 x} \right) \left| \nu_\alpha \right\rangle \\ &= -iU_{\beta 2}U^*_{\alpha 2}\Delta_{12} + \left(U_{\beta 3}U^*_{e3}\delta_{\alpha e} + \delta_{\beta e}U_{e3}U^*_{\alpha 3} - 2U_{\beta 3}U^*_{\alpha 3}|U_{e3}|^2 \right)\left(e^{-i\Delta_{13}} - 1\right)\frac{a_0 L}{2\Delta_{13}E} \\ &\quad -i\left[\delta_{\beta e}\delta_{\alpha e} - U_{\beta 3}U^*_{e3}\delta_{\alpha e} - \delta_{\beta e}U_{e3}U^*_{\alpha 3} + U_{\beta 3}U^*_{\alpha 3}|U_{e3}|^2\left(e^{-i\Delta_{13}} + 1\right)\right]\frac{a_0 L}{2E} \end{aligned} \tag{89}$$

$$\begin{aligned} S_1^{(2)}(L)_{\beta\alpha} &= -i\left\langle \nu_\beta \right| \left(\int_0^L dx e^{iH^0(x-L)} \delta V(x) e^{-iH^0 x} \right) \left| \nu_\alpha \right\rangle \\ &= \sum_{n\neq 0} \left[U_{\beta 3}U^*_{e3}\delta_{\alpha e} f_- + \delta_{\beta e}U_{e3}U^*_{\alpha 3} f_+ - U_{\beta 3}U^*_{\alpha 3}|U_{e3}|^2 (f_- + f_+) \right]\left(e^{-i\Delta_{13}} - 1\right)\frac{a_n L}{2\Delta_{13}E}, \end{aligned} \tag{90}$$

$$f_\pm \equiv \left(1 \pm \frac{2\pi n}{\Delta_{13}}\right)^{-1}. \tag{91}$$

In eq. (90), we do not divide a_n to real part and the imaginary part in order to integrate easily. When we divide the a_n, the Fourier mode factor is changed as

$$\sum_{n\neq 0} f_\pm a_n = \sum_{k=1}^{\infty} Re(a_k)\frac{2\Delta_{13}^2}{\Delta_{13}^2 - 4\pi^2 k^2} \mp Im(a_k)\frac{8\pi^2 k^2}{\Delta_{13}^2 - 4\pi^2 k^2}. \tag{92}$$

matsu, who gave an impetus to me during my Ph. D period. The numerical calculations were carried out on Altix3700 BX2 at YITP in Kyoto University.

A The approximation formula of the time eveolution matrix

In this appendix, we would like to show the approximation formula of the time-evolution operator.

First of all, the leading order is can be calculated as,

$$\begin{aligned} S_0(L)_{\beta\alpha} &= U_{\beta 1}U^*_{\alpha 1} + U_{\beta 2}U^*_{\alpha 2} + U_{\beta 1}U^*_{\alpha 1} \\ &= U_{\beta 3}U^*_{\alpha 3}\left(e^{-i\Delta_{13}} - 1\right). \end{aligned} \tag{87}$$

S_1, NLO, can be divided into two part, the contributions from $\bar{V}$ and δV. We obtain the both expressions by integrating eq. (35)

$$S_1(L)_{\beta\alpha} = S_1^{(1)}(L)_{\beta\alpha} + S_1^{(2)}(L)_{\beta\alpha}, \tag{88}$$

$$\begin{aligned} S_1^{(1)}(L)_{\beta\alpha} &= -i\left\langle \nu_\beta \right| \left(\int_0^L dx e^{iH^0(x-L)} \bar{V}(x) e^{-iH^0 x} \right) \left| \nu_\alpha \right\rangle \\ &= -iU_{\beta 2}U^*_{\alpha 2}\Delta_{12} + \left(U_{\beta 3}U^*_{e3}\delta_{\alpha e} + \delta_{\beta e}U_{e3}U^*_{\alpha 3} - 2U_{\beta 3}U^*_{\alpha 3}|U_{e3}|^2 \right)\left(e^{-i\Delta_{13}} - 1\right)\frac{a_0 L}{2\Delta_{13}E} \\ &\quad -i\left[\delta_{\beta e}\delta_{\alpha e} - U_{\beta 3}U^*_{e3}\delta_{\alpha e} - \delta_{\beta e}U_{e3}U^*_{\alpha 3} + U_{\beta 3}U^*_{\alpha 3}|U_{e3}|^2\left(e^{-i\Delta_{13}} + 1\right)\right]\frac{a_0 L}{2E} \end{aligned} \tag{89}$$

$$\begin{aligned} S_1^{(2)}(L)_{\beta\alpha} &= -i\left\langle \nu_\beta \right| \left(\int_0^L dx e^{iH^0(x-L)} \delta V(x) e^{-iH^0 x} \right) \left| \nu_\alpha \right\rangle \\ &= \sum_{n\neq 0} \left[U_{\beta 3}U^*_{e3}\delta_{\alpha e} f_- + \delta_{\beta e}U_{e3}U^*_{\alpha 3} f_+ - U_{\beta 3}U^*_{\alpha 3}|U_{e3}|^2 (f_- + f_+) \right]\left(e^{-i\Delta_{13}} - 1\right)\frac{a_n L}{2\Delta_{13}E}, \end{aligned} \tag{90}$$

$$f_\pm \equiv \left(1 \pm \frac{2\pi n}{\Delta_{13}}\right)^{-1}. \tag{91}$$

In eq. (90), we do not divide a_n to real part and the imaginary part in order to integrate easily. When we divide the a_n, the Fourier mode factor is changed as

$$\sum_{n\neq 0} f_\pm a_n = \sum_{k=1}^{\infty} Re(a_k)\frac{2\Delta_{13}^2}{\Delta_{13}^2 - 4\pi^2 k^2} \mp Im(a_k)\frac{8\pi^2 k^2}{\Delta_{13}^2 - 4\pi^2 k^2}. \tag{92}$$

Finally, the second order correction, S_2 is can be expressed as.

$$
\begin{aligned}
S_2(L)_{\beta\alpha} &= -i\int_0^L dx \left\{ \frac{m_2^2 - m_1^2}{2E} U_{\beta 2} U_{i2}^* + \frac{a_0}{2E} \left[\delta_{\beta e}\delta_{ie} + U_{\beta e} U_{e3}^* \delta_{ei} \left(e^{i\Delta_{13}(x-L)} - 1 \right) \right] \right\} \times S_1^{(1)}(x)_{i\alpha} \\
&= -\frac{1}{2}\Delta_{12}^2 U_{\beta 2} U_{\alpha 2}^* - \frac{\Delta_{12}}{2}\frac{aL}{2E} \left(\delta_{\beta e} U_{e2} U_{\alpha 2}^* + U_{\beta 2} U_{e2}^* \delta_{\alpha e} - U_{\beta 3} U_{e3}^* U_{e2} U_{\alpha 2}^* - U_{\beta 2} U_{e2}^* U_{e3} U_{\alpha 3}^* \right) \\
&+ i\frac{\Delta_{12}}{2}\frac{a_0 L}{\Delta_{13} E} \left(U_{\beta 3} U_{e3}^* U_{e2} U_{\alpha 2}^* + U_{\beta 2} U_{e2}^* U_{e3} U_{\alpha 3}^* \right) \\
&+ \frac{\Delta_{12}}{\Delta_{13}^2}\frac{aL}{2E} \left(U_{\beta 3} U_{e3}^* U_{e2} U_{\alpha 2}^* + U_{\beta 2} U_{e2}^* U_{e3} U_{\alpha 3}^* \right) \left(e^{-i\Delta_{13}} - 1 \right) \\
&- \frac{1}{2}\left(\frac{aL}{2E}\right)^2 \left\{ \left(1 - |U_{e3}^2| \right) \left(\delta_{\beta e}\delta_{\alpha e} - U_{\beta 3} U_{e3}^* \delta_{\alpha e} - \delta_{\beta e} U_{e3} U_{\alpha 3}^* \right) + U_{\beta 3} U_{\alpha 3}^* |U_{e3}|^2 \right. \\
&\qquad \left. \times \left[1 + |U_{e3}|^2 \left(e^{-i\Delta_{13}} - 1 \right) \right] \right\} \\
&- \frac{i}{\Delta_{13}}\left(\frac{aL}{2E}\right)^2 \left[-\delta_{\beta e}\delta_{\alpha e} + \left(1 - 3|U_{e3}|^2 \right) \left(-U_{\beta 3} U_{e3}^* \delta_{\alpha e} - \delta_{\beta e} U_{e3} U_{\alpha 3}^* + 2U_{\beta 3} U_{\alpha 3}^* |U_{e3}|^2 \right) \right] \\
&- \frac{i}{\Delta_{13}}\left(\frac{aL}{2E}\right)^2 |U_{e3}|^2 \left[U_{\beta 3} U_{e3}^* \delta_{\alpha e} + \delta_{\beta e} U_{e3} U_{\alpha 3}^* + U_{\beta 3} U_{\alpha 3}^* \left(1 - 3|U_{e3}|^2 \right) \right] \left(e^{-i\Delta_{13}} - 1 \right) \\
&- \frac{1}{\Delta_{13}^2}\left(\frac{aL}{2E}\right)^2 \left[\delta_{\beta e}\delta_{\alpha e}|U_{e3}|^2 - \left(1 - 3|U_{e3}|^2 \right) \left(U_{\beta 3} U_{e3}^* \delta_{\alpha e} + \delta_{\beta e} U_{e3} U_{\alpha 3}^* - 2U_{\beta 3} U_{\alpha 3}^* |U_{e3}|^2 \right) \right] \\
&\qquad \times \left(e^{-i\Delta_{13}} - 1 \right) . \qquad (93)
\end{aligned}
$$

For the ν_μ survival mode S_2 is negligibly small term, and we do not have to pay attention such terms. For $\nu_\mu \to \nu_e$ case, the leading term can be small easily due to the small $\sin^2 2\theta_{\rm RCT}$, or the suppression by the matter effect for the inverted hierarchy and the $\sin\delta$; see eqs. (56) and (57d). When we include S_2 term to the calculations, we can estimate the transition probability with 90% accuracy for up to $\sin^2 2\theta_{\rm RCT} = 0.15$, which is present upper limit given by CHOOZ experiment[9, 20].

References

[1] The Super-Kamiokande Collaboration, Phys. Ltt. B433, 9 (1998)

[2] M. Ambrosio *et al.* (MACRO Collaboration), Phys. Lett. **B566** 35 (2003) [hep-ex/0304037]; M. C. Sanchez *et al.* (Soudan 2 Collaboration), Phys. Rev. **D68**, 113004 (2003) [hep-ex/0307069]; Y. Ashie *et al.* (Super-Kamiokande Collaboration), Phys. Rev. **D71**, 112005 (2005) [hep-ex/0501064].

Finally, the second order correction, S_2 is can be expressed as.

$$
\begin{aligned}
S_2(L)_{\beta\alpha} &= -i\int_0^L dx \left\{ \frac{m_2^2 - m_1^2}{2E} U_{\beta 2} U_{i2}^* + \frac{a_0}{2E} \left[\delta_{\beta e}\delta_{ie} + U_{\beta e} U_{e3}^* \delta_{ei} \left(e^{i\Delta_{13}(x-L)} - 1 \right) \right] \right\} \times S_1^{(1)}(x)_{i\alpha} \\
&= -\frac{1}{2}\Delta_{12}^2 U_{\beta 2} U_{\alpha 2}^* - \frac{\Delta_{12}}{2}\frac{aL}{2E} \left(\delta_{\beta e} U_{e2} U_{\alpha 2}^* + U_{\beta 2} U_{e2}^* \delta_{\alpha e} - U_{\beta 3} U_{e3}^* U_{e2} U_{\alpha 2}^* - U_{\beta 2} U_{e2}^* U_{e3} U_{\alpha 3}^* \right) \\
&+ i\frac{\Delta_{12}}{2}\frac{a_0 L}{\Delta_{13} E} \left(U_{\beta 3} U_{e3}^* U_{e2} U_{\alpha 2}^* + U_{\beta 2} U_{e2}^* U_{e3} U_{\alpha 3}^* \right) \\
&+ \frac{\Delta_{12}}{\Delta_{13}^2}\frac{aL}{2E} \left(U_{\beta 3} U_{e3}^* U_{e2} U_{\alpha 2}^* + U_{\beta 2} U_{e2}^* U_{e3} U_{\alpha 3}^* \right) \left(e^{-i\Delta_{13}} - 1 \right) \\
&- \frac{1}{2}\left(\frac{aL}{2E}\right)^2 \left\{ \left(1 - |U_{e3}^2| \right) \left(\delta_{\beta e}\delta_{\alpha e} - U_{\beta 3} U_{e3}^* \delta_{\alpha e} - \delta_{\beta e} U_{e3} U_{\alpha 3}^* \right) + U_{\beta 3} U_{\alpha 3}^* |U_{e3}|^2 \right. \\
&\qquad \left. \times \left[1 + |U_{e3}|^2 \left(e^{-i\Delta_{13}} - 1 \right) \right] \right\} \\
&- \frac{i}{\Delta_{13}}\left(\frac{aL}{2E}\right)^2 \left[-\delta_{\beta e}\delta_{\alpha e} + \left(1 - 3|U_{e3}|^2 \right) \left(-U_{\beta 3} U_{e3}^* \delta_{\alpha e} - \delta_{\beta e} U_{e3} U_{\alpha 3}^* + 2U_{\beta 3} U_{\alpha 3}^* |U_{e3}|^2 \right) \right] \\
&- \frac{i}{\Delta_{13}}\left(\frac{aL}{2E}\right)^2 |U_{e3}|^2 \left[U_{\beta 3} U_{e3}^* \delta_{\alpha e} + \delta_{\beta e} U_{e3} U_{\alpha 3}^* + U_{\beta 3} U_{\alpha 3}^* \left(1 - 3|U_{e3}|^2 \right) \right] \left(e^{-i\Delta_{13}} - 1 \right) \\
&- \frac{1}{\Delta_{13}^2}\left(\frac{aL}{2E}\right)^2 \left[\delta_{\beta e}\delta_{\alpha e}|U_{e3}|^2 - \left(1 - 3|U_{e3}|^2 \right) \left(U_{\beta 3} U_{e3}^* \delta_{\alpha e} + \delta_{\beta e} U_{e3} U_{\alpha 3}^* - 2U_{\beta 3} U_{\alpha 3}^* |U_{e3}|^2 \right) \right] \\
&\qquad \times \left(e^{-i\Delta_{13}} - 1 \right) . \qquad (93)
\end{aligned}
$$

For the ν_μ survival mode S_2 is negligibly small term, and we do not have to pay attention such terms. For $\nu_\mu \to \nu_e$ case, the leading term can be small easily due to the small $\sin^2 2\theta_{\rm RCT}$, or the suppression by the matter effect for the inverted hierarchy and the $\sin\delta$; see eqs. (56) and (57d). When we include S_2 term to the calculations, we can estimate the transition probability with 90% accuracy for up to $\sin^2 2\theta_{\rm RCT} = 0.15$, which is present upper limit given by CHOOZ experiment[9, 20].

References

[1] The Super-Kamiokande Collaboration, Phys. Ltt. B433, 9 (1998)

[2] M. Ambrosio *et al.* (MACRO Collaboration), Phys. Lett. **B566** 35 (2003) [hep-ex/0304037]; M. C. Sanchez *et al.* (Soudan 2 Collaboration), Phys. Rev. **D68**, 113004 (2003) [hep-ex/0307069]; Y. Ashie *et al.* (Super-Kamiokande Collaboration), Phys. Rev. **D71**, 112005 (2005) [hep-ex/0501064].

[3] M. H. Ahn *et al.* (K2K collaboration) [hep-ex/0606032]

[4] P. Adamson *et al.* (MINOS Collaboration), Phys. Rev. **D73**, 072002 (2006) [hep-ex/0512036]; N. Tagg, (MINOS Collaboration), hep-ex/0605058; D.G. Michael, *et al.* (MINOS Collaboration), Phys. Rev. Lett. **97**, 191801 (2006) [hep-ex/0607088].

[5] R. J. Davis, D. S. Harmer and K. C. Hoffman, Phys. Rev. Lett. **20**, 1205 (1968).

[6] B.T. Cleveland *et al.* (Homestake Collaboration), Astro. J. **496** 505 (1998); J.N. Abdurashitov *et al.* (SAGE Collaboration), J. Exp. Theor. Phys. **95** 181 (2002) [Zh. Eksp. Teor. Fiz. **95**, 211 (2002)] [astro-ph/0204245]; W. Hampel *et al.* (GALLEX Collaboration), Phys. Lett. **B447**, 127 (1999); M. B. Smy *et al.* (Super-Kamiokande Collaboration), Phys. Rev. **D69**, 011104 (2004) [hep-ex/0309011]; B. Aharmim *et al.* (SNO Collaboration), Phys. Rev. **C 72**, 055502 (2005) [nucl-ex/0502021]; M. Altmann *et al.* (GNO Collaboration), Phys. Lett. **B616**, 174 (2005) [hep-ex/0504037].

[7] T. Araki *et al.* [KamLAND Collaboration], Phys. Rev. Lett. **94**, 081801 (2005) [arXiv:hep-ex/0406035].

[8] J. Hosaka *et al.* (Super-Kamiokande Collaboration), Phys. Rev. **D73**, 112001 (2006) [hep-ex/0508053].

[9] M. Apollonio *et al.* Eur. Phys. J. **C27** 331 (2003) [hep-ex/0301017].

[10] F. Boehm *et al.*, Phys. Rev. Lett. **84**, 3764 (2000) [hep-ex/9912050].

[11] Y. Itow *et al.*, [hep-ex/0106019]. see also the T2K official home page, http://jnusrv01.kek.jp/public/t2k/.

[12] D. S. Ayres *et al.* (NOvA Collaboration) [hep-ex/0503053].

[13] The Double-CHOOZ Collaboration [hep-ex/0405032]. M. G. T. Lasserre,[hep-ex/0606025].

[14] X. Guo *et al.* [Daya Bay Collaboration], arXiv:hep-ex/0701029.

[15] K. K. Joo [RENO Collaboration], Nucl. Phys. Proc. Suppl. **168**, 125 (2007).

[16] J-PARC home page, http://j-parc.jp/.

[17] K. Hagiwara, Nucl. Phys. Proc. Suppl. **137**, 84 (2004) [hep-ph/0410229].

[18] M. Ishituka *et al.*, Phys. Rev. **D72**, 033003 (2005) [hep-ph/0504026]

[19] K. Hagiwara, N. Okamura, K. Senda, Phys. Lett. **B637** 266 (2006) [hep-ph/0504061].

[20] K. Hagiwara, N. Okamura and K. Senda, Phys. Rev. D **76**, 093002 (2007) [hep-ph/0607255].

[21] T. Kajita, H. Minakata, S. Nakayama and H. Nunokawa, Phys. Rev. D **75**, 013006 (2007); K. Hagiwara and N. Okamur, JHEP **01**, 02 (2008), [hep-ph/0611058].

[22] P. Huber, M. Mezzetto and T. Schwetz, [0711.2950 (hep-ph)].

[23] N. C. Ribeiro, H. Nunokawa, T. Kajita, S. Nakayama, P. Ko and H. Minakata, [0712.4314 (hep-ph)].

[24] Z. Maki, M. Nakagawa and S. Sakata, Prog. Theor. Phys. **28**, 870 (1962).

[25] N.Cabbibo,Phys.Rev.Lett.10,531(1964); M.Kobayashi and T.Maskawa Prog.Theor.Phys.49,652(1973)

[26] S.P. Mikheyev and A.Yu. Smirnov, Yad. Fiz. **42**, 1441 (1985) [Sov.J.Nucl.Phys.**42**, 913 (1986)]; Nuovo Cimento **C9**, 17 (1986).

[27] K. Hagiwara and N. Okamura, Nucl. Phys. **B548**, 60 (1997).

[28] K. Abe *et al.* [Super-Kamiokande Collaboration],Phys. Rev. Lett. **97**, 171801 (2006)[arXiv:hep-ex/0607059].

[29] A.K. Ichikawa, private communication; the flux datas for various off-axis angles are available this web page; http://jnusrv01.kek.jp/~ ichikawa/jhfnu/nubeam/655km

[30] M. Koike and J. Sato, Mod. Phys. Lett. A **14**, 1297 (1999) [hep-ph/9803212].

[31] W. J. Ludwig, J. E. Nafe. and C. L. Drake; 'Seismic Refraction, in the sea.' Edited by A. E. Maxwell, Wiley-Interscience, New York

[32] A. M. Dziewonski and D. L. Anderson, Phys. Earth Planet. Interiors **25**, 297 (1981).

[33] T. Takeda *et al.*Earth Planets Space, **56**, 1293, (2004).

[34] Geological Sheet Map 1:500,000 No. 8 TOKYO (2nd ed., 2nd print); Fig. 1 in ref. [30].

[35] D. Zhao, S. Horiuchi, and A. Hasegawa, Tectonophys. **212** 389 (1992)

[36] H. M. Cho *et al.*, Geophys. Res. Lett. **33** L06307 (2006)

[37] T. W. CHung, Geophys. J. Int **109** 620, 1992

[38] H. J. Kim *et al.*, Tectonophys. **364** 25 (2004)